NELSON MANDELA UNIVERSITY

Design, Development and Testing of a Low-cost Sub-Joule µPPT for a PocketQube

J.E. BAE

2022

NELSON MANDELA UNIVERSITY

Design, Development and Testing of a Low-cost Sub-Joule µPPT for a PocketQube

Ji Eun Bae

215065506

Submitted in fulfillment of the requirements for the degree of

Master of Engineering (MEng) in Mechatronics

Awarded by the **Faculty of Engineering, the Built Environment, and Technology** at the **Nelson Mandela University**

April 2022

Supervisor: Prof. Farouk Smith

Declaration

I, *JI EUN BAE 215065506*, hereby declare that the dissertation for *Master of Engineering (MEng)* in *Mechatronics* to be awarded is my own work and that it has not previously been submitted for assessment or completion of any postgraduate qualification to another University or for another qualification.

SIGNATURE: 

NAME: JI EUN BAE

DATE: 4/02/2022

Official use:

In accordance with Rule G5.11.4, I hereby declare that the above-mentioned treatise/ dissertation/ thesis is my own work and that it has not previously been submitted for assessment to another University or for another qualification. However, material from publications by the student may be embodied in a treatise/dissertation/ thesis.

NELSON MANDELA UNIVERSITY

PERMISSION TO SUBMIT FINAL COPIES

OF TREATISE/DISSERTATION/THESIS TO THE EXAMINATION OFFICE

Please type or complete in black ink

FACULTY: Faculty of Engineering, the Built Environment, and Technology

SCHOOL/DEPARTMENT: Department of Mechatronics

I, (surname and initials of supervisor) F. Smith

(student number) 215065506 a candidate for the (full description of qualification)

Masters of Engineering in Mechatronics

with a treatise/dissertation/thesis entitled (full title of treatise/dissertation/thesis):

Design, Development and Testing of a Low-cost Sub-Joule µPPT for a PocketQube

It is hereby certified that the proposed amendments to the treatise/dissertation/thesis have been effected and that **permission is granted to the candidate to submit** the final bound copies of his/her treatise/dissertation/thesis to the examination office.

18 March 2022

SUPERVISOR **DATE**

Acknowledgements

I want to acknowledge that the Department of Mechatronics at Nelson Mandela University has provided the necessary fund for this research.

I want to thank Prof. Farouk Smith for his encouragement to pursue a Master of Engineering in Mechatronics as well as supervising the research. His interest and passion in the field of satellite and space technology have given me the inspiration for this dissertation topic.

I would like to acknowledge my parents, Mr. Sung Ho Bae and Mrs. Eun Gyeoung Han, and my sisters, Dr. Yeong Eun Bae and Ms. Ha Eun Bae, who have constantly supported and encouraged me throughout my time at Nelson Mandela University. Their steadfast faith in me has helped me push through a difficult time during the pandemic.

And finally, my thanks go to Helen Steyn, who tutored me in English throughout my life here in South Africa. She has helped nurture a love of writing and reading in me.

Abstract

Small satellites are unmanned spacecraft with small size and mass weighing less than 500kg. A small satellite called the CubeSat was created by two university professors to help students understand satellite design. The idea of small satellites caught on and they became popular due to their low cost, quick development time and easy deployment. The inexpensive nature of small satellites has helped lower the entry barrier to space and led to a movement called the “democratisation of space”. The popularity of small satellites has also caught the eye of private companies that recognise the potential of commercialising small satellite technologies. Nowadays, small satellites are being considered for more complex and challenging space missions. However for a small satellite to reach its full potential, it needs to be equipped with a proper propulsion system.

Governments, space agencies, companies and universities around the world have started to research new innovative miniaturised space propulsion technologies. Nowadays, there are many newly developed miniaturised propulsion technologies available. The new propulsion systems are either sold by the companies and universities at a very high price, or research and development is closely guarded due to the potential commercial value of the propulsion system. Companies and universities have primarily focused on researching and developing top-of-the-line micro-propulsion devices to win lucrative research funds. This has resulted in a lack of research into cheap reliable micro-propulsion as there have been no incentives for companies and universities to develop this area. As a result, fund-limited students and individuals have been left behind, defeating the purpose of small satellites.

This dissertation focuses on designing and developing a low-cost sub-joule micro-PPT propulsion system for a PocketQube satellite. The first section covers the literature review, which looks at the different space propulsion technologies currently available. The next section covers the micro-PPT propulsion system’s mechanical and electrical design and development process. After the development process, the performance of the prototype is tested using various input parameters, as well as in vacuum conditions and over its lifetime. The test results show that the optimal performance is obtained with an input voltage supply of 5V at a pulse frequency of 0.5Hz, which achieves a minimal impulse bit

of 0.698μNs and thrust range of 0.349~1.071μN. In comparison to the STRaND-1 3U CubeSat's PPT, performance data show that the developed μPPT propulsion system is a competitive propulsion solution, as it achieves more thrust with similar minimal impulse bit, using only one third of the power consumption. The μPPT propulsion system is able to produce 1980 shots so far, which is far lower relatively than other established PPTs due to the limitations resulting from capacitor failure.

Table of Contents

List of Figures 3
List of Equations 4
List of Tables 4
Abbreviations 5
1 Introduction 6
1.1 Rational for Low-Cost Micro-propulsion System for PocketQube 8
1.2 Research Aim 9
1.3 Objectives 9
1.4 Methodology 10
1.5 Hypothesis 10
1.6 Dissertation Outline 10
1.7 Conclusion 11
2 Literature Review 12
2.1 Current Space Propulsion Technologies for Space Missions 12
2.1.1 Chemical Propulsion (CP) 13
2.1.2 Electric Propulsion (EP) 14
2.1.2.1 Electrothermal Propulsion 15
2.1.2.2 Electrostatic Propulsion 17
2.1.2.2.1 Electrospray Propulsion 18
2.1.2.2.2 Gridded-Ion Propulsion 19
2.1.2.2.3 Hall-Effect Thrusters (HET) 21
2.1.2.3 Electromagnetic Propulsion 23
2.1.2.3.1 Pulsed Plasma Thruster (PPT) 24
2.1.2.3.1.1 Basics of PPT Physics 25
2.1.2.3.1.2 Different PPT Types 26
2.1.2.3.1.3 PPT System Characteristics 26
3 Design Objectives and Requirements 33
3.1 Electrical Design Requirements and Analysis 34
3.2 Mechanical Design Requirements and Structural Analysis 36
4 Electrical Design 37
4.1 Micro-PPT Circuit Design 37
4.1.1 Arduino UNO 38
4.1.2 ECMO High Voltage Supply 39
4.1.3 Capacitors 40

4.1.4 Trigger Coil 41
4.1.5 SCR 41
4.16 High Voltage Dividers 41
4.1.7 Schottky Diodes 42
4.2 Circuit Simulation 42
Circuit Model Simulation Results and Discussions 46
4.3 PCB Design 47
5 Mechanical Design 50
5.1 Electrodes Design 50
5.2 Spark Plug Design 51
5.3 Micro-PPT Material Selection 53
5.4 Housing Propellant Feeding Mechanism Analysis 55
5.4.1 Housing and Propellant Feeding Mechanism 56
5.5 Final Micro-PPT Design 58
6 Development and Assembly 59
6.1 Micro-PPT Assembly 59
6.2 Circuit Board Development 61
7 Experimental Setup, Results and Discussion 62
7.1 Ultra-Lightweight Micro-Pendulum Test Stand 62
7.2 Experiment Setup 63
7.4 Results and Discussion 64
8 Conclusion and Future Recommendation 68
9 Reference 74
Appendix A - PocketQube standards 76
Appendix B – Technical Drawings 77
Appendix C – Ultem 1010 Datasheet 78
Appendix D – Arduino Code Simulation 79
Appendix E – MATLAB GUI Code 81
Appendix F – Electronics BoM 85
Appendix G – Simulation Results 86
Appendix H – 0.25Hz Results 93
Appendix I – 0.5Hz Results 94
Appendix J – Total BoM 95
Appendix K – KiCAD Circuit Schematic and PCB Layout 96
Appendix L –Micro-pendulum Test Stand 97

List of Figures

Figure 1.1: SpaceX's Starlink satellite with Hall-effect thrusters. Sourced from: GeekWire 7
Figure 1.2: PocketQube. Sourced from: Build UBO 8
Figure 2.1: Thrust vs specific impulse of different propulsion. Sourced from: NASA 16
Figure 2.2: Schematics of Resistojet and Arcjet . Sourced from: (Kraft and White, 2013) 17
Figure 2.3: Schematics of a) Electrospray. Sourced from: Matsusada Precision and b) Ion thrusters. Sourced from: IntechOpen 18
Figure 2.4: Schematics of DC Discharge Gridded-Ion propulsion. Sourced from: NASA 20
Figure 2.5: Schematics of RF Discharge Gridded-Ion Propulsion. Sourced from: NASA 20
Figure 2.6: Schematics of HET. Sourced from: NASA 22
Figure 2.7: Schematics of a) Coaxial PPT and b)Rectangular PPT. Adapted from: (Ziemer and Choueiri, 2001) 24
Figure 2.8: Schematics of side-fed rectangular PPT. Adapted from: (Gessini et al., 2013) 26
Figure 3.1: 1P PocketQube. Sourced from: Goawesomeness 33
Figure 3.2: CAD model of 1P PocketQube. 34
Figure 4.1: Micro-PPT's firing cycle 37
Figure 4.2: General circuit of the micro-PPT 38
Figure 4.3: Arduino UNO. Sourced from: Arduino 39
Figure 4.4: EMCO Q20-5 0.5W 2kV. Sourced from: Digikey 40
Figure 4.5: Ceramic capacitor. Sourced from: Digikey 40
Figure 4.6: Trigger coil transformer. Sourced from: Xenon Flash Tube 41
Figure 4.7: BT258S-800LT SCR. Sourced from: Digikey 41
Figure 4.8: GeneSiC Semiconductor Schottky diode. Sourced from: Digikey 42
Figure 4.9: Model of the micro-PPT circuit in Proteus 43
Figure 4.10: Arduino set up in Proteus 44
Figure 4.11: COMPIM set up 44
Figure 4.12: Arduino UNO pin set up with COMPIM 45
Figure 4.13: MatLab GUI and a virtual port emulator 45
Figure 4.14: Simulation of the circuit with the GUI and digital oscilloscope. 46
Figure 4.15: A voltage vs frequency graph for different input voltages 46
Figure 4.16: KiCAD 3Dviewer of finished Micro-PPT PCB circuit board 47
Figure 4.17: First module PCB circuit board 48
Figure 4.18: Second Module PCB circuit board 48
Figure 4.19: Third Module PCB circuit board 49
Figure 5.1: Geometry of electrodes 51
Figure 5.2: Rimfire Micro Viper Z3 spark plug. Sourced from: NoZipCode 52
Figure 5.3: Schematics of a cylindrical spark plug 52
Figure 5.4: CAD model of the micro-PPT's electrodes 56
Figure 5.5: CAD model of the micro-PPT's electrodes and housing with an L-shaped notch 57
Figure 5.6: Final CAD model of the micro-PPT 58
Figure 6.1: CAD model of a modified version of micro-PPT used in the experiments 59
Figure 6.2: Photo of 3D printed micro-PP used in the experiments 59
Figure 6.3: Dimension of the electrode cut from the copper sheet. 60
Figure 6.4: Anode and cathode electrode 60

Figure 6.5: Assembled micro-PPT prototype 61
Figure 6.6: Circuit prototype 61
Figure 7.1: Impulse bits of a micro pendulum 62
Figure 7.2: Plasma plume of Experiment 1 66
Figure 7.3: Failed capacitor 67
Figure 7.4: Before and after on the cathode electrode and propellant cube 68
Figure 7.5: Erosion of the spark Plug 68

List of Equations

Equation 1: Lorentz Force Equation 23
Equation 2: Thrust-to-Power ratio's relationship to the aspect ratio 27
Equation 3: Energy of a Capacitor Equation 40
Equation 4: Voltage Divider Equation 42
Equation 5: Electrode Gap Equation 51
Equation 6: Electrode Width Equation 51
Equation 7: Impulse Bit for micro-pendulum 63

List of Tables

Table 1: Summary of chemical propulsion technologies surveyed. Sourced from: (Dunbar, 2020) 13
Table 2: Summary of electric propulsion technologies surveyed. Sourced from: (Dunbar, 2020) 15
Table 3: Past PPT missions 24
Table 4: Past micro-PPT missions. Sourced from: ((Wie and Murphy, 2005) 25
Table 5: PPT Configurations matrix 26
Table 6: Different methods for vacuum ignition system. Sourced from: (Clark et al., 2011) 30
Table 7: Thruster requirements for a 1P PocketQube. 33
Table 8: Pin connections of Arduino UNO 44
Table 9: Summary of the PCB weight and size 49
Table 10: Design parameters of micro-PPT 50
Table 11: Weight of the micro-PPT 58
Table 12: Summary of experiment parameters 63
Table 13: Summary of results for micro-PPT performance at different frequencies 65
Table 14: Comparison of micro-PPT prototype and STRaND-1 PPT 66
Table 15: Summary of the micro-pendulum properties 97

Abbreviations

Commercial-Off-The-Shelf (COTS)

Chemical Propulsion (CP)

Electrical Propulsion (EP)

Power Processing Unit (PPU)

Power Supply Unit (PSU)

Direct Current (DC)

Alternating Current (AC).

Filed Emission Electric Propulsion (FEEP)

Radio Frequency (RF)

Gridded-Ion thruster (GIT)

Power Processing Unit (PPU)

Pulsed Plasma Thruster (PPT)

Attitude Determination and Control System (ADCS)

Micro-Pulsed Plasma Thruster (μppt)

National Astronautics Space Administration (NASA)

Onboard Computer (OBC)

Bill of Materials (BoM)

Capacitor-Discharge Ignition (CDI)

Graphic User Interface (GUI)

Low Earth Orbit (LEO)

Pulse Width Modulation (PWM)

1 Introduction

Humans have always had an intrinsic urge to explore and investigate their surroundings. This has led to them exploring and conquering Earth's sky, land and sea. Now, with most of Earth discovered and researched, our focus has shifted towards outer space, the last frontier. Since 1957, with the launch of the world's first satellite, Sputnik 1, thousands of satellites have been launched from Earth. These satellites marked the era of new technologies such as GPS and research into space. Nowadays, with advances in miniaturisation and an increase in electronic capabilities, the use and development of smaller satellites has been on the rise. Small satellites offer reduced complexity in satellite design, development and testing. Additionally, small satellites have the added benefit of lower deployment costs and the ability to be launched in multiples.

The small satellite trend started with a CubeSat, which was a 10cm cube-shaped satellite (Lal et al., 2017). One CubeSat is connotated as 1U (1 Unit) and weighs approximately 1.3 kg which can be combined with sizes ranging from 1U to 6U. To date, the biggest CubeSat that was launched was a 6U CubeSat called Mars Cube One (MarCO). The concept behind the CubeSat was to simplify the complex design and development process and lower the costs of a traditional satellite (Shiroma et al., 2011). It does this through the standardisation of design requirements such as size and weight, and utilisation of COTS electronics. CubeSat became very popular with academic institutions, students and individuals looking to explore space. In the early days, CubeSat was typically launched without a propulsion system due to its strict size and weight requirements which led to limited lifetime and capabilities. As the interest in and usage of small satellites increased over the years, their lifetime and capabilities needed to be drastically increased to achieve their full potential.

The utilisation of micro-propulsion is the key to increasing the reliability, capabilities and lifetime of small satellites. Small satellites with micro-propulsion systems allow them to take on more complex space missions which requires them to be in space for a longer period. Currently, micro-propulsion technologies such as cold gas thrusters, chemical and electric propulsion, and even propellant-less propulsion technologies such as solar sails and electrodynamic tethers are being researched and developed for small satellite applications (Chigier and Gemci, 2003). Small satellites equipped with micro-propulsion capability are quickly becoming on par with the capabilities of

traditional satellites. This has resulted in governments and space agencies utilising small satellites more widely, and an increasing demand for the advancement of small satellite technologies.

Commercial companies saw the demand for small satellites as an opportunity to commercialise the space industry. Privately-own businesses started to develop and sell miniaturised space technologies to governments, space agencies and private individuals. As space exploration headed towards deep space and interplanetary research, governments and space agencies started to offer lucrative research funds for new and innovative space technologies for small satellites, such as micro-propulsion, to further increase the reliability, capabilities and lifetime of small satellites (Berner, 2019). Lucrative grants led to fierce competition between companies and academic institutions which led to a boom in micro-propulsion research and development. However, this also resulted in the research and development of micro-propulsion systems becoming closely guarded due to their potential commercial and research value.

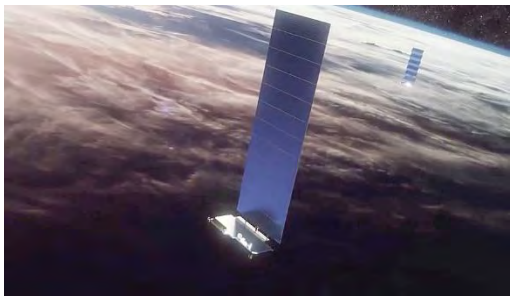

Figure 1.1: SpaceX's Starlink satellite with Hall-effect thrusters. Sourced from: GeekWire

Nowadays, there are many different micro-propulsion technologies available on the market even though they are very expensive. For example, an ion thruster used on NASA Dawn cost $50 million (Manzella, 2007). Existing micro-propulsion systems are often expensive due to companies and academic institutions primarily focusing on researching and developing the 'best of the best' micro-propulsion devices to win lucrative research funds. This has resulted in difficulty in obtaining cheap reliable micro-propulsion as there are no incentives for companies and universities to develop it. While their eventual goal is to reduce the price, fund-limited students and DIY hobbyists are being left behind in this new space age. This monetary barrier defeats the original purpose of small satellites which was to break down the entry barrier into space research, i.e. the democratising of space.

1.1 Rational for Low-Cost Micro-propulsion System for PocketQube

There is a current need for a low-cost micro-propulsion system for the PocketQube Satellite. A PocketQube is a “pocket-sized” femtosatellite that is a 5cm cube or 1P in size and weighs below 250g, which is one eighth of the volume and weight of a CubeSat as seen in *Figure 1.2*. PocketQubes were developed as a cheaper alternative to CubeSat for students and individuals looking to access space on a tight budget. For example, developing and launching a 3U CubeSat can cost up to $300 000 compared to a basic PocketQube kit sold by PocketQube Shop, which costs around $6000. However, there is no commercial micro-propulsion system available currently for a PocketQube, with current EP propulsion development mostly geared towards CubeSats. This dissertation aims to address this need by designing and developing a low-cost electric micro-propulsion system that can be used on a PocketQube. A typical PocketQube launched in Low Earth Orbit (LEO) has a lifetime of around 6 months, and because PocketQubes are launched without a micro-propulsion system, their capabilities are severely limited. Studies done on CubeSat report that its life can be extended by a factor of 2 or 3 with the implementation of a minimal micro-propulsion system. Therefore, the utilisation of even a simple micro-propulsion system can be expected to double the lifetime of a PocketQube, which in turn increases its capabilities, thereby providing more value for money for students and academic institutions on projects with a tight budget. This results in further democratisation of space.

Figure 1.2: PocketQube. Sourced from: Build UBO

1.2 Research Aim

The aim of this research is to design and develop a low-cost sub-joule micro-propulsion system suitable for a PocketQube. The aim also includes the testing and analysis of the developed prototype's performance in a vacuum environment.

1.3 Objectives

The objectives of this dissertation consist of the following:

1. The carrying out of a literature review that covers the following main topics:
    - Current space propulsion technologies
    - Different types of chemical propulsion
    - Different types of electric propulsion
    - Advantages and disadvantages of each propulsion technology
2. The development of micro-propulsion to be used in a PocketQube:
    - Establish the electrical architecture of the micro-propulsion system to define the interaction between the components used. An overall aim of decreasing the system's cost, size, weight and power.
    - Establish the mechanical architecture of the micro-propulsion system to define the interaction of the components used. An overall aim of decreasing the system's cost, size, weight and machining.
3. The development of micro-propulsion's circuit module:
    - Develop a circuit that can provide the necessary high voltage to the developed thruster module in a vacuum environment.
    - The circuit can control the firing sequence according to the desire pulsed frequency.
4. The development of micro-propulsion's thruster:
    - Develop a micro-propulsion thruster that can be tested in a vacuum environment.
    - The thruster can produce the necessary thrust, where the desired pulsed frequency is given.

1.4 Methodology

An iterative design methodology will be used to design and develop the micro-propulsion system. Once the design requirements are established, the iterative design process will follow a cycle of design/analysis, simulation/testing and review until a satisfactory prototype solution is designed and developed. To determine if the developed prototype is a viable micro-propulsion solution, the prototype will undergo performance and lifetime testing in a vacuum environment.

1.5 Hypothesis

A low-cost sub-joule micro-propulsion system can be designed and developed as a viable micro-propulsion solution for a PocketQube.

1.6 Dissertation Outline

The dissertation will consist of the following chapters:

1. Chapter 1: Introduction
    - This chapter will introduce the background and history pertaining to the research, and will discuss the rationale, aim, objectives, methodology and dissertation outline.
2. Chapter 2: Literature Review
    - This chapter will present all relevant sources of literature used as the foundation for this research.
3. Chapter 3: Design Objectives and Requirements
    - This chapter will present the overall design objectives and requirements of the electrical and mechanical design.
4. Chapter 4: Electrical Design
    - This chapter will detail the design process used to obtain the final electrical design and will include the selection of the electrical components.
5. Chapter 5: Mechanical Design
    - This chapter will detail the design process used to obtain the final mechanical design and will include the selection of the material, components and manufacturing method.
6. Chapter 6: Development and Assembly

- This chapter will detail the development and assembly of the propulsion prototype to be used in the experiment.

7. Chapter 7: Experimental Setup, Results and Discussion
    - This chapter will detail the experiment setup used in testing the prototype as well as the testing equipment and program used for performance data collection. Additionally, the results of the experiments will be presented, analysed and discussed.
8. Chapter 8: Conclusion and Future Recommendations
    - This chapter will discuss whether the aim, objectives and hypothesis of the research were achieved. Future recommendations for the research will also be discussed.

1.7 Conclusion

This chapter provided an overall introduction to the research, which was defined to be the development of a low-cost sub-joule micro-propulsion solution for a PocketQube. The section presented the aim of the research and the objectives that needed to be achieved in the research. The rationale for the research was discussed, highlighting the reasons why there is a need for this research in the space industry. Additionally, the hypothesis for the research was presented. A layout of the dissertation was provided to show the contents of each chapter.

2 Literature Review

The literature review section will investigate and summarise the different types of space propulsion systems currently available to satellites.

2.1 Current Space Propulsion Technologies for Space Missions

Any given space mission will have a delta-v requirement for each part of its mission whether rapid manoeuvre or non-impulsive manoeuvre. Delta-v, in physics, is referred to as a change in velocity. However, in spacecraft flight dynamics, it is defined as the change in velocity it can achieve on its propellant capacity i.e. the range of velocity it can achieve on its propellant capacity. For example, a space mission that requires a spacecraft to complete a rapid manoeuvre will need to achieve a high delta-v in a short period. Therefore, the propulsion system will need to have high thrust.

For deep space missions and interplanetary travel, the propulsion system's goal will be to achieve high delta-v. The optimal way for a propulsion system to achieve this goal is by performing a non-impulsive manoeuvre. This manoeuvre is carried out by applying low thrust over a longer burn period. Therefore, the propulsion system should have a combination of high specific impulses and low thrust (Jahn and Choueiri, 2003). Specific impulse is defined as thrust produced per unit rate of propellant consumption and is thus used as an indicator of the efficiency of the propulsion system. The advantage of using a propulsion system with a high specific impulse is that less propellant is needed, thus reducing the volume and storage space required. This results in the minimisation of the total mass of the spacecraft, so, a higher delta-v can be achieved with a lower deployment cost and a higher payload can be achieved (Jahn and Choueiri, 2003).

Usually, it is not beneficial to use low thrust in space. However, for deep space and interplanetary missions, applying low thrust over a longer burn period can bring huge benefits. For example, if a propulsion system can produce 9.2mN for a spacecraft weighing 1000kg, it can produce an acceleration of 0.0000982 m/s^2. Due to the frictionless and microgravity nature of space, in a week worth of burn time of 604 800s, the spacecraft can travel at 55.6m/s. In a year's worth of burn time of 315 000 000s, it can travel at 2898m/s which is nearly equivalent to 8.5 Mach i.e. 8.5 times the speed of sound. In the following sections, different available propulsion systems will be reviewed.

2.1.1 Chemical Propulsion (CP)

Chemical propulsion is by far the most mature propulsion technology option available for a spacecraft. It has a long successful track record for past and current missions. It is flight-proven, highly capable, extensively researched and reliable, whether it is required to be used for attitude control or as the main propulsion system. Chemical propulsion makes use of a large variety of thrusters, which can be subcategorised in many ways. Chemical propulsion can be categorised according to the different types of propellants it uses: solid, liquid and hybrid (Sutton, 1992). Liquid chemical thrusters can be further divided into subcategories according to the propellant they use: cold gas thrusters, liquid monopropellants (single propellant fluid), or liquid bipropellants (fuel and oxidiser).

Chemical thrusters are fundamentally based on the idea of producing thrust through an exothermic chemical reaction of the propellant. For most chemical thrusters, a chemical reaction of the propellant is created using an oxidiser and fuel. The contact between these fuels results in the creation of a highly pressurised fluid which is then accelerated through a convergent-divergent nozzle called the de Laval nozzle. This results in the creation of thrust. Cold gas thrusters are an exception to the chemical reaction used to create thrust. Rather the spacecraft stores the gas at high pressure, and it is then directly injected into the nozzle through-feed system using a control valve. *Table 1* summarises the chemical propulsion technologies.

Table 1: Summary of chemical propulsion technologies surveyed. Sourced from: (Dunbar, 2020)

Technology	Thrust Range	Specific Impulse Range (seconds)
Chemical Propulsion		
Hydrazine Monopropellant	0.25 - 0.22N	200 - 235
Other Mono- And Bipropellant	10mN - 30N	160 - 310
Hybrids	1 - 10N	215 - 300
Cold/Warm Gas	10μN – 3N	30 - 10
Solid Motors	0.3 – 260 N	180 – 280

Advantages and Disadvantages of Chemical Propulsion

Chemical propulsion is a good solution when high thrust is required, such as in a rapid maneuver. However, the huge disadvantage of chemical propulsion technology is that the spacecraft's delta-v is dependent on the amount of propellant it can carry for that mission. This limitation makes chemical thrusters unable to perform the mission economically or within a reasonable timeframe (Johnson, 2011). For example, Voyager 1 was fitted with a monopropellant rocket as its main propulsion system and attitude control. It took the spacecraft 35 years to leave the solar system. This was also a result of the process of changing chemical reaction to thrust being very inefficient, i.e. it had a low specific impulse. This requires spacecraft to carry a large amount of propellant and reserve huge storage spaces. Another disadvantage is that propellants used in chemical thrusters requiring specialised feed and storage systems require more space and weight than microsatellites can provide. Thus, chemical thrusters are not a feasible solution for microsatellites such as the PocketQube.

2.1.2 Electric Propulsion (EP)

Electric propulsion is an immature technology compared to chemical propulsion technologies as it has had limited application in past space missions. In the past, electric propulsion was typically only used for maintaining satellite stations as it could only produce a low thrust (Micci and Ketsdever, 2000). Current electric propulsion has a higher specific impulse than chemical propulsion, which is advantageous for deep space missions and for improving mission performance. Recently, a huge number of companies and academic institutions and space agencies have started to pursue research, development and innovation in electric propulsion systems, and at the current rate, electric propulsion technology may overtake chemical propulsion technology (Goebel et al., 2005).

Electric propulsion is fundamentally based on converting electrical energy to kinetic energy. Electric propulsion can be grouped into three subcategories according to the type of techniques it uses to create thrust: electrothermal, electrostatic and electromagnetic propulsion. Any combination of these techniques can also be employed to make an even more efficient electric propulsion system. *Table 2* summarises electric propulsions.

Table 2: Summary of electric propulsion technologies surveyed. Sourced from: (Dunbar, 2020)

Technology	Thrust Range	Specific Impulse Range (seconds)
Electrothermal	2 - 100mN	50-185
Electrosprays	10μN – 1mN	250 - 5000
Gridded Ion	0.1 - 15mN	1000 - 3500
Hall Effect	1 – 60mN	800 - 1900
Pulsed Plasma and Vacuum Arc Thrusters	1 - 600 μN	500 - 2400
Ambipolar	0.25 – 10mN	500 - 1400

Advantages of Electric Propulsion over Chemical Propulsion

Electric propulsion is a more viable and popular option over chemical propulsion for deep space and interplanetary missions. As discussed in the previous section, the optimal propulsion solution for deep space and interplanetary mission is to have a combination of low thrust and high specific impulse, and electric propulsion systems meet all the requirements. It can produce a high specific impulse and depending on which technique is used, it requires little or no propellant, thus requiring little or no space. It is also proven to reliably create thrust over a long period. For example, a NASA-developed electric thruster called NEXT set a world record for continuously producing thrust for 43 000 hours, which is equivalent to nearly five years. A huge advantage of electric propulsion is that it can be designed to be miniaturised as it requires little to no propellant due to its high specific impulse and technique used to produce thrust. This results in savings in space and weight, which helps meet the strict design standards of microsatellites and maximise the payload. Another advantage of electric propulsion is that it is safer than chemical propulsion systems as it does not depend on chemical reactions to create thrust. This allows microsatellites to piggyback larger payloads thus saving deployment costs. The following sections will give more detail on the different electric propulsion systems available.

2.1.2.1 Electrothermal Propulsion

Electrothermal propulsion includes electric propulsion systems in which electrical energy is utilised to electrically heat a propellant. The resultant high pressurised fluid

is then expelled out of a nozzle to convert the thermal energy into kinetic energy. The propellant used is usually an inert gas such as ammonia. There are three types of electrothermal propulsion, as seen in *Figure 2.2*:

1. *Resistojets devices* utilise a heater coil to heat the chamber surface to increase the temperature of the gaseous propellant.
2. *Arcjet devices* utilise an electric discharge through an ionised gaseous propellant. This results in joule or ohmic heating.
3. *Electrodeless thrusters* utilise inductive or capacitive coupled discharges or radiation to heat the gaseous propellant.

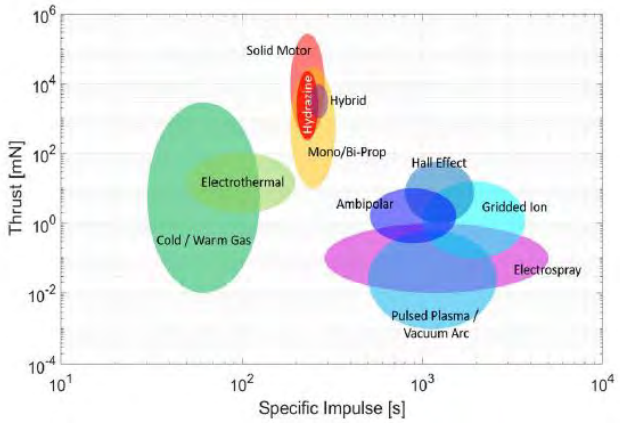

Figure 2.1: Thrust vs specific impulse of different propulsion. Sourced from: NASA

As seen in *Figure 2.1*, electrothermal propulsion achieves a similar magnitude of specific impulses to chemical propulsion. It can achieve a specific impulse range of (500s~1000s), which is lower than most electric and chemical propulsion systems (Kraft and White, 2013). Electrothermal thrusters, like chemical-based thrusters, are limited by the spacecraft's working material temperature limit. However, electrothermal thrusters can achieve higher exhaust velocity as there are fewer limitations on propellant storage (Dunbar, 2020).

Advantages and Disadvantages of Electrothermal Thrusters

The advantage of using electrothermal propulsion is that it has the most lenient restriction on propellant selection. For example, chemical propulsion systems require propellant (i.e. fuel and oxidiser) to have the right chemical and physical properties for the right amount of chemical reaction to happen, while electrothermal propulsion only requires the gas propellant to have the right physical property (i.e. low molecular weight such as inert gases). This allows electrothermal propulsion to use waste products such as water or carbon dioxide as a propellant.

However, there are many disadvantages to electrothermal propulsion. Firstly, the propellant needs to be stored in a specialised highly pressurised tank. This complicates the satellite's design and increases the cost of development. Secondly, the thruster operates at a very high temperature in which thermal soak-back to other components can happen. Thermal soak-back can happen through the mounting structure, propellant line, cable harness, etc. Thirdly, the performance of electrothermal propulsion is limited by the temperature limit of working material surfaces. Tungsten and molybdenum alloys are typically used as they can withstand very high temperatures, however they are very hard to work with as they are brittle and therefore prone to breaking. Lastly, electrothermal devices require a complex power processing unit (PPU). The design and integration of the large PPU into a microsatellite is challenging, and costs might even exceed that of the thruster (Micci and Ketsdever, 2000). For example, a radio-frequency electrodeless thruster requires inverters that convert a direct current (DC) power bus to high-frequency alternating current (AC).

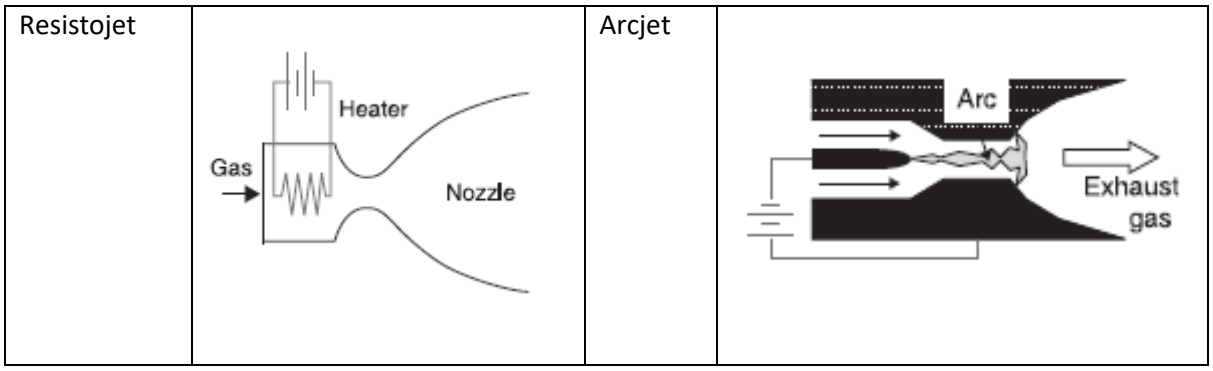

Figure 2.2: Schematics of Resistojet and Arcjet . Sourced from: (Kraft and White, 2013)

2.1.2.2 Electrostatic Propulsion

Electrostatic propulsion uses electrostatic force, also known as Coulomb's force, to accelerate ionised propellants or droplets. In Coulomb's Law, opposite charges attract and like charges repel. Using Coulomb's Law, electrostatic propulsion works first by ionising the propellant particles to have the same charge so that the particles can move in the same direction (Sutton, 1992). Electrostatic propulsion uses positively charged ions because a proton ($m_p = 1.67x10^{-27}kg$) is 1836 times heavier than an electron ($m_e = 9.11x10^{-31}kg$) (Sutton, 1992). The most typically used electrostatic propulsions are electrospray propulsion, the gridded-ion thruster (GIT) and the Hall-

Effect thruster. These electrostatic propulsion technologies can achieve the highest specific impulses of all chemical and electric propulsion technologies available.

2.1.2.2.1 Electrospray Propulsion

Electrospray propulsion creates thrust through electrostatically accelerating ions or droplets between two high voltage electrodes. The propellant consists of electrically conductive liquid propellants such as molten metals, liquid salt, or electrolyte solutions. There are two types of electrospray propulsions. They are categorised according to the propellant that they use, as seen in *Figure 2.3*:

1. An *Ionic-Liquid Electrospray thruster* uses liquid salt or electrolyte solutions as a propellant. The propellant is stored as a liquid, and onboard heaters are used to keep the temperature of the propellant within operational range.
2. A *Field Emission Electric Propulsion (FEEP) thruster* uses liquid metal as the propellant. The propellant chosen must have a low melting point as it is stored as a solid, and before usage an onboard heater is used to liquefy it for thruster operation. Commonly used propellants are indium, mercury and cesium.

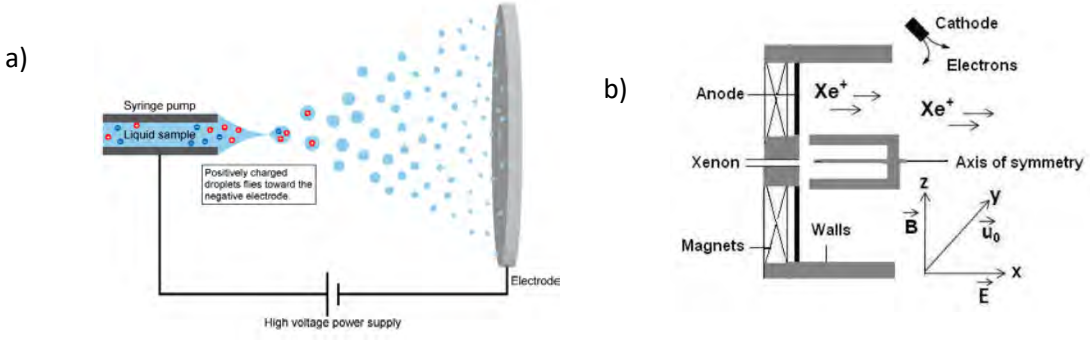

Figure 2.3: Schematics of a) Electrospray. Sourced from: Matsusada Precision and b) Ion thrusters. Sourced from: IntechOpen

The thruster has two electrodes, called the emitter and the accelerator, which maintain a large potential difference (~10kV). The electric field creates tension on the propellant surface as it is electrically conductive, and this is balanced by the surface tension. Thus, sharp liquid menisci (i.e. shape formed by liquid's surface due to adhesion) are formed, which help amplify the applied field force by two to three magnitudes of order (Kraft and White, 2013). This results in the creation of charged ions, droplets, or both. The particles are then accelerated by the accelerator, which results in thrust.

Advantages and Disadvantages of Electrospray Thrusters

The advantage of using electrospray thrusters is that they can produce very high specific impulses (e.g. droplets can achieve 100s or ions can achieve 500s) with high efficiency of up to 90%. Unfortunately, electrospray thrusters produce very low thrust (i.e. ranges of micro- to milli-newton). However with pulsed modulation of the voltage, precise impulse bits of <10 μNs can be achieved. This makes them suitable for attitude control and precise manoeuvring. The disadvantage of using electrospray thrusters is plume contamination. Plume contamination affects the performance and lifetime of the thrusters. For example, plume contamination can cause the propellant deposit to collect between the two electrodes, which can lead to a short circuit of the spacecraft. Also, during thruster operation where the propellant is expelled from the thruster, the propellant can condense back into solids due to the freezing temperatures that occur in space, which can cause surface contamination on the solar panels. This may affect electrical power generation, thereby leading to a decrease in performance over time.

2.1.2.2.2 Gridded-Ion Propulsion

The gridded-ion thruster (GIT) uses plasma discharge to ionise a heavy gaseous propellant which is accelerated via electrostatic grids. After the expulsion of the ions, it uses an external neutraliser cathode to maintain plume neutrality. Plume neutrality is important to prevent the spacecraft from gaining a negative charge which might attract back the expelled ions towards the spacecraft, thus cancelling the thrust created when ions were first expelled away from the spacecraft. Propellants mostly used in gridded-ion thrusters are noble gases (e.g. iodine and xenon).

GIT is categorised in the following through the type of plasma discharge used:

1. DC Discharge: A hollow cathode or electron emitter is used to cause electron bombardment on the propellant, which results in ionising the propellant. See the following diagram in *Figure 2.4*.
2. Radio Frequency (RF) Discharge: A RF generator is used to produce RF or microwave to excite and ionise the propellant. See following diagram in *Figure 2.5*.

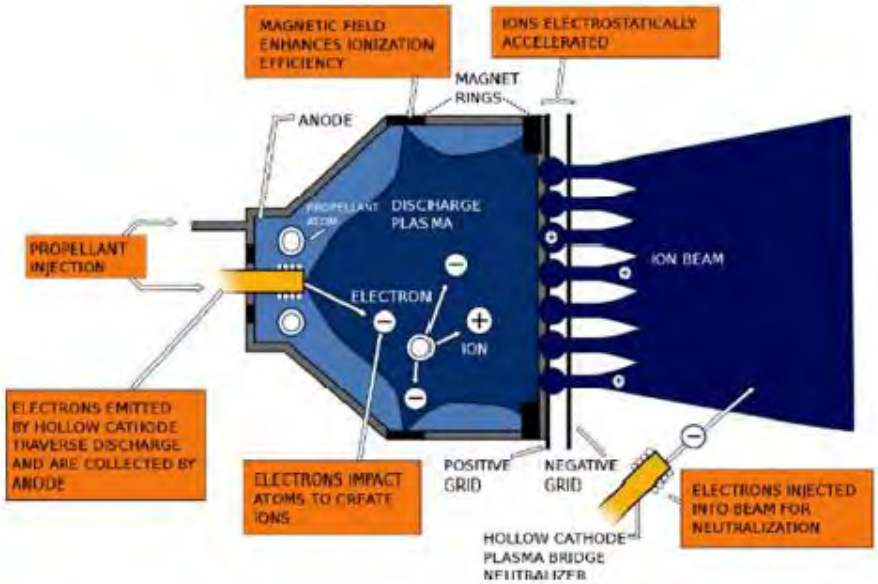

Figure 2.4: Schematics of DC Discharge Gridded-Ion propulsion. Sourced from: NASA

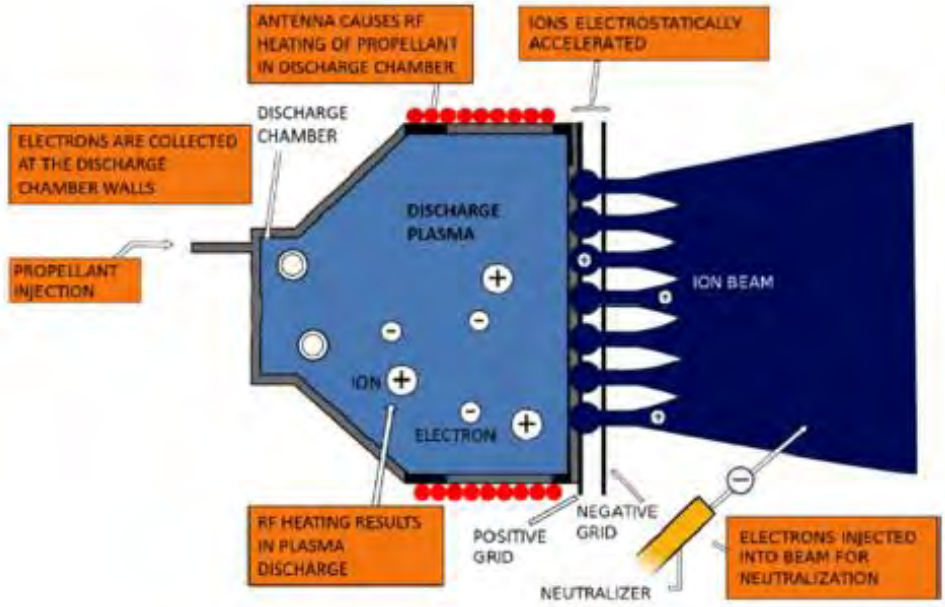

Figure 2.5: Schematics of RF Discharge Gridded-Ion Propulsion. Sourced from: NASA

Advantages and Disadvantages of GIT

The advantage of using GIT is that testing can reliably predict the performance of the thruster compared to other devices (i.e. Hall-effect thrusters). This is due to it being less sensitive and more robust, therefore giving more accurate results during testing, which is essential for the prediction of the flight performance of the spacecraft. Furthermore, thrust calculation is more straightforward due to the calculations for ion generation and ion velocity being considered as separate mechanisms. A GIT can achieve the highest specific impulse range (e.g. 3000s~5000s) compared to other propulsion technologies, with an efficiency of 75% (Kraft and White, 2013).

However, there are many disadvantages to using GIT thrusters. Gridded-ion thrusters require complex and expensive power electronics such as multiple high voltage power supply units. This is due to the cathodes requiring a large amount of power for ion generation, ion acceleration and plume neutralisation. This complex and multiple PPU can take up a large amount of an already limited available space in a microsatellite and it is nearly impossible to integrate it into a PocketQube. Grid erosion is one of the main causes of failure of a GIT on a satellite. Examples are grid structural failure, back streaming of discharged ions, and inter-grid electrical shorts. Grid erosion is caused over time by the flow of ions between the two grids (ion optics). However, grid erosion can be accelerated through improper grid alignment, thermal expansion and vibration. An improper grid alignment can also cause roll torque on the spacecraft. Another GIT failure can also be caused by foreign contamination. For example, as

GIT usually utilises high voltage grids that are less than 1mm apart to maximise performance, foreign contamination can easily bridge the gap and cause an electrical short.

2.1.2.2.3 Hall-Effect Thrusters (HET)

Hall-effect thrusters (HET) represent one of the most successful EP technologies to make it into mainstream satellite propulsion as a huge of them are flown in space. HET thrusters work in the same way as electrospray thrusters. However, the difference is that HET thrusters apply a magnetic field to electrostatically accelerated low-density plasma, as seen in *Figure 2.6*. They use propellants such as noble gases (e.g. xenon and krypton). Most HETs in the past used xenon as their propellant as it has a high molecular weight, low ionisation energy and is easy to handle. Xenon is a better propellant than krypton in terms of efficiency, and has fewer strict storage requirements. However, companies such as SpaceX are switching to krypton as it is much cheaper than xenon, therefore making it possible to launch thousands of satellites while saving money for development and launching. Many other propellants have been tested but up to date only xenon and krypton have been used in space operations.

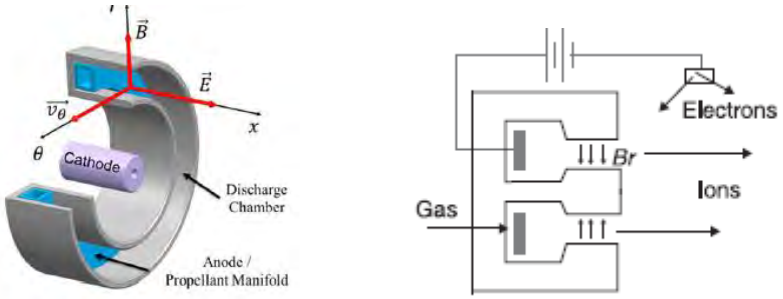

Figure 2.6: Schematics of HET. Sourced from: NASA

Advantages and Disadvantages of HET

The popularity of HET technology can be attributed to the advantages of its simple design and the favourable balance of cost, reliability, good efficiency, high specific impulse and high thrust-to-power ratio. HET thrusters can achieve specific impulses between 1200s and 2000s with the efficiency ranging between 20% to 60% depending on the power or discharge voltage level (Kraft and White, 2013). However, HET is designed to operate optimally at a specific throttle condition. Any deviations such as changing the power level can result in the decrease of specific impulse and efficiency. For example, a GIT thruster can achieve a higher specific impulse than a HET thruster. However, HET has a higher thrust-to-power ratio which shortens the mission period. HET does not need high voltage grids and plume neutrality, unlike the other electrostatic propulsion technologies, thus eliminating the need for a cathode for plume neutrality and a complex Power Supply Unit (PSU). Another example, Arcjet, can achieve higher thrust than HET, however the limitations from material properties make Arcjet less efficient and it has lower specific impulses than HET. Notable companies that use HET thrusters are OneWeb (68 satellites in 2020) and SpaceX Starlink (475 satellites in 2020).

However, there are disadvantages to HET thrusters. HET can have thermal soak-back due to the HET core reaching up to 400ºC, with the cathode temperature reaching 1000ºC. Failure can occur caused by plasma erosion on spacecraft discharge wall chamber surfaces, which can lead to structural failures and degraded performance and lifetime. HET may also require an extra propulsion system or reaction wheel to correct its direction. This is due to the roll torque created by the thruster that is produced due to the non-uniformed plasma, magnetic field, propellant flow, or temperature variation.

2.1.2.3 Electromagnetic Propulsion

Electromagnetic propulsion technologies work on a similar principle to Arcjets. A strong discharge is used to create highly ionised gas (plasma) which is accelerated through an interaction with the electromagnetic field, as seen in *Figure 2.7*. The plasma is made of electrons, positive ions and neutral particles and is highly conductive at a high temperature around 4700ºC (Patel, 2015). The magnetic field is either generated by the ionised gas or externally with an electromagnet. This interaction between the current density vector and magnetic field causes an electromagnetic force called the Lorentz force to produce thrust. A Lorentz force is created when the current density vector is applied perpendicular to a magnetic field, and the resultant force is also perpendicular to the current and magnetic field.

$$\vec{F} = \vec{j} \times \vec{B} \; [N/m^3]$$

Equation 1: Lorentz Force Equation

$\vec{j} \; [A/m^2]$	Current density field
$\vec{B}[T]$	Magnetic field

There are many advantages of electrostatic propulsion over other propulsion methods. Firstly, electrostatic propulsion has a higher efficiency than electromagnetic propulsion, which means that lower power input is needed. However, they have low energy density, which makes higher power configuration very large (Sutton, 1992). Electromagnetic propulsion, on the other hand, has a higher energy density. Hence, it can have a more compact design, which makes it suitable for smaller microsatellites like the PocketQube (Sutton, 1992). Secondly, unlike the other propulsion technologies, electromagnetic thrusters can be used with a wide range of power and frequencies. For example, it is suitable for use for microsatellites (<1W) for an interplanetary mission (200W) (Johnson, 2011). Lastly, electromagnetic propulsion technologies have more flexibility and simplicity in design than other electric propulsion systems. This allows for a broad range of thruster configurations and a wide variety of propellants (Jahn and Choueiri, 2003).

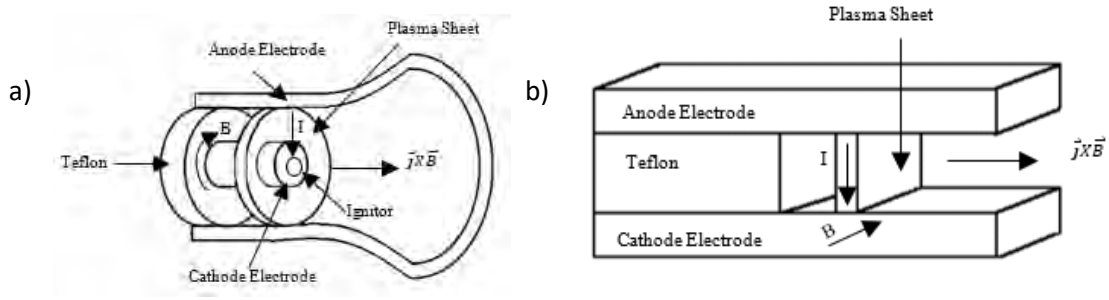

Figure 2.7: Schematics of a) Coaxial PPT and b)Rectangular PPT. Adapted from: (Ziemer and Choueiri, 2001)

2.1.2.3.1 Pulsed Plasma Thruster (PPT)

Pulsed plasma thruster (PPT) was the first electric propulsion technology used for a space mission. In 1964, a Soviet satellite called the Zond-2 was the first to utilise PPTs in its propulsion system. The Zond-2 was fitted with six breech-fed coaxial PPTs that used Teflon® as its propellant. Unfortunately, there is little record of the PPT performance during this mission due to radio communication being lost shortly after launch. During the space race, there were many experimental studies done to develop PPT. However, due to technological hurdles with the ignitor, electrode erosion and capacitor lifetime, interest in optimising and researching PPT waned. Nevertheless, due to the current increasing demand for simple electric propulsion systems for microsatellites, there is a growing need and renewed interest in micro-PPT research. *Table 3* shows some of the documented satellites that used PPT.

Table 3: Past PPT missions

Spacecraft	Year	Thruster Application
Zond-2	1964	Attitude control and station keeping
LES-6	1968	Station keeping
TIP II/III	1975/1976	Orbit insertion and drag correction
LES 8/9	1981/1988	Attitude control
NOVA-3	1984	Orbit insertion and drag correction
EO-1	200	Orbit insertion and drag correction
Dawgstar	2001	Attitude and orbit control
FalconSAT-3	2007	Attitude stabilisation

2.1.2.3.1.1 Basics of PPT Physics

The PPT's firing cycle contains two stages of acceleration for creating thrust. The firing cycle starts by creating a pilot electric arc or discharge with an ignitor initiated by a high voltage. The pilot discharge produces electrons which impact the surface of the propellant with high velocity. This results in some of the neutral, ions and electron particles escaping from the propellant's surface. The strong electric field created between the two electrodes accelerates the ions, which keep on bombarding the propellant, creating more particles to be released. The frequent collision between the particles and propellants creates a plasma between the electrodes. The plasma plume consists of carbon, fluorine and fluorocarbons such as CF, CF_2 and CF_3 (Dali et al., 2008). The formation of plasma leads to the main discharge between the two electrodes that ablates the surface of the solid propellant, thus creating more particles and increasing the pressure and temperature near the surface of the propellant, as seen in *Figure 2.7*. The increase in pressure and heat leads to the first acceleration (i.e. electrothermal acceleration). In the first stage of acceleration, plasma created has a low density with no electromagnetic acceleration (Dali et al., 2008).

The second stage of acceleration is caused by the electric field between the two electrodes. Since plasma is electrically conductive, a current flow through the plasma between the two high voltage electrodes. The interaction between the current flow and the self-generated magnetic field creates a Lorentz force that accelerates the propellant. *Table 4* shows the performance of some past micro-PPT propulsion systems.

Table 4: Past micro-PPT missions. Sourced from: ((Wie and Murphy, 2005)

Parameter	Dawnstar	AFRL-μPPT	FalconSat-3	AMSAT-Genesis
Thrust (μN)	120	10	100	0.22
Thrusters per module	2	1	3	1
Pulsing frequency (Hz)	2	1	2	0.33
Impulse bit (μN-s)	60	10	50	0.65
Pulse energy (J)	5	6.6	2	0.06
Total module mass (kg)	51	0.1	1.6	0.034

Power (W)	115	1	8	0.15~0.5
I_{sp} (s)	1524	-	-	-
Efficiency (%)	242	-	-	-
Total impulse (μN-s)	1.8	-	-	650
Propellant (g)	30	-	-	99
Number of shots	-	-	-	2000

2.1.2.3.1.2 Different PPT Types

There are a variety of PPT configurations that exist. PPT can be classified according to the electrode configuration along with how the propellant is fed into the propulsion system. *Table 5* shows a PPT configuration matrix, and *Figures 2.7* and *2.8* show the schematics of the different PPT configurations. Each configuration exposes the propellant to the main discharge in different ways, which affect the plasma formation, thus the performance of the PPT.

Table 5: PPT Configurations matrix

Electrodes Configuration	Propellant Configuration
Rectangular	Breech-fed
Coaxial	Side-Fed

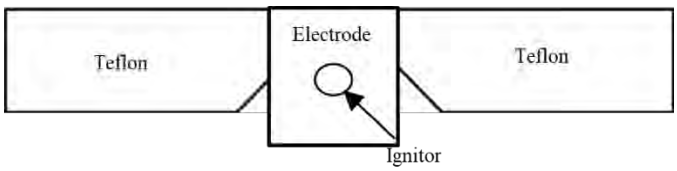

Figure 2.8: Schematics of side-fed rectangular PPT. Adapted from: (Gessini et al., 2013)

2.1.2.3.1.3 PPT System Characteristics

Despite PPT being the simplest form of electric propulsion, PPT's performance is highly sensitive to thruster characteristics. PPT does have some form of electrothermal forces but relies mainly on electromagnetic forces. According to a study done by Mingo Pérez et al. (2011), these are the main critical characteristics that need to be considered when designing or optimising a PPT:

1) Electrodes: There are two characteristics of an electrode that must be considered regarding the performance of a PPT: the geometry and the material. There have been many research studies regarding the various design parameters, such as the spacing

between the electrodes, flare angle, length, etc. Rectangle electrode configuration is the most used and studied electrode configuration for PPT to date. Studies done by Arrington et al. (1998) and Palumbo and Guman (1976) conclude some notable findings for rectangle electrode configuration regarding its design characteristics:

- **Electrode Gap**: As space between the electrode increases, the thrust-to-power ratio decreases (decrease in performance) while specific impulse and efficiency increase. Arrington et al. (1998) concluded that increased exposure to the surface area of the propellant leads to more ablation of propellant which leads to an increase of mass loss per pulse. This results in increased efficiency and specific impulse with lower performance.
- **Exposed Width**: The increase in electrode width results in a decrease in thrust-to-power ratio, while specific impulse and efficiency increases. This is also due to increases in the exposure of the propellant surface.
- **Aspect Ratio**: A general thruster equation is used to relate the thrust-to-power ratio to the aspect ratio. *Equation 2* is a general guide and assumes that there is no limit to increasing the aspect ratio (Palumbo and Guman, 1976). An aspect ratio as high as 30:1 has successfully been achieved (Micci and Ketsdever, 2000).

$$\frac{T}{P} \propto \frac{h_0}{d_0}$$

T	Thrust
P	Power
d_0	Electrode width
h_0	Electrode gap

Equation 2: Thrust-to-Power ratio's relationship to the aspect ratio

However, if the aspect ratio is too high, it could cause non-uniformity in the electromagnetic field, thus reducing thruster efficiency and requiring higher voltage for the thruster to function.

- **Electrode Length**: There have been contradicting studies in this area. Guman and Peko (1968) studied the influence of electrode length on impulse bits and specific impulses. The experiment was to increase the length from 0.5inch to 3inch with discharge energy ranging from 5J to 10J. They concluded that

smaller electrode lengths produced more thrust-to-power ratio (specific thrust) and specific impulse. However, Arrington et al. (1998) tried an increase of 2.54cm to 3.81cm with a discharge energy of 43J. Their experiment found that as the length increased, the efficiency and the specific impulse increased, and there was no notable difference in thrust-to-power ratio. Arrington et al. (1998) concluded that a longer electrode allowed the particles time to get enough kinetic energy to reach a higher velocity through the magnetic field created by the two electrodes. The discrepancy between these two conclusions could be due to the different discharge energy used in the experiments.

- **Spark plug distance**: The distance from the propellant surface can also influence the performance of the PPT. A study done by Vondra and Thomassen (1974), shows that there is an optimum distance that can be reached in each PPT design, which in their study was 1/16inch (1.5mm) to 3/16inch (4.7mm).Studies done by Schönherr et al. (2009) and Zhe et al. (2017) found that incorporating these designs also helped optimise the PPT:
- **Flare Angle**: A study done by Palumbo and Guman (1976) found that the optimal angle between the electrode was 20º, which increased thrust, impulse bits, thrust-to-power ratio, specific impulse and efficiency.
- **Electrode Shape**: Electrodes are traditionally shaped as rectangles, however a study done by Schönherr et al. (2009) found that using tongue-shaped electrodes increased the specific impulse, impulse bits and efficiency by almost 10%.
- **Segmented Electrodes**: Rectangular electrodes that were segmented with a ceramic insulator (2mm in length located 4mm from the propellant surface) were found to have an improved thrust efficiency of 49%, 75% higher current density, impulse bits increased by 28% and better discharge topography.

Coaxial electrode configuration is the least researched electrode configuration of PPT. However, there are some notable findings from experimental studies done by Edamitsu et al. (2021), Miyasaka et al. (2013), Rysanek and Burton (2001) and Huang et al. (2015):

- **Cavity length**: The cavity length refers to the distance between the two electrodes. Edamitsu et al. (2021) noted that when the cavity length was decreased from the optimal value, the efficiency and specific impulse

decreased. This decrease was attributed to transmission loss. However, if the cavity length was increased from the optimal value, the efficiency decreased due to acceleration loss.

- **Cavity Diameter**: The cavity diameter refers to the difference between the diameter of the two electrodes. Edamitsu et al. (2021) noted that as the cavity diameter was decreased from the optimal value, the transmission loss was due to high plasma resistance and high pressure created by the small cavity diameter. However, if the diameter increased, the specific impulse and efficiency increased, while the impulse bit (precision) of the thruster decreased.

PPT electrodes have been made from various metals in the past. The main metals used are copper, brass, molybdenum, aluminium, stainless steel and copper-tungsten alloy. Copper is the most popular option for electrodes and has been utilised on flight-tested PPTs. However, a study done by Dali et al. (2008) found that alloy metals such as copper-tungsten alloy and molybdenum might provide better performance than copper.

2) Different types of propellant: Although Teflon® is the main propellant used for PPT, there have been studies conducted using different propellants. Experimental studies conducted by Palumbo and Guman (1976) and Scharlemann and York (2002) compared Teflon® with other polymers, such as Celcon®, Halar®, Tefzel® and Halon®. The parameters compared were the specific thrust, specific impulse and efficiency produced by each propellant. However, most experimental studies concluded that in overall performance, Teflon® remained the most efficient and reliable propellant for PPT. A different experiment by Pencil and Kamhawi (2003) studied the effect of the density, porosity and carbon particles of Teflon® on the ablation rates, thrust and impulse bits of a thruster. A summary of the study results is given below:

- **Porosity**: The porosity of Teflon® increased the ablation rate, but it did not have any effect on the thrust produced.
- **Density**: The higher the density of Teflon®, the higher the electromagnetic component produced.
- **Carbon**: Teflon® infused with carbon particles had a slightly better specific impulse and efficiency than pure Teflon®.

3) Ignition System: The ignition system is one of the most critical parts of the thruster operation. The ignitor system consists of a spark plug and a high voltage circuit. The traditional spark plug consists of two electrodes that create an electric spark. A spark plug is important to the function of the thruster as it is needed to create the initial discharge to ablate the needed amount of Teflon® to initiate the main discharge. However, ablation of Teflon® creates a problematic by-product of carbon and fluorine which can cause erosion and contamination of the ignitor electrode surface. This can severely reduce the ignitor's lifetime. Various alternative ignitor systems are being studied, such as using a laser (Wu et al., 2018) to start the ablation process or taking out the ignitor system with a self-initiating discharge between the two main PPT electrodes. *Table 6* gives a summary of different methods for a vacuum ignition system.

Table 6: Different methods for vacuum ignition system. Sourced from: (Clark et al., 2011)

Triggering Mechanisms	Advantages	Disadvantages
High-Voltage Vacuum breakdown	No contamination of metal plasma	Requires a high voltage; breakdown voltage changes with electrode conditioning; Not usable for repetitive mode operation
Fuse Wire Explosion	No contamination of metal plasma	Not usable for repetitive mode operation
Contact Separation	Reliable, Simple, Repeatable	Low repetition rate; contacts may weld
Mechanical Triggering	Reliable, Relatively Simple (depending on actuator mechanisms)	Low repetition rate; contacts may weld and wear; limited number of triggering events (less than 10^4) large jitter
High-Voltage Surface Discharge	High repetition rates, reliable typically up to 10^5 pulses, low jitter	Needs high-voltage pulser; fails when approaching 10^5 pulses; plasma contamination by erosion of insulator
Plasma Injection Triggering	No Trigger Supply	Needs sufficiently high pressure in the discharge vicinity; metal plasma contamination by gas species; very large jitter
Low-voltage or 'triggerless' vacuum arc initiation	Reliable for 10^5 pulses, simple, high repetition rate possible, works without high voltage	Needs arc switch and moderate 'booster' voltage; may fail for low-melting-point and easily oxidizing cathode materials

4) Power System

The power system consists of a power processing unit (PPU) and a capacitor bank for the ignitor and main discharge systems. The PPU is responsible for supplying the required energy for the capacitor banks. The power available for the PPU is usually determined by the spacecraft. Available supply voltages can range from 3.3V to 35V. A flyback transformer or a high voltage transformer are usually used to increase the voltage to several kV for the capacitor banks and ignition system. There are many varieties of methods and PPU designs, with most power systems being 100W/kg (Gessini et al., 2013).

Advantages and Disadvantages of PPT

PPT is overall the best electric propulsion system that can meet the design standards and limitations of a PocketQube. The largest advantage of PPT over other propulsion systems is its simplicity and compact design. This easily allows PPT to meet the space, weight and cost standards of a PocketQube. Its simplicity comes from requiring no moving parts for it to function. This provides a higher degree of reliability, which makes it more robust than other propulsion systems. Alternative or more complex PPTs can have propellant feed system designs that can include a negator spring.

Another big advantage of PPT is that it uses a solid propellant like Teflon®. This makes PPT safe and robust, which allows it to piggyback bigger payloads, thus lowering deployment costs. Teflon® is also cheaper compared to Xenon gas and easily available. PPT can typically achieve a high specific impulse and efficiency compared to chemical thrusters. However, compared to other electric propulsion systems, PPT suffers from low thrust, efficiency and performance.

Another big advantage of PPT is its pulsed nature. PPT can be used to provide precise small impulse bits (~μN.s) by controlling and varying the frequency and discharge voltage. This makes PPT suitable for precise attitude control and pointing manoeuvres. PPT is also very scalable for different power requirements. It can be easily scaled to satellites with low- and high-power budgets and can be powered from the satellite's power bus and solar panels. However, PPT operating in low-frequency mode has very low efficiency (10%~20%). This is caused mainly by late-time ablation. Late-time

ablation occurs when the propellant continues to ablate after the discharge, i.e. misfiring of the PPT.

One of the biggest disadvantages of PPT is that it is limited to the lifetime of electronic components used for its ignition and main capacitor charge circuit. For example, PPTs are prone to capacitor failures as the capacitor's banks typically store tens of joules of energy at thousands of volts. Capacitor failure can also be caused by the shorting of the main electrodes or ignitor. The main electrodes can be bridged when there is enough accumulation of carbon from the ablation of Teflon®, therefore causing capacitor failure.

3 Design Objectives and Requirements

The main goal is to design and develop a low-cost micro-propulsion system for a 1P PocketQube as shown in *Figure 3.1*. The goal is to keep development costs as low as possible and simplify the micro-propulsion system design to include the least amount of moving and machined parts, to make the developed micro-propulsion easily integratable and more feasible for budget-tight satellite projects.

Figure 3.1: 1P PocketQube. Sourced from: Goawesomeness

A typical micro-propulsion system's design process is to evaluate the PocketQube's mission and design requirements which dictate the size and performance specification. It is important to note that PocketQubes, unlike CubeSat, have a sliding backplate that is used for ejection from the spacecraft, as seen in *Figure 3.2*. *Table 7* shows a summary of 1P PocketQube design requirements:

Table 7: Thruster requirements for a 1P PocketQube.

Size without the sliding backplate (mm)	50x50x50
Size with the sliding backplate (mm)	58x64x1.6
Weight	<250g
Power	<1W
Bus Voltage Level	3.3V

Refer to Appendix A for the PocketQube Design Standards document.

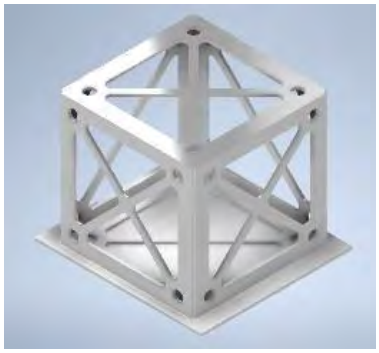

Figure 3.2: CAD model of 1P PocketQube.

As reviewed in the literature section, PPT is chosen to be developed over other electric propulsion systems as it can best meet the overall PocketQube design standard and limitations. The design of the micro-PPT propulsion system in the dissertation is broken into two parts: the mechanical design and the electrical design. The mechanical design section consists of the micro-PPT housing, electrode and spark plug design, while the electrical design section consists of designing a high voltage supply circuit for the ignition system and the main capacitor bank for the main discharge.

It is important to note that the micro-propulsion system was manufactured with the available budget, materials and machinery available to the author and tested with equipment available. This implies that the final prototype's budget, limitations, tolerances and test results can differ depending on the manufacturer or components used.

3.1 Electrical Design Requirements and Analysis

Electrical Design and Development Requirements

1. The electrical circuit must be designed to operate at input voltage levels of 3.3/5V so that it can be powered by the PocketQube's solar panels or from the Arduino UNO power bus (5V or 3.3V) with an instantaneous power of <1W (sub-Joule micro-PPT).
2. The circuit for the ignition system will need to generate a timed pulse of at least 10kV to ablate the propellant's surface (Teflon®) for the designed micro-PPT.
3. The high voltage supply unit must be able to supply the main capacitor bank with at least 2kV for the main discharge.

4. The electrical circuit must be designed to use COTS components and be easily manufactured with available basic equipment to keep costs and development time low. This requirement is to ensure that the developed prototype offers a cost-effective solution and is easy to manufacture for budget-tight individuals.
5. The electronics components must be chosen keeping in mind that they must be able to withstand a vacuum environment.
6. The final circuit design must be able to fit into a 1P PocketQube and be 10% of the PocketQube's weight.

Electrical Design Method and Approach

1. Design a basic micro-PPT control circuit based on a CDI circuit that fills the above design and development requirements.
2. Create 2D electrical schematics.
3. Simulate and test the circuit in the Proteus (LabCenter Electronics) for different frequency and voltage inputs. This is to ensure that the designed circuit can be powered and controlled from an Arduino UNO.
4. Once the designed circuit is successfully simulated, design a 3D PCB layout in KiCAD using SMD components to ensure the electronics fit the size and weight requirement.
5. Create a prototype of the circuit on a breadboard using available electric components
6. Conducti atmospheric testing of the prototype circuit before vacuum testing to ensure ignition of the spark plug and to make sure there are no electric arcs between components.

3.2 Mechanical Design Requirements and Structural Analysis

Mechanical Design and Development Requirements

1. The micro-PPT must be designed to fit within 1P of a PocketQube i.e., a 5cm cube.
2. The micro-PPT must be less than 5% of the PocketQube volume of 125 000mm^3.
3. The micro-PPT must be designed to be under or equal to 15% of PocketQube's standard weight of 250g.
4. The material selected for the micro-PPT, ignitor and propulsion housing must be able to withstand high temperatures created by the Teflon® ablation process and plasma.
5. The designed micro-PPT must be able to withstand a vacuum environment.
6. The material used for the electrodes and spark plug must be made from a highly conductive material and must be able to resist to some degree the sputter disposition caused by the plasma i.e. it must be chemically resistant to the by-products of Teflon®.
7. The material selected for the micro-PPT propulsion system must be easily available and be manufactured using minimal machining. This is to ensure development costs and time are kept as low as possible.
8. The micro-PPT propulsion system must use Teflon® as its propellant according to the PocketQube design standards.
9. The micro-PPT propulsion system must be robust and reliable.

Mechanical Design Method and Approach

1. Use Autodesk InventorCAD and knowledge gained from the literature review to design a single channel micro-PPT through an iterative design process to meet all the design requirements as mentioned above.
2. Design the micro-PPT to have minimal moving parts to ensure it is robust and reliable.
3. Using 3D printing as a manufacturing process for the micro-PPT, select the material for the micro-PPT housing that meets all the design requirements.
7. Using knowledge from the literature review select material for the electrodes and spark plug to meet the design requirements.

4 Electrical Design

This section contains details of the design process and method used to develop the electrical design to meet the design requirements of the micro-PPT. The micro-PPT electrical design included the high voltage supply circuit for the ignition of the spark plug for the pilot discharge and the main capacitor bank for the main discharge. First, the vacuum ignition system circuit was designed, and basic electrical components were chosen. This followed by the development of a circuit model in Proteus with a MatLab Graphic User Interface (GUI). After this, a simulation of the circuit model was run, and the results were analysed. Once the circuit simulation was successful, a prototype of the circuit was developed and tested in atmospheric conditions. Once the prototype circuit was successful a PCB version of the circuit was made. Final circuit schematics, codes for the Arduino UNO and MatLab GUI and the BoM are included in the Appendixes.

4.1 Micro-PPT Circuit Design

The electrical circuit for the micro-PPT is responsible for supplying the necessary high voltage needed for the pilot and main discharge and controlling the micro-PPT propulsion operation at the desired frequency. A typical micro-PPT firing cycle is powered by the main onboard computer (OBC). PocketQube typically uses an Arduino UNO as the OBC. Micro-PPT can also be powered directly from the Li-ion battery which is recharged by solar panels. Once powered, the supply voltage is boosted to a high voltage, typically by a transformer which is then used to charge the main capacitor bank and the ignitor capacitor bank. After the capacitor banks are fully charged, the OBC sends trigger pulses to start the thruster's pulsed operation. *Figure 4.1* illustrates the sequence of operations of the micro-PPT.

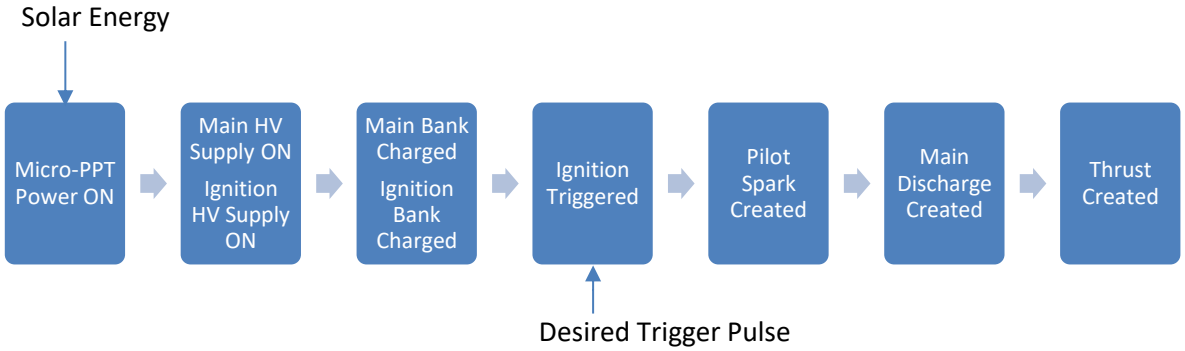

Figure 4.1: Micro-PPT's firing cycle

Based on the thruster firing cycle and the set design requirements, the electric circuit design was divided into two parts, both powered by the same voltage supply from an Arduino UNO. An Arduino UNO has two different voltages of 3.3V or 5V, too low for the required voltage in the design requirements. Therefore, a high voltage converter was used to boost the low voltage from 3.3V to 2kV. The 2kV was directly stored in the main capacitor bank for the main discharge and the ignition capacitor bank for the pilot discharge. However, 2kV was too low for the required voltage for the spark plug and a way was needed to control the thruster's pulses. Therefore, based on a capacitor discharge ignition (CDI) circuit and a disposable camera circuit, the OBC was used to send signals to the gate of the SCR, which allowed a high rush of current to be produced from the ignition capacitor bank connected to the trigger coil. Trigger coils are miniature transformers with a high turn ratio and are typically used in disposable camera flash circuits to produce a very high current for flash tubes. The trigger coil was able to produce the required high voltage for the pilot spark. *Figure 4.2* shows the general guide used to design the electrical circuit and selection of the electrical components as described in the next subsections. The final designed circuit cost ZAR 5024.80. The circuit schematics can be found in Appendix K and the final electronics BoM can be found in Appendix F.

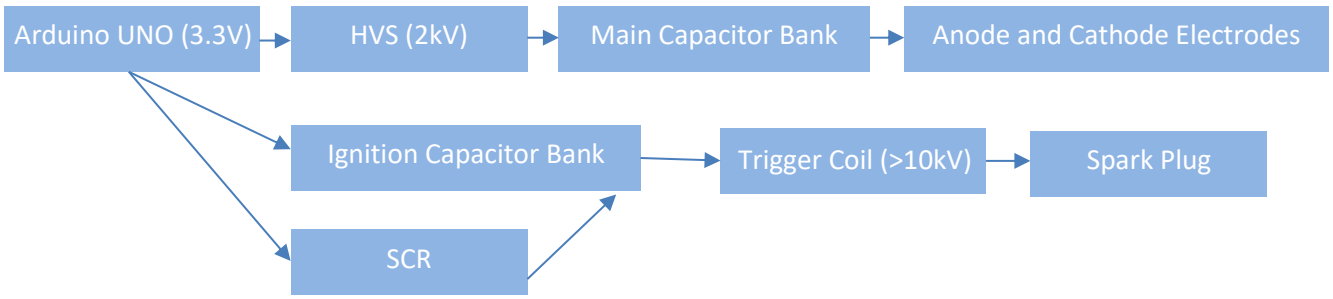

Figure 4.2: General circuit of the micro-PPT

4.1.1 Arduino UNO

The Arduino UNO was chosen as the main processor for controlling the triggering of the micro-PPT and as the main voltage supply. Arduinos are a popular choice as the OBC in many micro-satellites, which have a supply voltage of 3.3V or 5V with a maximum current draw of 40 to 50mA. Their popularity is due to the low cost, availability and open-source software. They are also supported by a strong established

community where there are already a variety of open-source code libraries, sensors and systems available. For example, ArduSat is a crowd-funded nanosatellite designed around utilising the Arduino boards and sensors. The Arduino UNO is used to trigger the micro-PPT at a desired pulsed or frequency. *Figure 4.3* shows a picture of an Arduino UNO.

Figure 4.3: Arduino UNO. Sourced from: Arduino

4.1.2 ECMO High Voltage Supply

The design goal of the circuit was to charge the main capacitor bank at 2kV. The first challenge of designing the micro-PPT control circuit was designing a circuit that was fully compatible with the power and size restrictions of the 1P PocketQube. As stated before, a standard PocketQube's supply voltage is 3.3V or 5V, with available instantaneous power of <1W. Based on the power restriction, a high voltage supply model called the EMCO 0.5W Q-series made by XP Power was chosen. This was a result of its compact size (0.5" cube) and isolated outputs which were beneficial to pulsed operation. Additionally, EMCO 0.5W Q-series modules had already been flight-tested and utilised in many micro-satellites and electric propulsion technologies. However, a shortcoming of the EMCO 0.5W Q-series module was its low-efficiency rating of 66%.

EMCO 0.5W Q-series modules have a recommended input voltage supply rated at 5V. A voltage booster module is necessary to boost the 3.3V to 5V for the Li-ion battery. Many voltage booster modules are available which are highly efficient (90%). However, an additional circuit module would introduce higher power loss and take up additional space in the circuit board. Further examination of the EMCO 0.5W Q-series modules data sheet revealed that the ECMO high voltage supply modules can be used in a voltage range between 0.7V and 5V with a linearly proportional output. Therefore, it can be used with a 3.3V supply voltage. The Q20-5 model with an input of 0.7V-5V

produces an output of 280V to 2kV, as seen in *Figure 4.4*. Therefore, the Q20-5 can produce and charge 1.32kV or 2kV for the main and ignitor capacitor bank with a voltage supply input of 3.3V or 5V.

Figure 4.4: EMCO Q20-5 0.5W 2kV. Sourced from: Digikey

4.1.3 Capacitors

Ceramic capacitors were selected as the ignitor and main capacitors bank. Ceramic capacitors are best suited for applications such as high-frequency pulse discharge and are rated at a very high voltage and temperature. They are easy to acquire, compact and vacuum rated. The ignition capacitor bank used a 0.1μF ceramic capacitor rated at 1250V. The main capacitor bank used two parallel 0.068μF KEMET ceramic capacitors which had an equivalent total capacitance of 0.136μF. The capacitor was rated at 2kV. *Equation 3* shows that the main capacitor had an estimated energy of 0.118J or 0.272J for an input voltage supply of 3.3V or 5V. *Figure 4.5* shows the ceramic capacitor used for the main capacitor bank.

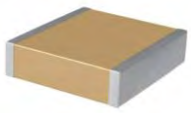

Figure 4.5: Ceramic capacitor. Sourced from: Digikey

Equation 3: Energy of a Capacitor Equation

$$E_o = \frac{1}{2} * C * U^2$$

E_o	Energy (J)
C	Capacitance (F)
U	The voltage of the Capacitor (V)

4.1.4 Trigger Coil

A trigger coil transformer was selected as these are used in the disposable flash circuit as a step-up transformer to produce rapid high voltage pulses for ionisation of the gas in xenon flash tubes. They are also very compact and have a high winding ratio. The selected trigger coil transformer was used with an input voltage of 300V and an output voltage of 12kV which was calculated to a 1:40 winding ratio. The 1.32kV or 2kV was brought down to around 300V or 750V in the circuit by two 10MΩ resistors in series. This resulted in an output of 12kV or 30kV. *Figure 4.6* shows the trigger coil transformer used in the circuit.

Figure 4.6: Trigger coil transformer. Sourced from: Xenon Flash Tube

4.1.5 SCR

Since the voltage produced by the Q20-5 module was a DC voltage, the DC voltage needed to be changed to an AC voltage for the trigger coil transformer. SCR was chosen as the controlled switch for the thruster firing cycle. The advantage of a SCR is that it has high switching speed, high bidirectional voltage blocking capability and high thermal resistance. The chosen SCR component is made by a company named WeEN and is rated at 800V and used typically for applications like CDI circuits. Once SCR is triggered ON, the capacitor discharges through the SCR which creates a current rush resulting in a high voltage output by the trigger coil. A Vishay 12M resistor load rated at 3000V with a power rating of 1W was added to the circuit to dissipate any excess current when the SCR or the thruster was turned off. *Figure 4.7* shows the SCR used in the circuit.

Figure 4.7: BT258S-800LT SCR. Sourced from: Digikey

4.16 High Voltage Dividers

Since the high voltage cannot be easily measured with a typical multimeter, a high resistance voltage divider was included in the circuit for monitoring of capacitor banks

and circuit fault finding. Each capacitor bank had a high resistance voltage divider which lowered the voltages to between 0V to 5V so that they could be read by a multimeter or as an analog input by an Arduino UNO. *Equation 4* was used to calculate the voltage over the capacitor banks.

Equation 4: Voltage Divider Equation

$$V_{OUT} = V_{supply} / \left(\frac{R_2}{R1 + R2}\right)$$

V_{OUT}	The voltage of the capacitor
V_{supply}	The voltage of the supply
R_1, R_2	Resistor

4.1.7 Schottky Diodes

Two Schottky diodes were also included in the circuit for the safety of the Arduino UNO and EMCO Q20-5. A Schottky diode has many advantages over a normal diode and include a fast switching frequency, minimal power consumption and very low forward voltage (0.3V~-0.4V). The Schottky diode chosen was manufactured by GenSiC Semiconductor and had a rating of a maximum reverse voltage of 1.2kV and 2.5A. *Figure 4.8* shows the Schottky diode used in the circuit. See Appendix F for the BoM for the circuit components and Appendix K for a full detailed schematic of the circuit designed in KiCAD.

Figure 4.8: GeneSiC Semiconductor Schottky diode. Sourced from: Digikey

4.2 Circuit Simulation

Before the designed circuit was manufactured it was modelled in Proteus. A real-time simulation helped determine the performance of the circuit designed in the previous section. A MatLab GUI was designed and used to set the desired frequency and plot the voltage of the capacitor banks read by the virtual Arduino UNO in Proteus. Proteus is a popular circuit simulation program used by engineers, developers and students to simulate electrical circuits. It is often used for running simulations of microprocessors

and microcontrollers models such as Arduinos. Another advantage of using Proteus is that it has a digital oscilloscope and other analysis tools for circuit analysis. Additionally, Proteus and MatLab can be interfaced with each other by using a virtual serial port emulator. *Figure 4.9* shows a complete model of the circuit designed in the previous section in Proteus.

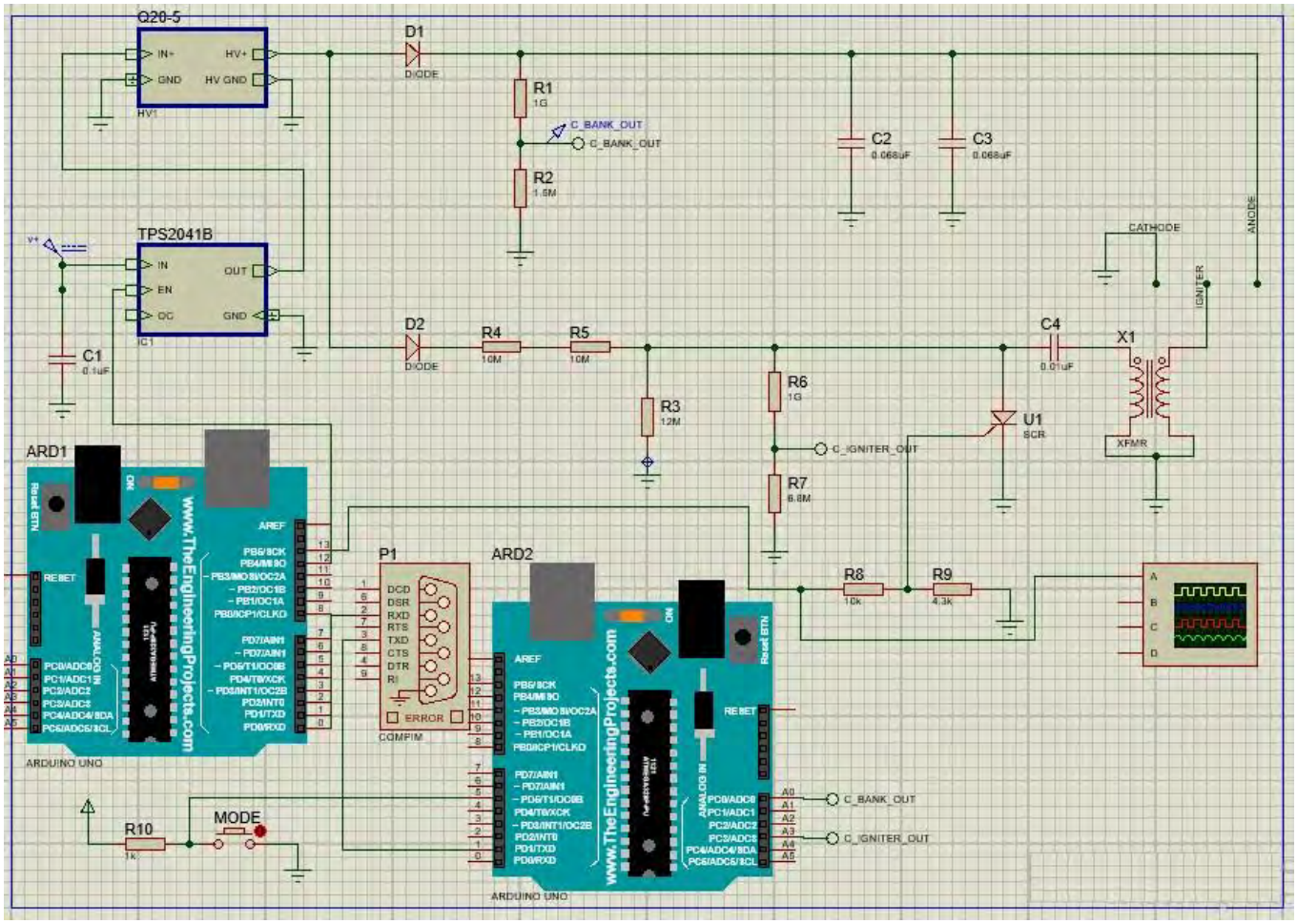

Figure 4.9: Model of the micro-PPT circuit in Proteus

After the circuit model was made, the two Arduino UNO models were set up in Proteus. Each of the Arduino UNO models were set up to use the hex files of the compiled Arduino programs to generate the trigger pulse at the desired frequency and collect the data of the capacitor banks' voltage. See Appendix D for the Arduino codes. The program called arduino_pulser.ino uses the delay(), digitalWrite() functions to generate a trigger pulse between 0.3Hz to 3Hz. This method was used instead of using the Pulse Width Modulation (PWM) pin due to the limited range of frequencies PWM pins can generate (e.g. minimum of 490Hz). The second Arduino UNO uses the program called arduino_reader.ino which uses the function called analogRead(). It

takes an analog input (0V-5V) from analog pin A0 and A3 which is then sent to the MatLab GUI. Both Arduinos are with a clock frequency of 16Hz. *Figure 4.10* shows the setup of the Arduino UNO in Proteus.

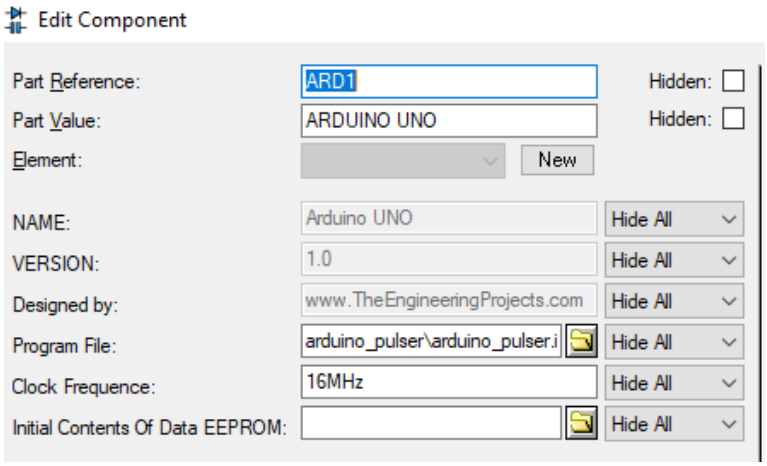

Figure 4.10: Arduino set up in Proteus

Table 8 shows the pin connection of the Arduino UNO used.

Table 8: Pin connections of Arduino UNO

Pin	Label
13	Trigger Pulse
A0	Main Capacitor Voltage Reading
A3	Igniter Capacitor Voltage Reading
12	Enable Signal

Next, the COM port model called COMPIM was used to send and receive data from the MatLab GUI. The COMPIM was set up to connect to COM4 and set up with a baud rate of 9600 bits per second. *Figure 4.11* shows the setup of the COMPIM.

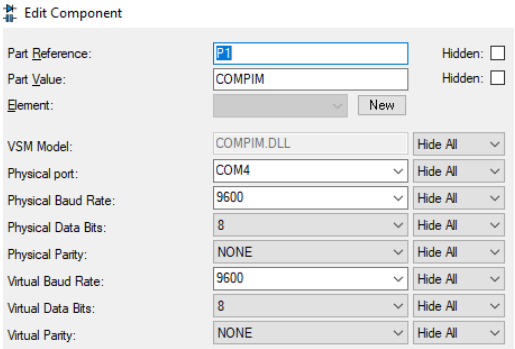

Figure 4.11: COMPIM set up

MatLab GUI was used to set the desired frequency of the trigger pulse. The trigger pulse generation Arduino UNO's pin RxD was connected to the RxD of the COMPIM to receive the desired frequency from the MatLab GUI. The voltage reader Arduino's pin TXD was connected to the TxD of the COMPIN to transmit the analog inputs from pin A0 and A3. The toggle button called mode was used to toggle between the plotting of the graph between the ignitor and main capacitor bank. *Figure 4.12* shows the pin setup of the Arduinos with the COMPIM.

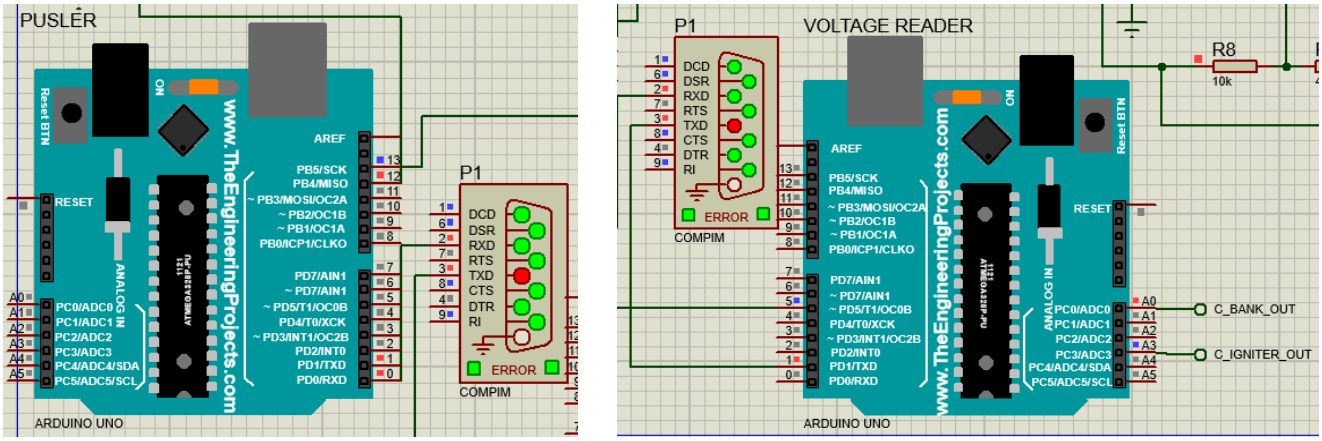

Figure 4.12: Arduino UNO pin set up with COMPIM

A simple GUI was designed in MatLab. The MatLab GUI contains a pop-up menu where the user chooses the COM port where the COM port is paired with the Arduino UNO in the virtual port emulator. Once the push button 'Open' is pressed the GUI and the Arduinos start communicating via the ports. Another pop-up menu called 'Set Trigger PWM Frequency' becomes visible after communication is established. The user then chooses the desired frequency between 0.3Hz and 3Hz. A graph of real-time data is plotted in a MatLab figure. *Figure 4.13* shows the MatLab GUI and the virtual port emulator, and *Figure 4.14* shows the simulation of the circuit and GUI with a digital oscilloscope. Appendix E contains the code for the MatLab GUI.

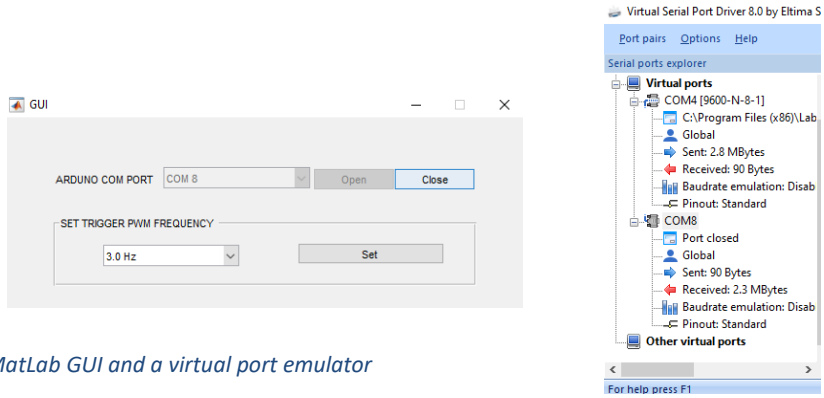

Figure 4.13: MatLab GUI and a virtual port emulator

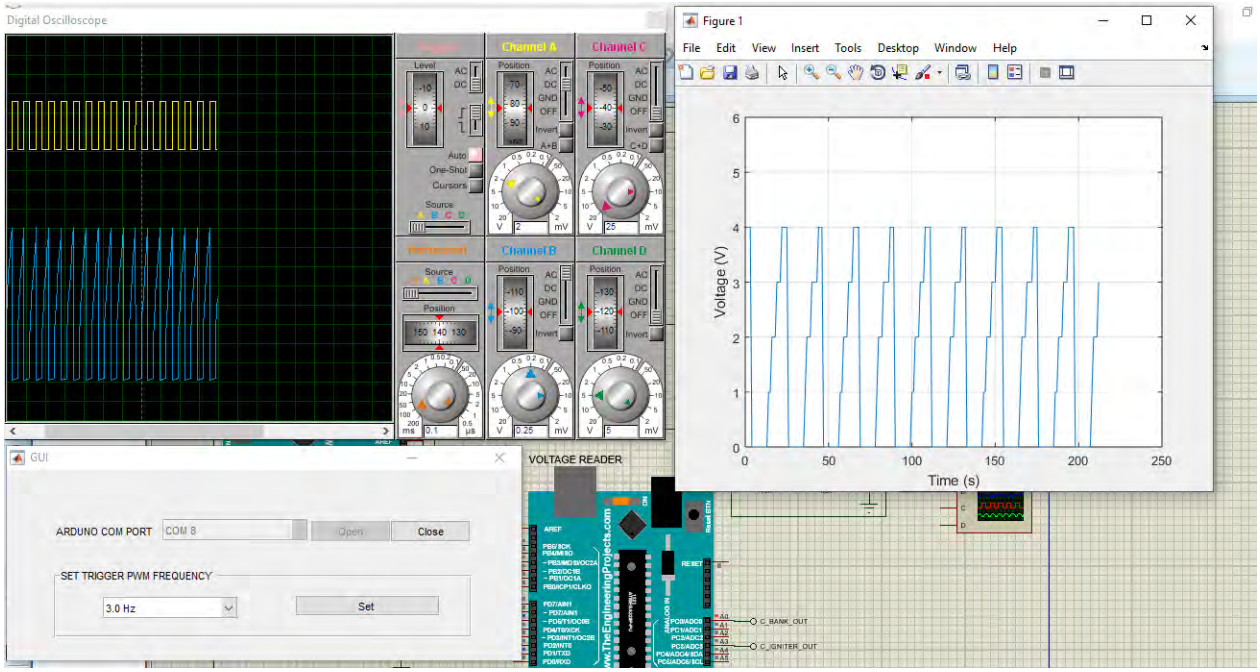

Figure 4.14: Simulation of the circuit with the GUI and digital oscilloscope.

Circuit Model Simulation Results and Discussions

A simulation of the circuit was run on different frequencies between 0.3Hz and 3Hz with a different input voltage of 3.3V, 4V and 5V. The voltage of the ignitor capacitor bank was captured with a digital oscilloscope. *Figure 4.15* shows the graph of the results from the simulation of the circuit. See Appendix G for full detailed results from the simulation.

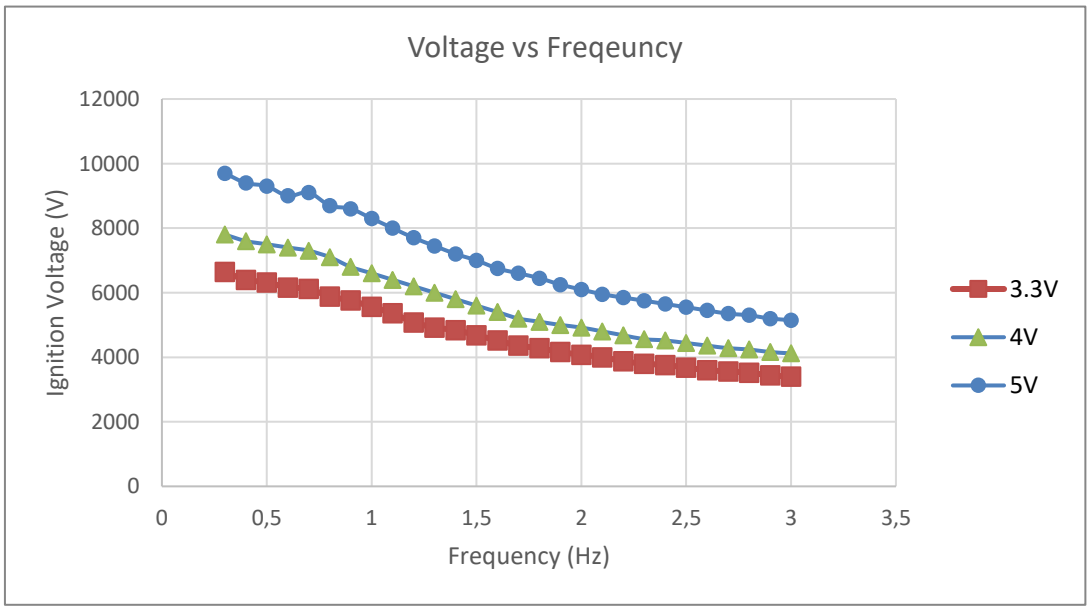

Figure 4.15: A voltage vs frequency graph for different input voltages

The simulation showed that when there was an increase in input voltage, there was a huge increase in voltage output in the ignitor. For example, the output voltage difference between 3.3V and 5V was nearly 3kV. Therefore, the increased voltage output of the ignition voltage would result in a more stable and reliable ignition of the thruster.

The results also showed that when there was an increase in the frequency of the trigger pulse, the voltage output decreased significantly in the ignitor voltage. For example, the 3.3V input voltage had its output voltage halved from 6.64kV to 3.4kV when the input frequency was changed from 0.3Hz to 3Hz. Therefore, as the frequency of the pulsed operation decreased, it resulted in increased charge time for the capacitor bank. The increased charge time increased the voltage output of the ignitor, which resulted in a more stable ignition of the thruster.

4.3 PCB Design

Once the prototype circuit was successfully simulated, a PCB design was needed to fulfil the electrical design requirements of weight and size. A PCB layout using SMD components greatly reduces the weight of the circuit to less than 250g. KiCAD was used to design a prototype PCB layout. KiCAD is a popular open-source electronic design software used by electronic designers for schematic capturing, PCB layout and 3D PCB model. The advantage of using programs like KiCAD is that most of the footprints and symbols of the electrical components' can be found online on open-source websites such as SnapEDA and Ultra Librarian. The micro-PPT PCB was designed into three separate one-layer 1.5mm thick PCB modules for a modular circuit design, which made it easy for modification and mounting inside a PocketQube. *Figure 4.16* shows the 3D visualisation of the designed PCB modules.

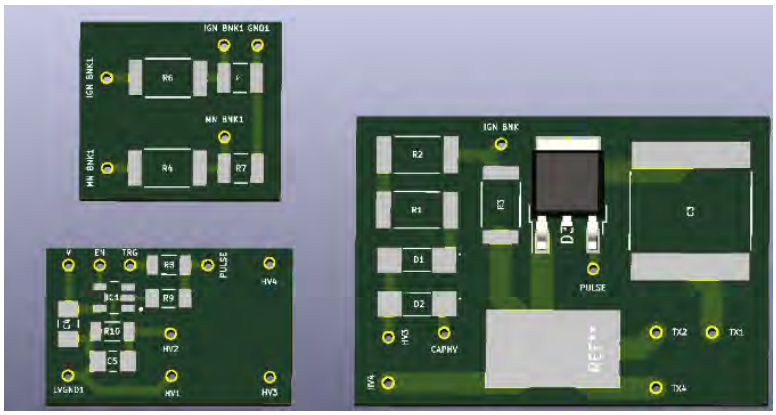

Figure 4.16: KiCAD 3Dviewer of finished Micro-PPT PCB circuit board

The first PCB module layout contained the integrated circuit (IC) load switch, trigger pulse circuit and the Q20-5 HV supply module. The layout included 0.75mm mounting hole pads added for Arduino UNO pin connections. Additionally, 0.75mm mounting hole pads were added for the Q20-5 HV module. The first PCB module was to ensure the isolation of the low and high-voltage circuits. The total footprint of the first PCB module was 22x14x12.7mm with an estimated weight of 0.846g. *Figure 4.17* shows the PCB layout for the first PCB module.

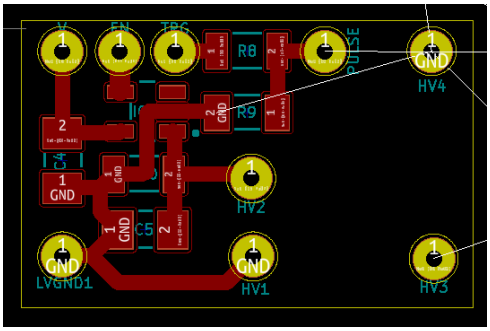

Figure 4.17: First module PCB circuit board

The second PCB module contained the high voltage circuits which contained the ignitor and main capacitor bank. The capacitor of the ignitor bank accounted for the most footprint on the PCB board: 11.40mm by 10.20mm. Therefore, to save space the ignitor capacitor bank was designed to be installed upright. There were 0.75mm mounting hole pads added for Arduino UNO and the HV pin connections. Additionally, there were 0.75mm mounting hole pads for the main and ignitor capacitor bank for voltage level monitoring. The total footprint of the second PCB module was 26x37x10mm with an estimated weight of 2.644g. However, the second PCB module had the heaviest components with the ECMO Q20-5 (4.25g) and parallel capacitor (3g). Therefore, the total estimated weight was 9.894g. *Figure 4.18* shows the PCB layout for the second PCB module.

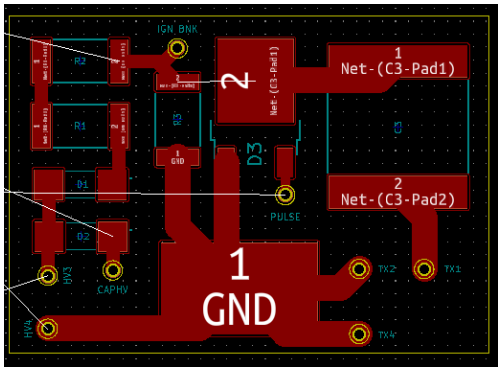

Figure 4.18: Second Module PCB circuit board

The third PCB module contained the high resistance voltage dividers for safe monitoring of the main and ignitor capacitor bank voltage level by Arduino UNO or a multimeter. The third PCB module was not necessary for the operation of the micro-PPT but could be integrated into the PocketQube for monitoring capacitor bank failure etc. The total footprint of the third PCB module was 18x16x1.6mm with an estimated weight of 0.796g. *Figure 4.19* shows the PCB layout for the second PCB module.

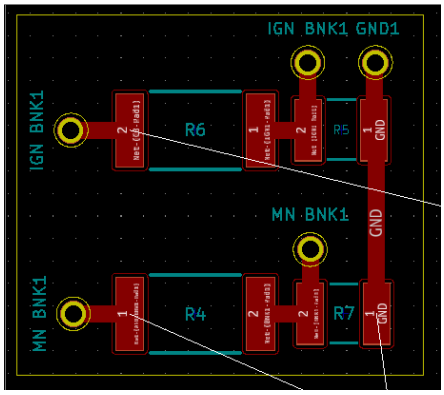

Figure 4.19: Third Module PCB circuit board

The final combined weight for the PCB module was estimated to be 11.537g, with each PCB module size measuring less than 5x5x5cm. There was enough weight left over for the other smaller SMD components, solder and the weight of the copper wire. Therefore, the final PCB module design met the size and weight requirement. *Table 9* shows a summary of the estimated size and weight of each PCB module excluding the solder weight and assuming the other SMD components on the PCB have negligible weight.

Table 9: Summary of the PCB weight and size

Component	Weight (g)	Size (mm)
First Module	0.846	22x14x12.7
Second Module	9.894	26x37x10
Third Module	0.796	18x16x1.6
Total		11.537g

5 Mechanical Design

This section discusses the methodology and process that was followed for designing the mechanical design for a rectangular breech-fed micro-PPT propulsion system. Various iterations of designs were made before the final design. The design process started with the electrode design parameters and spark plug design followed by the material section and lastly ended with the housing structure design and material selection.

5.1 Electrodes Design

The electrode geometric characteristics have a huge influence on the performance of the PPTs. However, as reviewed in the literature section, there are still major challenges and ambiguity regarding the guidelines for designing and choosing the geometries of a micro-PPT. Therefore, the design focused on making the micro-PPT as simple, robust and compact as possible to take up less space and weight in the PocketQube. The designed electrodes were placed 10mm apart with a 10mm cube of Teflon®. This electrode gap would theoretically require 30kV for a voltage breakdown to occur in an atmospheric condition, which is a dielectric voltage breakdown of 3kV/mm. According to the studies reviewed in the literature section, the electrodes were designed to have a 20º flare angle and were tongue-shaped to increase the specific impulse, impulse bits and efficiency of the thruster. The length was chosen as 20mm to keep the length as short as possible due to the micro-PPT being a sub-joule thruster. *Table 10* shows a summary of the design parameters of the prototype micro-PPT.

Table 10: Design parameters of micro-PPT

Parameter	Value
Flare angle α (degree)	20º
Electrode shape (T)	Tongue-Shape
Electrode gap h_0 (mm)	10mm
Electrode width d_0 (mm)	10mm
Electrode width *de* (mm)	0.5mm
Electrode Length l_e (mm)	20mm
Electrode thickness (mm)	1.5mm
Spark distance from Propellant surface (mm)	3mm

Figure 5.1 shows the geometry and generalised equations for calculating the design parameters of the micro-PPT. The length of the propellant bar can be determined according to the mission's impulse bits requirements.

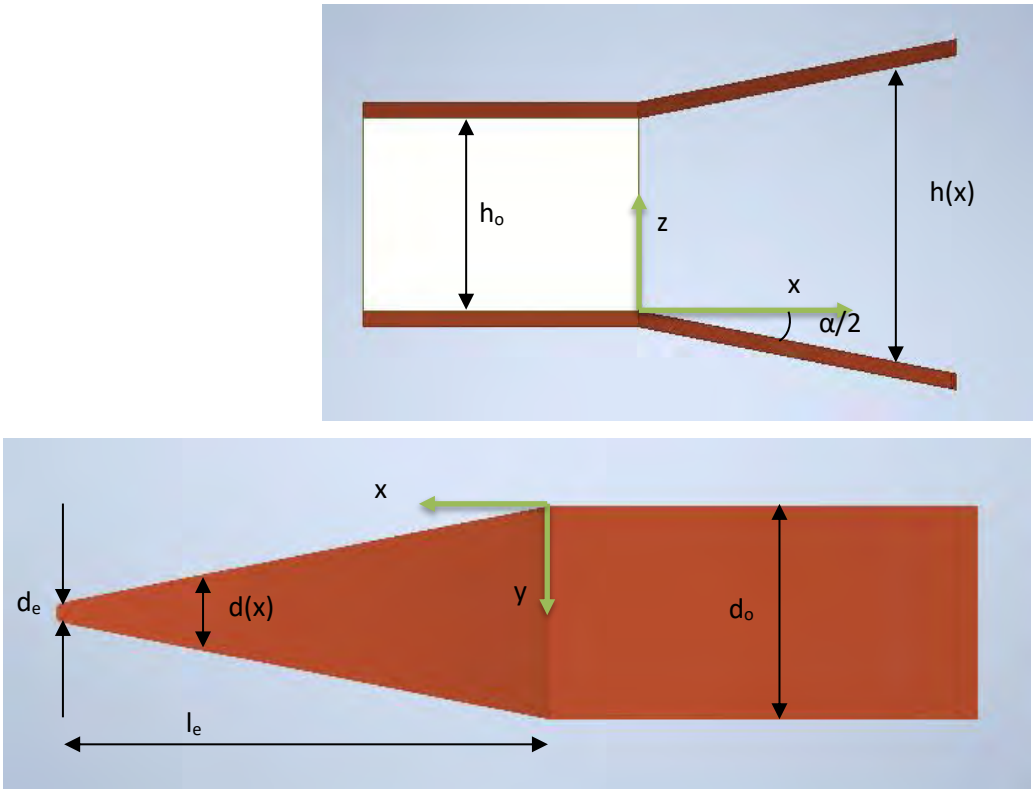

Figure 5.1: Geometry of electrodes

Equation 5: Electrode Gap Equation

$$h(x) = h_o + 2\tan\left(\frac{\alpha}{2}\right)x$$

Equation 6: Electrode Width Equation

$$d(x) = d_o\left(1 - \frac{x}{l_e}\right) + \frac{d_e x}{l_e}$$

5.2 Spark Plug Design

The next iteration of the design focused on designing and integrating the micro-PPT's ignitor. The ignitor is a vital part component of the micro-PPT firing cycle. It is used to create a pilot arc to lower the impedance for the main discharge and create the initial ablation of the Teflon®. The factors that are considered when choosing a spark plug for PPT are the size, weight and required voltage. Most micro-satellites utilised

commercially have spark plugs. For example, Eslava et al. (2014) and Pottinger and Scharlemann (2007) used a Rimfire Micro Viper Z3 (6MM HEX) spark plug for a micro-PPT designed for a CubeSat. *Figure 5.2* shows a Rimfire Micro Viper Z3 spark plug. Typical commercial spark plugs are bulky and heavy and need their own PSU to operate. PocketQubes, already severely limited by size, weight and power compared to a CubeSat, will result in limited payload capacity if a commercial spark plug is used. Therefore, it would be beneficial to design and develop a simplified version of a spark plug for a PocketQube while sacrificing some of the lifetime and reliability that commercially made spark plugs provide.

Figure 5.2: Rimfire Micro Viper Z3 spark plug. Sourced from: NoZipCode

A spark plug is fundamentally two electrodes used to create a controlled pulsed spark. Most spark plugs used in PPT have a cylindrical design with a central high voltage electrode surrounded by a ground connector with a semiconductor material or an air gap (Teflon®). *Figure 5.3* shows a schematic of the spark plug.

Figure 5.3: Schematics of a cylindrical spark plug

During analysis of the designed electrical circuit, it was realised that the cathode could be utilised as the ground for the spark plug. The design also reduced the anode of the spark plug to a single copper wire with a sharpened point. This greatly simplified the micro-PPT design and reduced weight substantially. However, this may sacrifice the

lifetime of the thruster as the spark plug anode electrode may experience erosion muchsooner. The spark plug was designed to be placed 3mm away from the surface of the Teflon®. The ignition circuit was designed to produce 19.8kV or 30kV. This calculates to a maximum spark gap of 6.6mm or 10 mm in an atmospheric environment. The spark plug anode electrode, which consisted of 1.5mm diameter copper wire, was placed 3mm away from the cathode electrode of the thruster.

5.3 Micro-PPT Material Selection

The following sub-section details the material selection process for the electrodes and housing. Each part of the micro-PPT was first analysed, then its material was chosen according to the design requirements and analysis.

1) Electrode: Copper

An analysis of the micro-PPT electrode showed that the material needed to have the following properties:

1) Highly conductive
    - The electrodes needed to be highly conductive because, during the firing cycle, the micro-PPT had to form a high voltage discharge between the two electrodes.
2) High melting point
    - The electrodes needed to have a high melting point as, during the firing cycle, the discharge and ablation of the Teflon® produced plasma and electric discharge resulted in a very high temperature.
3) Low thermal expansion
    - The electrodes needed to have low thermal expansion because due to the high operating temperature and the pulsed operation mode, the heating and cooling of the electrodes might result in thermal expansion.
4) Erosion resistance
    - The electrodes needed to be resistant to the erosion caused by the by-products of the Teflon® ablation process.

Copper was chosen for the PPT's anode and cathode electrodes, as well as the spark plug. This is a popular material for electrodes that have been traditionally used in flight-tested PPT. There have been studies done on the utilisation of copper alloy for the

electrodes, and copper has been shown to provide the best balance of properties and cost (Dali et al., 2008).

2) Housing: 3D printed Ultem 1010

The material for the housing of the micro-PPT needed to have the following properties:

1) High melting point
    - The housing needed to withstand the high temperature resulting from the firing cycle. Failure would result in the destruction of the satellite.
2) Good heat insulator
    - It was important for the housing to be a good heat insulator to minimise the thermal soak-back of the satellite. The thermal soak-back can be caused by the high temperature of the firing cycle (i.e. discharge and thermal expansion of gas)
3) Good electrical insulator and dielectric
    - Good dielectric properties were important as the PPT needed to maximise the electric field produced by the two electrodes. It also needed to be a good electrical insulator as the housing needed to protect the satellite from the high voltage discharge between the two electrodes and prevent the spacecraft from charging.
4) Withstand vacuum environment.
    - The material had to maintain structural integrity in a vacuum environment. Outgassing could cause unwanted arcing between the electrodes which could lead to the destruction of the satellite.

First, before choosing the housing material, the manufacturing process of the housing was considered. To satisfy the design requirements, 3D printing technology was chosen as the preferred method of manufacturing. There are many benefits to using 3D printing technology such as rapid prototyping, affordable price and high accessibility, with a variety of materials and various 3D printing technologies. Although 3D printing has mostly been used for rapid prototyping with ABS and PLA, in recent years 3D printers have moved towards the production of finished products. This has increased the number of high-performance thermoplastics available for 3D printing with the development of FMD printing technology. These are some of the high-performance thermoplastics that were investigated: PEEK, ULTEM 1010 and ULTEM

9085. High-performance thermoplastics can withstand high temperatures, and are highly heat resistant flame resistant, and chemical resistant. They also have high rigidity, high dielectric strength and low thermal conductivity. ULTEM 1010 was chosen out of the other thermoplastics for the following reasons:

- It has a lower thermal expansion than ULTEM 9085
- It has a better chemical resistance than ULTEM 9085 and PEEK
- It offers similar properties to PEEK and PEKK but at a lower cost, for example, €150 per kilo vs €300 per kilo
- It has an easier manufacturing process than PEEK
- It has been used in aerospace components and as electrical housing
- It uses FDM 3D printing technology which has been proven to have 0-5% expected loss of mass in a vacuum environment (Fluitt, 2012)

Additionally, ULTEM 1010 has been used successfully used before as the housing material in an experimental micro-ion thruster which was tested in a vacuum environment (Bretti, 2020). A document on the mechanical properties of ULTEM 1010 can be seen in Appendix C.

5.4 Housing Propellant Feeding Mechanism Analysis

The housing design section contains the details of the final design of the micro-PPT, where there was improved iteration of the design until all the design requirements were satisfied. Once the electrode design parameters were finalised and the housing material selected, the housing structure was designed. The first step of the design was to identify the functions and sections of the housing structure:

The housing structure needed to house the following:

- A simple propellant feeding mechanism which needed to supply the micro-PPT continuously and reliably with the propellant.
- An ignitor area for the copper wire used to start the firing cycle.
- An electrode section to house the anode and cathode which i created the main discharge.
- A propellant section to house the propellant used for plasma creation.
- A robust protective shell to protect the other PocketQube's components from the intense heat from the plasma and the erosion caused by the by-products of

the Teflon® ablation process. It also needed to contain and protect all the parts: the electrode, spark plug and propellant.

5.4.1 Housing and Propellant Feeding Mechanism

This section is focused on the iterations of the design for the propellant feeding system. It was important to find ways to keep the propellant feeding mechanism as simple as possible to meet the design requirements and set goals for the micro-PPT. A simple spring mechanism was chosen for the propellant feed, and this was integrated into the housing structure itself. The spring mechanism was chosen due to its simplicity, which allowed a more compact design and improved the reliability of the micro-PPT because it had few moving parts. A more complex propellant feed mechanism could introduce complications and potential failure during operations. The electrodes together with the propellant were first modelled in order InventorCAD to develop a solution for a possible configuration for the propellant feeding mechanism. The modelled Teflon propellant block had a dimension of 10mmx10mmx10mm. It is important to note that the length of the propellant block can be changed according to the mission's impulse bits requirements and the size restriction of the microsatellite.

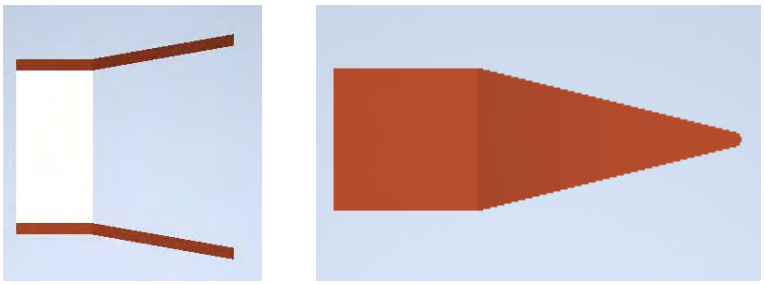

Figure 5.4: CAD model of the micro-PPT's electrodes

After analysing the electrode configuration, the first identified problem was to prevent the components from slipping out. As seen in *Figure 5.4*, the Teflon propellant can easily slide out between the two electrodes from the spring's compressive force. Various configurations of the electrode, propellants and housing were investigated, reviewed and experimented with to find the most feasible and simple solution. The simplest and lowest cost solution was to alter the electrodes and micro-PPT housing shape to form an L-shaped notch. *Figure 5.5* shows an L-shaped notch formed on both electrodes.

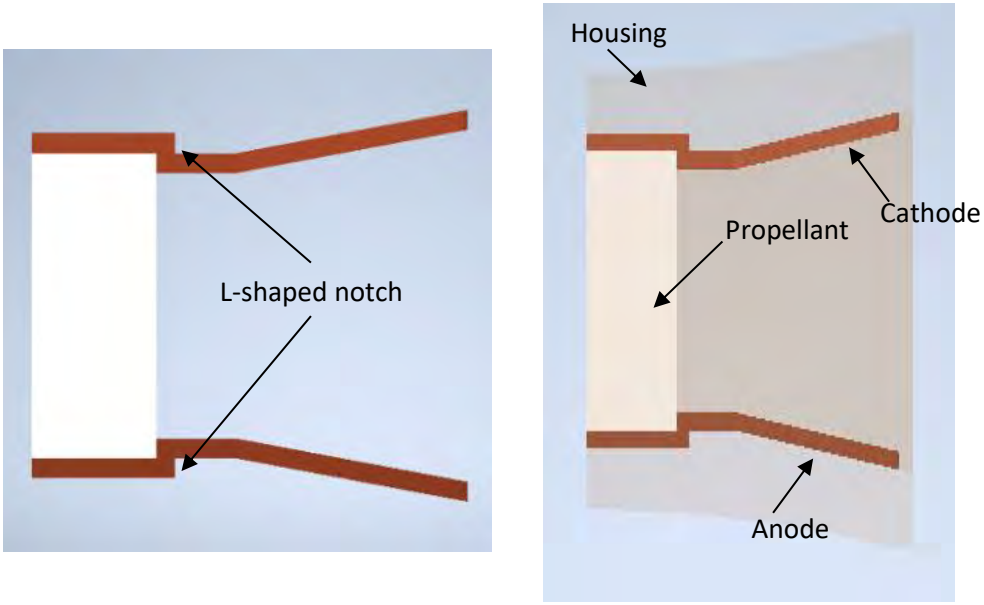

Figure 5.5: CAD model of the micro-PPT's electrodes and housing with an L-shaped notch

The L-shaped notch worked by first using the spring's compressive force on the propellant to compress the propellant bar onto the electrode in the desired position. The housing design had a corresponding L-shaped notch built into it. This allowed the mated L-shaped notch from the electrode and the housing to utilise the spring's compressive force from the propellant to lock the electrodes into the desired position. The utilisation of the spring's compressive force alone greatly helped to simplify and reduce the weight and size of the micro-PPT. *Figure 5.5* shows a general micro-PPT design cadded in Inventor Autodesk with the electrodes, the propellant block and the housing with the L-shaped notch.

Once the general housing was designed for the propellant and electrodes, the spring mechanism was integrated into the back part of the housing. The back part of the housing was designed to be a 5mm plate with a cylindrical node. The node was integrated to ensure the spring position for the propellant feeding mechanism. The back housing was also designed to be assembled onto the front part of the housing with two M2 screws.

5.5 Final Micro-PPT Design

Once the final version of electrodes, spark plug and the propellant feeding mechanism was designed, it was cadded and assembled in AutoCAD Inventor. *Figure 5.6* shows a final design iteration of CAD and assembled micro-PPT. Using Autodesk iProperties, the total weight of the micro-PPT was estimated to be 32.010g excluding the spring and two M2 screws which were just 12% of the PocketQube's weight, thus meeting the weight requirement set out with more than enough left over for the spring and screws. *Table 11* shows a summary of the weights of each part of the micro-PPT. The final size of the micro-PPT came to 50x29x20mm which is 2900mm^3 in volume. This is just 2% of the PocketQube's volume. Therefore, the final micro-PPT design met the size and volume requirement set out in the design requirements. Refer to Appendix B for the technical drawing of the micro-PPT.

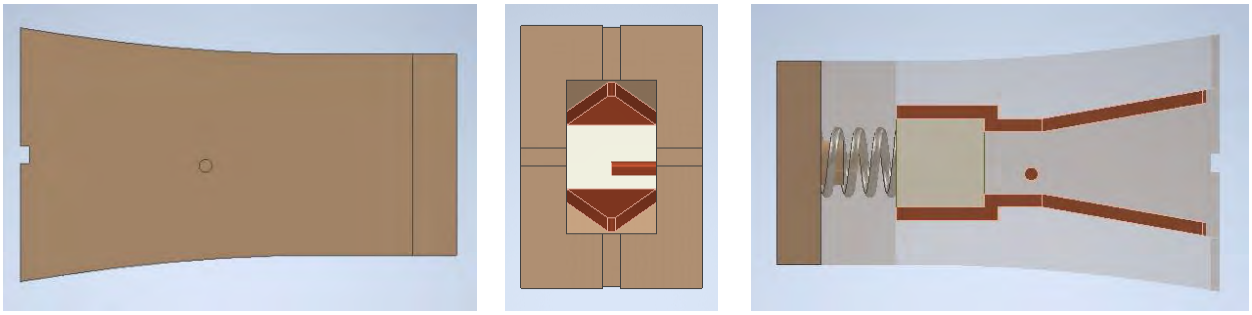

Figure 5.6: Final CAD model of the micro-PPT

Table 11: Weight of the micro-PPT

Part	Estimated Weight (g)
Front Housing	19.417
Back Housing	2.923
Teflon®	2.020
Spark Plug	0.158
Anode Electrode	3.746
Cathode Electrode	3.746
Total Estimated Weight	32.010

6 Development and Assembly

This section contains a detailed development process for the micro-PPT and the circuit. The first subsection details development and assembly of the micro-PPT. This is followed by the development of the PCB design and development of the circuit prototype after atmospheric testing on the breadboard.

6.1 Micro-PPT Assembly

For the experimental part of the dissertation, a modified version of the final micro-PPT design was developed and assembled. The modified version had four mounting legs which were used to mount the micro-PPT onto the micro-pendulum stand. *Figure 6.1* shows the CAD model of a modified version of the micro-PPT thruster.

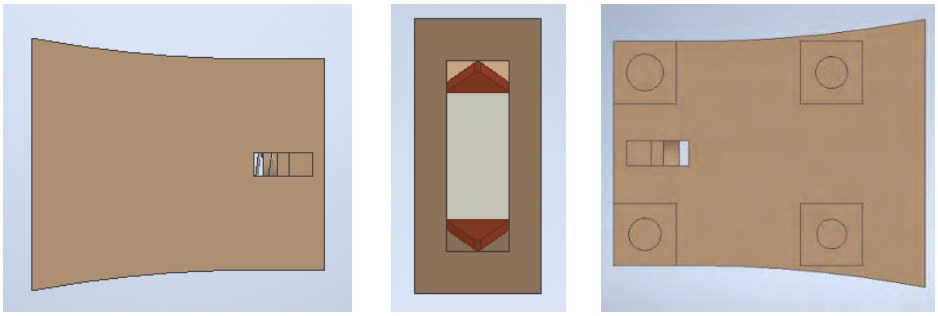

Figure 6.1: CAD model of a modified version of micro-PPT used in the experiments

Using an FDM 3D printer with a solid infill setting, an ULTEM 1010 micro-PPT was 3D printed. The prototype used in the experiment weighed 28g compared to the estimated weight of 33.279g. The 5.279g difference in weight was due to the tiny air gaps left by the 3D printing technique. A transparent version was also printed out using 3D printed with Formlabs High Temp V2 liquid using SLA 3D technology. This was used in the experiments to analyse the plasma plume. Figure 6.2 shows the ULTEM 1010 3D printed version of the modified micro-PPT thruster.

Figure 6.2: Photo of 3D printed micro-PP used in the experiments

The L-shaped notch of the electrodes was made by separating the electrode into two parts: the rectangle base and the tongue-shaped electrode. The electrodes were made from a 1.5mm thick copper sheet. As the electrode parts were very small, it was difficult to manufacture them using a CNC machine, therefore it was cut out by using a Dremel tool and a handsaw. Figure 6.3 shows the dimension of the separate electrode parts cut from the copper sheet. All dimensions were measured using a digital vernier calliper.

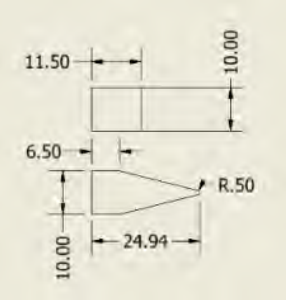

Figure 6.3: Dimension of the electrode cut from the copper sheet.

Once the electrodes parts were cut, the parts were weighed using a scale. The two electrode parts weighed about 7g in total which is about an average of 3.5g each. The tongue-shaped electrode was bent until 10 degrees apart as per the electrode design. After the electrode was weighed and the tongue-shaped electrode bent, the two parts were welded together using a blow torch, soldering wire and soldering flux. The finished electrode weighed 8g for the cathode, the anode and the attached copper wire for circuit connection. *Figure 6.4* shows the anode and cathode electrodes.

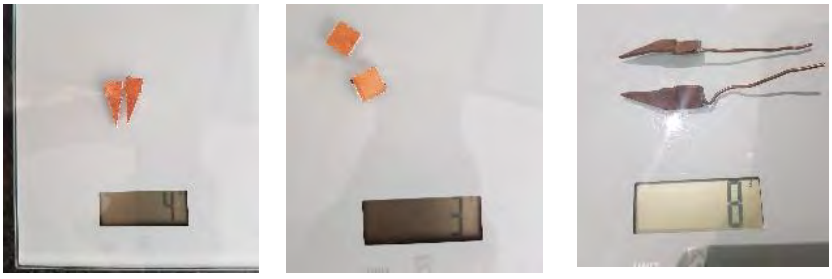

Figure 6.4: Anode and cathode electrode

Once the electrodes and housing were manufactured, the thruster was assembled. A 10mm cube of Teflon® propellant, weighing 2g, was used in the thruster experiment. *Figure 6.5* shows the finished assembled micro-PPT prototype with the propellant block.

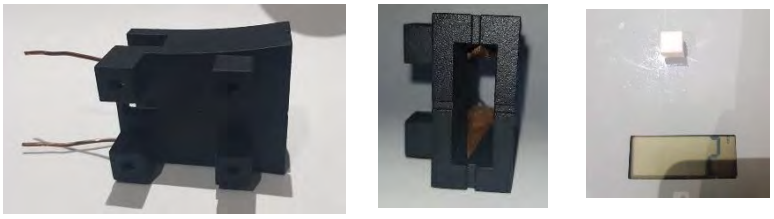

Figure 6.5: Assembled micro-PPT prototype

6.2 Circuit Board Development

Once the circuit and the programming logic were designed and simulated in Proteus, a prototype of the circuit was made on a breadboard. The prototype was made using the specified electronic components in the electric circuit design. However, some of the chosen SMD electronic components such as the resistors were replaced with similar breadboard electronic components. Once the circuit prototype was made, atmospheric testing was conducted on the circuit board's ignition function to ensure no arcs occurred between the components. The circuit was tested in atmospheric conditions at 0.25Hz pulse with an input supply voltage of 3.3V from an Arduino UNO. The 0.25Hz pulse was created using a simple low/high enable program sent to the gate of the SCR from the Arduino UNO with the discharge pulse being 100ms and the charge pulse being 4s. The atmospheric testing showed that the maximum distance between the trigger coil high voltage output wire (anode) and the high voltage ground plate (cathode) was 5mm. Calculations showed that the trigger coil was produced around 15kV for each spark. *Figure 6.6* shows a picture of the breadboard circuit prototype.

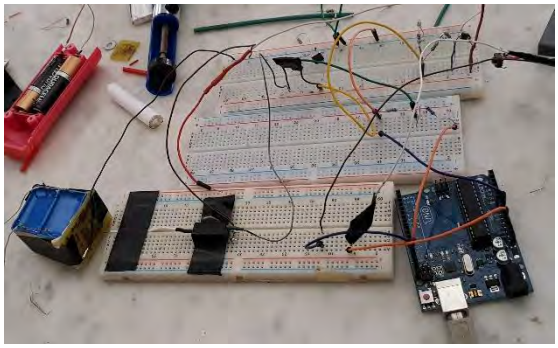

Figure 6.6: Circuit prototype

7 Experimental Setup, Results and Discussion

This section contains details of the experimental setup and results of the previously developed micro-PPT population system. It also contains the discussion of the results used to determine the success of the micro-PPT developed. Additionally, all captured data, plasma discharge and wear and tear of the micro-PPT are included.

7.1 Ultra-Lightweight Micro-Pendulum Test Stand

A micro-pendulum test stand was used to quantify the micro-PPT's impulse bits, in the order of μNs. The success of the micro-PPT design is dependent on the minimum impulse bits used as the standard for which thrusters are compared to each other. Impulse bits in thrusters are a measure of the precision level of the thruster. Lower minimal impulse bits translate to more propellant saving and prolonged life, which saves on cost, size, weight and power. Equipment such as a balanced thrust stand is usually used to quantify impulse bits (μNs). However, specialised equipment is expensive and complex, and is not designed to measure impulse bits for sub-joule propulsion systems (<1J). A study by Aheieva et al. (2016) successfully used an ultra-lightweight pendulum and a high-speed camera to measure impulse bits for a 0.45J vacuum arc thruster. These micro-pendulums are easily constructed and less costly and can roughly quantify impulse bits with reasonable precision. *Equation 7* was used to calculate the impulse bits and thrusts with reference to *Figure 7.1*. Refer to Appendix L for the details on the micro-pendulum test stand.

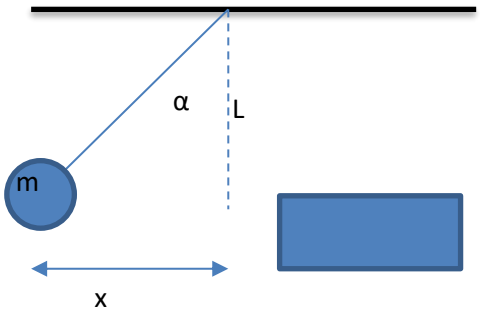

Figure 7.1: Impulse bits of a micro pendulum

Equation 7: Impulse Bit for micro-pendulum

$$I_{bit} = F\Delta t = m_{pend}\sqrt{2g(L - \sqrt{L^2 - x^2}}$$

I_{bit}	Impulse bits (Ns)
F	Thrust (N)
Δt	Time (s)
m_{pend}	Mass of the target mass (kg)
g	Acceleration due to gravity (m/s^2)
L	Length of the pendulum (m)
x	Displacement of the pendulum (m)

7.2 Experiment Setup

The micro-PPT was mounted on the micro-pendulum test stand before being placed in a vacuum chamber. After being placed in the vacuum chamber, the thruster was connected to the hermetically sealed connectors of the vacuum chamber. The vacuum pressure gauge used in the experiment had a measurement range of 0 ~ -760mmHg. The vacuum chamber used in the experiment reached a vacuum pressure reading of -720mmHg. After the vacuum chamber was pumped down to the appropriate vacuum pressure, the circuit was powered on from the Arduino UNO power pin. Once powered and the load switch enabled, the high voltage supply was switched on. Using a simple Arduino program, a 1V trigger pulse was issued to the SCR to start the firing cycle. A high-speed camera was used to record the test. This was placed horizontally to the ground facing the side of the micro-PPT. The micro-PPT was tested and observed for ignition performance for different input voltage, different pulse frequency performance and lifetime. See *Table 12* for the summary of experiment parameters.

Table 12: Summary of experiment parameters

Input Voltage	3.3V/5V
Frequencies	0.25Hz / 0.5Hz
Propellant	Teflon®

7.4 Results and Discussion

An ignition test of 50 shots was done with different input voltages at the initial 0.5Hz. The first ignition test of the micro-PPT was with an input voltage of 3.3V at 0.5Hz. Although the micro-PPT was designed for operation with an input voltage of 3.3V, the micro-PPT operation was unstable, with erratic ignition and many repetitive misfires. After the 50 shots, the frequency was lowered to 0.25Hz and another 50 shots were conducted. The frequency was lowered to try and achieve stable ignition through a longer charge time. However, this did not improve the thruster's ignition performance, with many misfires of the thruster occurring. Upon a closer inspection of the circuit using a multimeter, the main capacitor bank was measured to have an applied voltage of only 940V, which was much lower than the anticipated value of 1.32kV. Therefore, the ECMO high supply unit input and output were not linearly dependent as stated in the manufacturer's datasheet. Thus, due to the lower voltage level, the micro-PPT did not have enough energy in both the main and ignition capacitor bank to achieve a stable and reliable operation with an input voltage of 3V. It was also observed that the Arduino UNO would also occasionally glitch due to the plasma interference.

After the failure at stable operation with the input of 3.3V, the input voltage was increased to 5V. The thruster was tested for ignition reliability, first at 0.25Hz and then at 0.5Hz. The micro-PPT had 120 shots fired at each frequency. The main capacitor bank voltage was also measured with the multimeter and high voltage divider circuit to the correct 2kV. Unlike the unstable operation at 3.3V, the micro-PPT achieved stable operation with 5V at each different frequency. An immediate movement of the micro-pendulum was observed after each trigger pulse, with the flapper falling to the correct position and no misfires. Therefore, the micro-PPT stability and reliability relied on the voltage level of the main and ignition capacitor bank. During the testing of the micro-PPT at each frequency, the operation of the thruster was recorded.

After the tests were conducted, the video was analysed using a physics program called Tracker, which was used to quantify the inclination angles of each shot. After the inclination angle was quantified for each shot fired in the tests, the impulse bits and thrusts were calculated in Excel using the micro-pendulum's known values and equation 7. The results showed that at 0.25Hz frequency, the micro-PPT produced an inclination angle range of 4.2-14.3 degrees, which calculated to a minimum impulse bit of 0.838μN with an average thrust of 0.387 μN. For operation at 0.5Hz, the micro-

PPT was able to produce an inclination angle range of 3.5~10.6 degrees which was calculated to a minimum impulse bit of 0.698μNs with an average thrust of 0.713μN. This showed that the thruster operated best at 0.5Hz as it resulted in the lowest minimum impulse bits and produced the larger average thrust. The enhanced performance of the micro-PPT could be attributed to the operating frequency of 0.5Hz contributing to a higher temperature, which improved the electrothermal operation of the micro-PPT and creation of plasma, thus making the thruster more efficient and precise. *Table 13* shows a summary of the results for micro-PPT operation at different frequencies.

Table 13: Summary of results for micro-PPT performance at different frequencies

Frequency	0.25Hz	0.5Hz
Number of Shots	120	120
Input Voltage	5V	5V
Maximum Main Bank Voltage	2000V	2000V
Maximum Energy per shot	0.272J	0.272J
Min Angle (degrees)	4,2	3,5
Max Angle (degrees)	14,3	10,6
Average I_{bit} (μNs)	1,547	1,426
Max I_{bit} (μNs)	2,930	2,143
Min I_{bit} (μNs)	0,838	0,698
Average Thrust (μN)	0,387	0,713
Max Thrust (μN)	0,732	1,071
Min Thrust (μN)	0,209	0,349

During the test and video analysis, it was also observed that the thruster produced visible plasma plume only at certain shots, with most seen in the operating frequency of 0.5Hz. This might be due to the micro-PPT not ablating enough Teflon®, resulting in lower plasma plume density. and hence less visibility of the plasma plume. However, whether the plasma plume was visible or not, this did not result in a huge difference in inclination angle produced by the micro-PPT. Therefore, the micro-PPT operation did not depend on the ablation of Teflon® to operate. It was also noted during video analysis that there was a clear time delay of 0.01s (1 frame) between the firing and

plasma evolution to the interaction of the micro-pendulum. *Figure 7.2* shows some of the plasma plume formation during the test.

Figure 7.2: Plasma plume of Experiment 1

There is not a lot of research and recorded data available on sub-joule thruster performance. Therefore, the following results were also compared to a PPT in a similar power, size and energy class (Shaw, 2011). The chosen PPT was developed and used on the STRaND-1 3U CubeSat for attitude control. As i can be seen from *Table 14*, despite operating at one-third of the power of the STRaND-1, the micro-PPT prototype had a similar minimum impulse bit, larger than average thrust and faster-operating frequency. This shows that the developed micro-PPT's design was successfully optimised through the iteration design process of simplifying and improving the traditional PPT design. Hence, the micro-PPT performance showed that it could be a viable propulsion solution for a micro-satellite.

Table 14: Comparison of micro-PPT prototype and STRaND-1 PPT

Thruster	Vin (V)	Power (W)	Time (s)	Energy (J)	Min. Impulse Bit (μNs)	Avg. Thrust (μN)
STRaND-1	5	1.5	6	0.19	0.56	0.09
Micro-PPT	5	0.5	2	0.272	0,698	0,713

Next, the lifetime test of the micro-PPT was conducted. This part of the test aimed at helping to quantify the total lifetime of the designed micro-propulsion system. The micro-PPT was operated at the discovered optimised operating frequency of 0.5Hz with an input voltage of 5V. The thruster was operated at the set parameter until operation ceased. The first lifetime test ran a total of 18 minutes with a total of 540 shots. The micro-PPT was able to achieve a stable operation and reliable ignition throughout the test until operation breakdown. The first lifetime test had operation breakdown due to capacitor failure that occurred when the main energy bank blew.

After a search the capacitor's datasheet, the failure of the capacitors could be attributed to it being overdriven with the applied voltage of 2kV. The nominal rated voltage was around 1kV although the capacitors were rated for 2kV. Therefore, for the second lifetime test, the capacitor was replaced in the circuit and the input voltage was dropped to 4V. The micro-PPT was able to achieve stable operation at 0.5Hz with reliable ignition running a total of 40 minutes with 1200 shots fired. However, the operation failed again due to capacitor failure. Thus, it can be concluded that the applied voltage to the capacitor during charge time directly influenced the lifetime of the micro-PPT propulsion system. *Figure 7.3* shows a photo of the failed capacitors.

Figure 7.3: Failed capacitor

Despite the capacitor failure, the thruster was able to produce a total of 1740 shots during lifetime tests. Combined with the shots fired in previous tests, a total of 1980 shots were produced by the micro-PPT propulsion system minus the replacement of the capacitors for the main energy bank. A simple physical examination of the thruster showed that there was also no significant erosion or charring on any of the electrodes and spark plug. Upon a closer inspection, the cathode electrode and the spark plug electrode did have a few black char marks from the area where the ignition would have occurred with a slight erosion occurring at the spark plug electrode's edge. The physical examination of the propellant cube did not show any change in weight or size except a few very shallow lines on the surface where some of the ablations of the Teflon® occurred. Therefore, if the main energy bank's capacitor were to be replaced with a higher reliability pulsed capacitor the micro-PPT lifetime could reasonably be extended as there was no significant damage or erosion to the micro-PPT. See *Figures 7.4* and 7.*5* for before and after photos from physical inspection of the micro-PPT system.

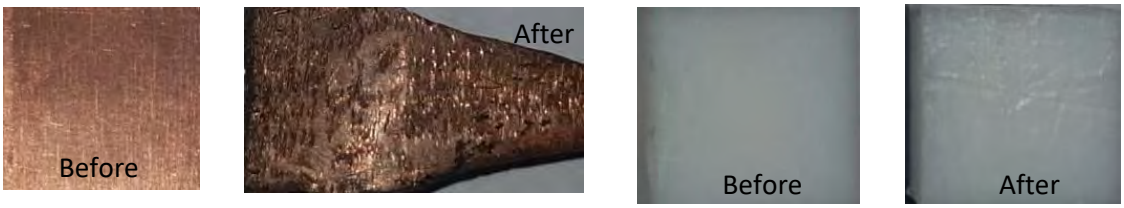

Figure 7.4: Before and after on the cathode electrode and propellant cube

Figure 7.5: Erosion of the spark Plug

8 Conclusion and Future Recommendation

The first generation of a low-cost sub-joule micro-PPT propulsion system for a PocketQube was successfully designed, developed and tested using typical equipment available to students and hobbyists with minimal machining. This was achieved through an iterative design process that focused on simplification and improvement upon the traditional PPT design. The designed and developed micro-PPT was able to achieve a large reduction in the cost, power, weight and size, and met all the design requirements that were set out.

Initial testing of the micro-PPT on a micro-pendulum established that the optimal operating parameter for the micro-PPT propulsion system was at 5V at 0.5Hz. It was discovered during tests that the micro-PPT ignition was erratic with most trigger pulses being of misfires when input voltage was 3.3V due to the lower voltage output than expected. The micro-PPT was able to achieve stable and reliable ignition with no misfires with an input voltage of 5V at both 0.25Hz and 0.5Hz. This showed that the voltage applied to the ignition and main capacitor bank directly influenced the reliability and stability of the micro-PPT operation. There were also larger thrusts and lower minimal impulse bits at 0.5Hz, where the improved performance was attributed to the improved electrothermal efficiency of the micro-PPT through observation of plasma plume.

Afterward, a comparison was made with a PPT that had a similar power, size and energy class. It showed that the micro-PPT's impulse bits and thrusts were found to be within a reasonable range. Compared to a STRaND-1 3U CubeSat, the micro-PPT

performance exceeded the STRaND-1 PPT and it produced a larger thrust and energy per shot with a similar level of precision. However, the reduction in the cost, size, power, weight and simplification of design and manufacturing made it a more compelling propulsion system option for PocketQube than the STRaND-1's PPT.

After the lifetime test, the micro-PPT, to date, was able to fire 1980 shots with no visible indication of significant wear, charring, or erosion of the electrodes and spark plug as well as no significant propellant depletion. However, the key factor limiting the lifetime of the micro-PPT propulsion system was the limiting lifetime of the ignition capacitors. Every lifetime test conducted was terminated due to capacitor failure which was attributed to the capacitors being overdriven. This was evident when the voltage dropped from 5V to 4V at 0.5Hz, and the lifetime increased from 540 shots to 1200 shots. The charging voltage applied during the charging period greatly influenced the lifetime of the capacitor. However, as shown in previous tests, the stability and reliability of the micro-PPT ignition were dependent on the increase of the applied voltage during the charge, while lifetime decreased when applied voltage increased. Therefore, the solution for extending the lifetime would be to find a balance between reliability and lifetime for the micro-PPT.

Future recommendations for the micro-PPT would be to replace the pulse capacitor and find a more reliable one with a higher rated voltage for a more extended lifetime. This would ensure that the micro-PPT has enough room without being overdriven, while maintaining the desired high voltage and energy for successful and reliable ignition of the micro-PPT. Additionally, another capacitor bank could be added to share the load, although at the cost of increased cost, size and weight. Furthermore, additional improvements can be made to the spark plug to enhance the voltage breakdown, reliability and lifetime through improvements to the ignitor profile design, manufacturing process and new ignitor materials.

9 Reference

AHEIEVA, K., TOYODA, K. & CHO, M. 2016. Vacuum Arc Thruster Development and Testing for Micro and Nano Satellites. *TRANSACTIONS OF THE JAPAN SOCIETY FOR AERONAUTICAL AND SPACE SCIENCES, AEROSPACE TECHNOLOGY JAPAN,* 14**,** Pb_91-Pb_97.

ARRINGTON, L., HAAG, T., PENCIL, E. & MECKEL, N. 1998. A Performance Comparison of Pulsed Plasma Thruster Electrode Configurations.

BERNER, J. 2019. Deep Space Network in the CubeSat Era. *IEEE Aerospace and Electronic Systems Magazine,* 34**,** 46-54.

BRETTI, M. 2020. *Applied Ion Systems* [Online]. Applied Ion Systems. Available: https://appliedionsystems.com/on-the-prospects-and-development-of-open-source-electric-propulsion-for-cubesats/ [Accessed 15 February 2020].

CHIGIER, N. & GEMCI, T. 2003. *A Review of Micro Propulsion Technology*.

CLARK, C., GUARDUCCI, F., COLETTI, M. & GABRIEL, S. M. An Off-the-shelf Electric Propulsion System for CubeSats. 2011.

DALI, H., WANSHENG, Z. & XIAOMING, K. 2008. Operation analysis of pulsed plasma thruster. *Acta Astronautica,* 62**,** 404-409.

DUNBAR, B. 2020. In-Space Propulsion. *In:* WESTON, S. (ed.) *State of the Art of Small Spacecraft Technology.* 1 ed. Ames Research Center: Small Spacecraft Systems Virtual Institute.

EDAMITSU, T., ASAKURA, H., MATSUMOTO, A. & TAHARA, H. 2021. Research and Development of a Pulsed Plasma Thruster in Osaka University.

ESLAVA, S., MARCHETTO, J. & SCOUGAL, E. 2014. *Micro-Pulsed Plasma Thruster Design MQP.* Undergraduate, Worcester Polytechnic Institute.

FLUITT, D. 2012. Feasibility Study Into the Use of 3D Printed Materials in CubeSat Flight Missions.

GESSINI, P., HABL, L., BARCELOS, M., FERREIRA, J. L., MARQUES, R. & COLETTI, M. Low Power Ablative Pulsed Plasma Thrusters. 2013.

GOEBEL, D., KATZ, I., ZIEMER, J., BROPHY, J., POLK, J. & JOHNSON, L. 2005. Electric Propulsion Research and Development at JPL.

GUMAN, W. & PEKO, P. 1968. Solid-propellant pulsed plasma microthruster studies. *Journal of Spacecraft and Rockets - J SPACECRAFT ROCKET,* 5**,** 732-733.

HUANG, T., WU, Z., LIU, X., XIE, K., WANG, N. & CHENG, Y. 2015. Study of breakdown in an ablative pulsed plasma thruster. *Physics of Plasmas,* 22**,** 103511.

JAHN, R. & CHOUEIRI, E. 2003. Electric Propulsion.

JOHNSON, I. K. 2011. *The Development of a Pulsed Plasma Thruster as a Solid Fuel Plasma Source for a High Power Helicon.* Master of Science Research, The University of Washington.

KRAFT, M. & WHITE, N. 2013. *Mems for Automotive and Aerospace Applications*.

LAL, B., BLANCO, E., BEHRENS, J., CORBIN, B., GREEN, E., PICARD, A. & BALAKRISHNAN, A. 2017. *Global Trends in Small Satellites*.

MANZELLA, D. 2007. Low Cost Electric Propulsion Thruster for Deep Space Robotic Missions.

MICCI, M. & KETSDEVER, A. 2000. Micropropulsion for Small Spacecraft. *Prog Astronaut Aeronaut*.

MINGO PÉREZ, A., COLETTI, M. & GABRIEL, S. B. 2011. Development of a Microthruster Module for Nanosatellite Applications. *32nd International Electric Propulsion Conference.* Wiesbaden, Germany.

MIYASAKA, T., ASATO, K., SAKAGUCHI, N. & ITO, K. 2013. Optical measurements of unsteady phenomena on coaxial pulsed plasma thrusters. *Vacuum,* 88**,** 52–57.

PALUMBO, D. & GUMAN, W. 1976. Effects of Propellant and Electrode Geometry on Pulsed Ablative Plasma Thruster Performance. *Journal of Spacecraft and Rockets,* 13**,** 163.

PATEL, A. 2015. *Magnetically Levitating Low-Friction Test Stand for the Evaluation of Micro-Thrusters.* M.Sc., The University of Alabama.

PENCIL, E. & KAMHAWI, H. 2003. *Alternate Propellants Evaluation for 100-Joule-Class Pulsed Plasma Thrusters*.

POTTINGER, S. & SCHARLEMANN, C. 2007. Micro Pulsed Plasma Thruster Development. *The 30th International Electric Propulsion Conference.* Florence: Space Propulsion & Advanced Concepts.

RYSANEK, F. & BURTON, R. 2001. Performance and Heat Loss of a Coaxial Teflon Pulsed Plasma Thruster.

SCHARLEMANN, C. & YORK, T. 2002. *Alternative Propellants for Pulsed Plasma Thruster*.

SCHÖNHERR, T., NAWAZ, A., HERDRICH, G., RÖSER, H.-P. & AUWETER-KURTZ, M. 2009. Influence of Electrode Shape on Performance of Pulsed Magnetoplasmadynamic Thruster SIMP-LEX. *Journal of Propulsion and Power,* 25**,** 380-386.

SHAW, P. 2011. *Pulsed Plasma Thrusters for Small Satellites.* Ph.D, University of Surrey.

SHIROMA, W., MARTIN, L., AKAGI, J., AKAGI, J., WOLFE, B., FEWELL, B. & OHTA, A. 2011. CubeSats: A bright future for nanosatellites. *Open Engineering,* 1**,** 9-15.

SUTTON, G. P. 1992. *Rocket propulsion elements - An introduction to the engineering of rockets (6th revised and enlarged edition)*.

VONDRA, R. J. & THOMASSEN, K. I. 1974. Flight Qualified Pulsed Electric Thruster for Satellite Control. *Journal of Spacecraft and Rockets,* 11**,** 613-617.

WIE, B. & MURPHY, D. 2005. MicroPPT-Based Secondary/Backup ACS for a 160-m, 450-kg Solar Sail Spacecraft.

WU, J., ZHANG, Y., CHENG, Y., HUANG, Q., LI, J. & ZHU, X. 2018. Plasma Generation and Application in a Laser Ablation Pulsed Plasma Thruster.

ZHE, Z., REN, J., TANG, H.-B., LING, W. & YORK, T. 2017. An ablative pulsed plasma thruster with a segmented anode. *Plasma Sources Science and Technology,* 27.

ZIEMER, J. & CHOUEIRI, E. 2001. Scaling laws for electromagnetic pulsed plasma thrusters. *Plasma Sources Science and Technology,* 10**,** 395.

Appendix A - PocketQube standards

The PocketQube Standard

Issue 1

7th of June, 2018

Contributors:

Organization Name	Authors	Reviewers
TU Delft	S. Radu	S. Radu
TU Delft	M.S. Uludag	M.S. Uludag
TU Delft	S. Speretta	S. Speretta
TU Delft	J. Bouwmeester	J. Bouwmeester
TU Delft	-	A. Menicucci
TU Delft	-	A. Cervone
Alba Orbital	A. Dunn	A. Dunn
Alba Orbital	T. Walkinshaw	T. Walkinshaw
Gauss Srl	P.L. Kaled Da Cas	P.L. Kaled Da Cas
Gauss Srl	C. Cappelletti	C. Cappelletti
Gauss Srl	-	F. Graziani

Important Note(s): The latest version of the PocketQube Standard shall be the official version.

Contents

1. Introduction 4

1.1 Purpose 4

2. PocketQube Specification 4

1.2 General requirements 5

2.2 Mechanical Requirements 5

2.2.1 Exterior dimensions 7

2.2.2 Mass 10

2.2.3 Materials 10

2.3 Electrical Requirements 11

2.4 Operational Requirements 11

2.5 Testing Requirements 11

2. Annexe 1 12

4. References 14

5. Contacts 14

Figure 1 CAD representation of a typical PocketQube 4

Figure 2 PocketQube Exterior Dimensions and Form Factor 6

Figure 3 PocketQube Axis Specification 7

Figure 4 Sliding backplate rail clamping 7

Figure 5 Components Envelope and Allowable Additional Envelope for Deployables 9

Figure 6 Contact Surface (red) Kill Switches location (green) options 9

Figure 7 Contact surface (hashed area) 10

Table 1. PocketQube external dimensions and sliding backplate dimensions for different number of units: 5

Table 2. Contacts: 14

List of Acronyms	
TU Delft	Delft University of Technology
TML	Total Mass Loss
CVCM	Collected Volatile Condensable Material
COTS	Commercial off-the-shelf
GAUSS	Group of Astrodynamics for the Use of Space Systems
MRFOD	Morehead Rome Femtosatellite Orbital Deployer
MSU	Morehead State University
LSP	Launch Service Provider

1. Introduction

The PocketQube concept (Figure 1) was first proposed in 2009, from an idea of professor Robert J. Twiggs, as a result of a collaboration between Morehead State University (MSU) and Kentucky Space which developed some specifications with respect to this new class of spacecraft [1,2]. These specifications were stipulated in order to help universities in performing space applications using this type of platform. The PocketQubes are a cube shaped platform of 50x50 mm with a mass of no more than 250 g for which typically COTS electronics are used. The first PocketQube was launched using the MRFOD (Morehead Rome Femto Orbital Deployer) installed inside the UniSat-5 microsatellite as a result of a cooperation between Morehead State University GAUSS Srl and Kentucky Space [1,2].

1.1 Purpose

This document aims to present a PocketQube Mechanical Standard which follows from a collaboration between Alba Orbital, Delft University of Technology and GAUSS Srl. This action started due to a need to converge towards common standards and interfaces for the PocketQube platform, in order to avoid uncertainties and allow the community to grow, starting from the same, shared standard. The aim is that for the next revisions, the standard would be extended to electrical, operational and testing requirements.

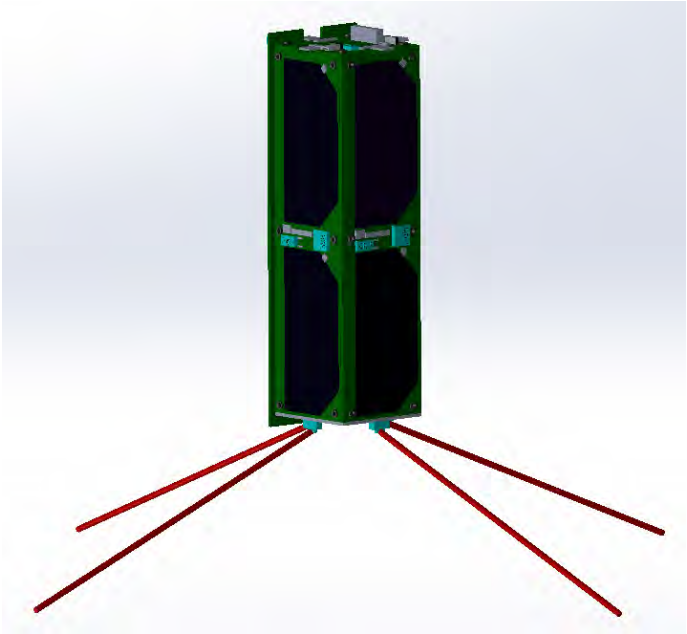

Figure 1 CAD representation of a typical PocketQube

The purpose of this standard is to facilitate the development of PocketQubes in the same way as the CubeSat Standard [3] facilitated the design and development of CubeSats in their infancy. The aim is also to enlarge the community and increase the overall access to space opportunities for this new type of satellite platform.

2. PocketQube Specification

This section presents basic general requirements that shall be applied on all PocketQubes in accordance with the Launch Service Provider as well as all mechanical dimensions.

2.1 General requirements

PQ-Gen-01: The PocketQube shall ensure no deliberate detachment of any components throughout the lifetime of the entire mission: launch, ejection and in orbit operation.
Rationale: This is a safety precaution.

PQ-Gen-02: Pyrotechnics shall not be allowed on board.
Rationale: This is a safety precaution.

PQ-Gen-03: Materials that can be toxic, flammable or potentially hazardous shall not be used. The use of Li-Ion batteries is exempted from this constraint, provided that there is adequate prevention against thermal runaway.
Rationale: This is a safety precaution for both the people handling the satellite and the other payloads. The launch service provider might ask for additional tests in order to prove that your system is capable of handling the thermal runaway.

PQ-Gen-04: The PocketQube shall meet the out-gassing requirement in order to prevent contamination of any other spacecraft during integration, testing and launch:

- TML ≤1.0%
- CVCM ≤0.1%

Rationale: This is a general requirement for space systems outgassing criteria as per ECSS-Q-70-02C [4].

2.2 Mechanical Requirements

PocketQubes are picosatellite platforms based on a cubic-shaped form factor (approximately 50x50x50 mm per unit) with each side one half smaller than a CubeSat (100x100x100 mm per unit). The external dimensions and features are outlined in Figure 2.

Unlike the CubeSat Standard [3] that is deployed along its long-side edges, the PocketQube uses a sliding backplate for ejection (visible in the 3D CAD in Figure 1), thus one side of the platform has slightly different dimensions as better outlined in Figure 2 and in Table 1 in the sliding backplate column.

PocketQubes external dimensions are slightly different depending on the number of units, as outlined in Table 1 for the 1P, 2P and 3P cases:

Table 1. PocketQube external dimensions and sliding backplate dimensions for different number of units:

Number of Units (P)	External dimensions without backplate (mm)	Sliding backplate dimension (mm)
1P	50x50x50	58x64x1.6
2P	50x50x114	58x128x1.6
3P	50x50x178	58x192x1.6

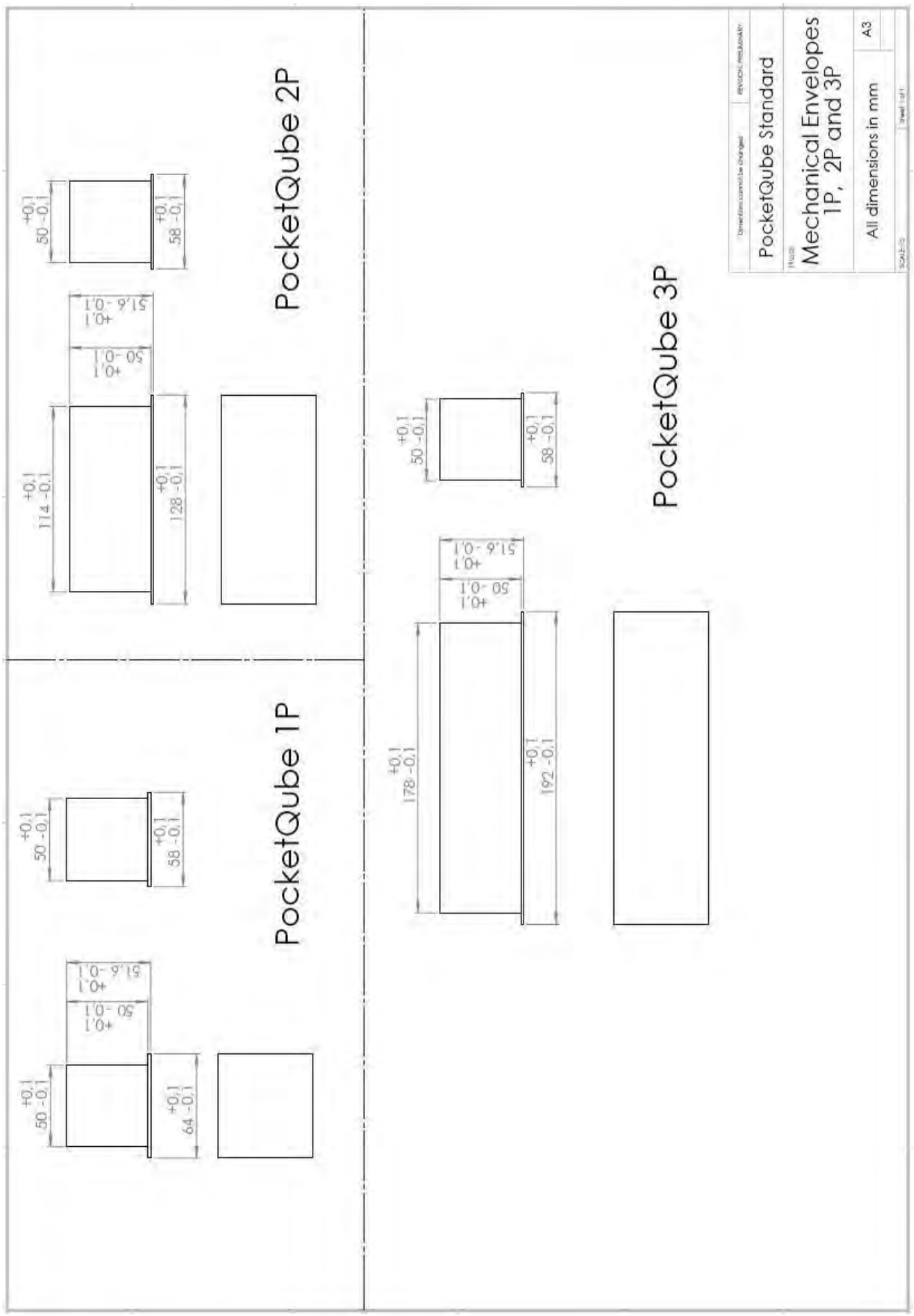

Figure 2 PocketQube Exterior Dimensions and Form Factor

2.2.1 Exterior dimensions

The axis and sides conventional nomenclature used while defining the requirements in this document are as shown in Figure 3.

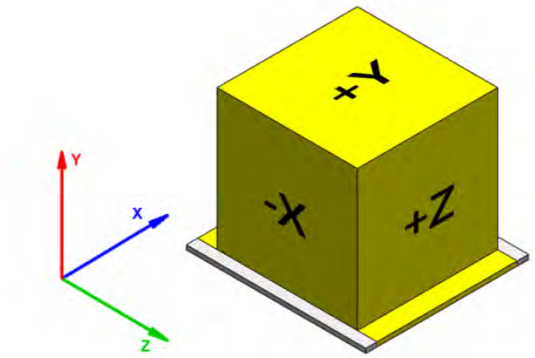

Figure 3 PocketQube Axis Specification

PQ-Mech-01: The PocketQube configuration and dimensions shall be in accordance with Figure 2.

PQ-Mech-02: A 1P PocketQube shall be 51.6±0.1 mm wide (Y dimensions as seen in Figure 2). This comprises 50.0 mm + 1.6 mm the thickness of the sliding plate.

PQ-Mech-03: A 1P PocketQube shall be 50.0±0.1 mm wide (X dimensions as seen in Figure 2) with sliding plate of 58.0±0.1 mm in the same direction.

PQ-Mech-04: A 1P PocketQube shall be 50.0±0.1 mm long (Z dimensions as seen in Figure 2) with sliding plate dimensions of 64.0 ±0.1 mm in the same direction.

PQ-Mech-05: A 2P PocketQube shall be 114.0±0.1 mm long (Z dimensions as seen in Figure 2) with sliding plate dimensions of 128.0±0.1 mm in the same direction.

PQ-Mech-06: A 3P PocketQube shall be 178.0±0.1 mm long (Z dimensions as seen in Figure 2) with sliding plate dimensions of 192.0±0.1 mm in the same direction.

PQ-Mech-07: The rail clamping dimensions shall be of 2 mm on each side of the sliding backplate as it can be seen in Figure 4 and in Figure 5. Please notice that the maximum envelope does not apply to the sliding backplate sides that are placed within the rail clamp (as seen in Figure 5).
Rationale: In order to allow the satellite to slide into the deployer, an empty area should be left for clamping.

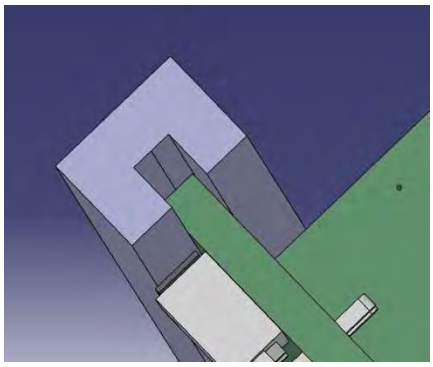

Figure 4 Sliding backplate rail clamping

PQ-Mech-08: The envelope around the PocketQube shall be no more than 7 mm for components. For appendages and deployables, maximum 10 mm is allowed if the Launch Service Provider can adapt to this requirement (as shown in Figure 5, in which the area of maximum appendages envelope is hashed differently). This procedure implies completing the waiver form attached in Annexe 1, which also includes a table and drawing with the relevant dimensions that cannot be exceeded.
Rationale: The envelope is 7 mm, however the waiver of 10 mm maximum envelope was accepted for the PocketQubes that have deployables (panels, GPS antennas, etc) assuming a Launch Service Provider can allow a bigger envelope.

PQ-Mech-09: All deployable components shall be constrained by the PocketQube and not by the deployer.

PQ-Mech-10: The minimum contact surface of the PocketQube backplate shall be 21.5 mm from both sides on the Z+ axis, as seen in Figure 6, the red area.
Rationale: Contact surface means either between satellite and pusher plate or between two satellites assuming they are stacked upon each other. This contact surface is required in order to make sure the kill switches are pressed.

PQ-Mech-11: The contact surface between the PocketQube and pusher plate or between two stacked PocketQubes shall be as outlined in Figure 7.

PQ-Mech-12: All PocketQubes shall use at least two kill switches to keep the satellite offline while in deployer.
Rationale: This is a safety precaution to assure the satellite is turned off while in the deployer.

PQ-Mech-13: The PocketQube kill switches shall make contact with the deployer rail or with another PocketQube (see green and blue surfaces from Figure 6).

PQ-Mech-14: Kill switches shall be located only on Z- axis. There are two different possible placement areas:

a) In the lateral side of the satellite within 20 mm from the Z- faces and touching the deployment rails (as shown in Figure 6, lateral green area);
b) Aligned with the sliding backplate in Z- face and in contact with the PocketQube below or the pusher plate (as shown in Figure 6, blue area).

PQ-Mech-15: The kill switches (Figure 6) shall not obstruct ejection of the satellite from the deployer.

Rationale: Depending on the direction of the kill switches force, pressure against deployment can be an issue.

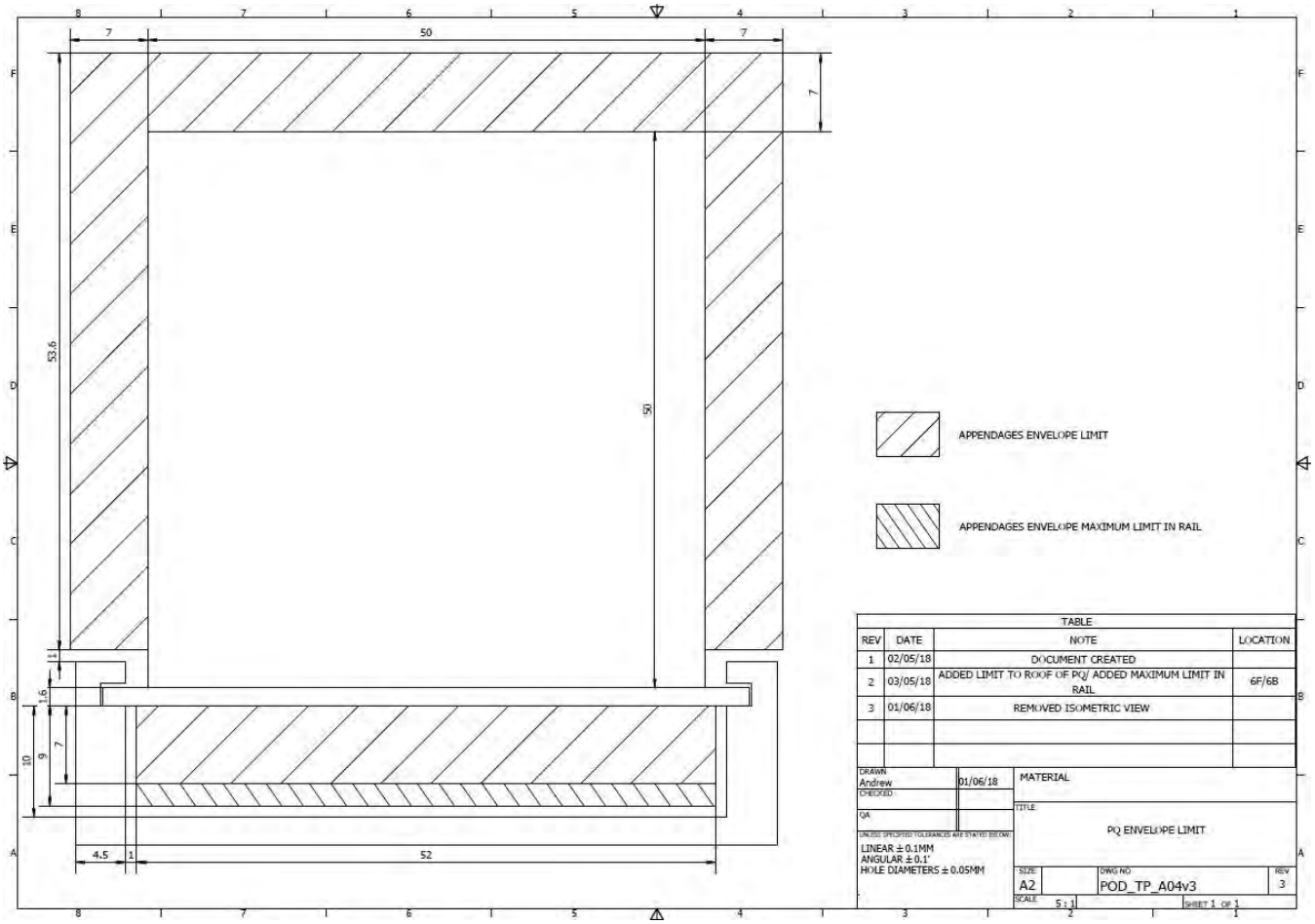

Figure 5 Components Envelope and Allowable Additional Envelope for Deployables

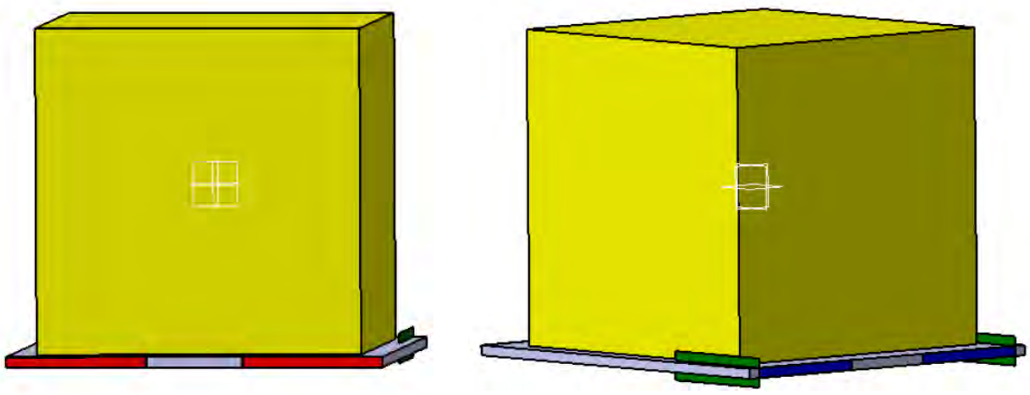

Figure 6 Contact Surface (red) Kill Switches location (green) options

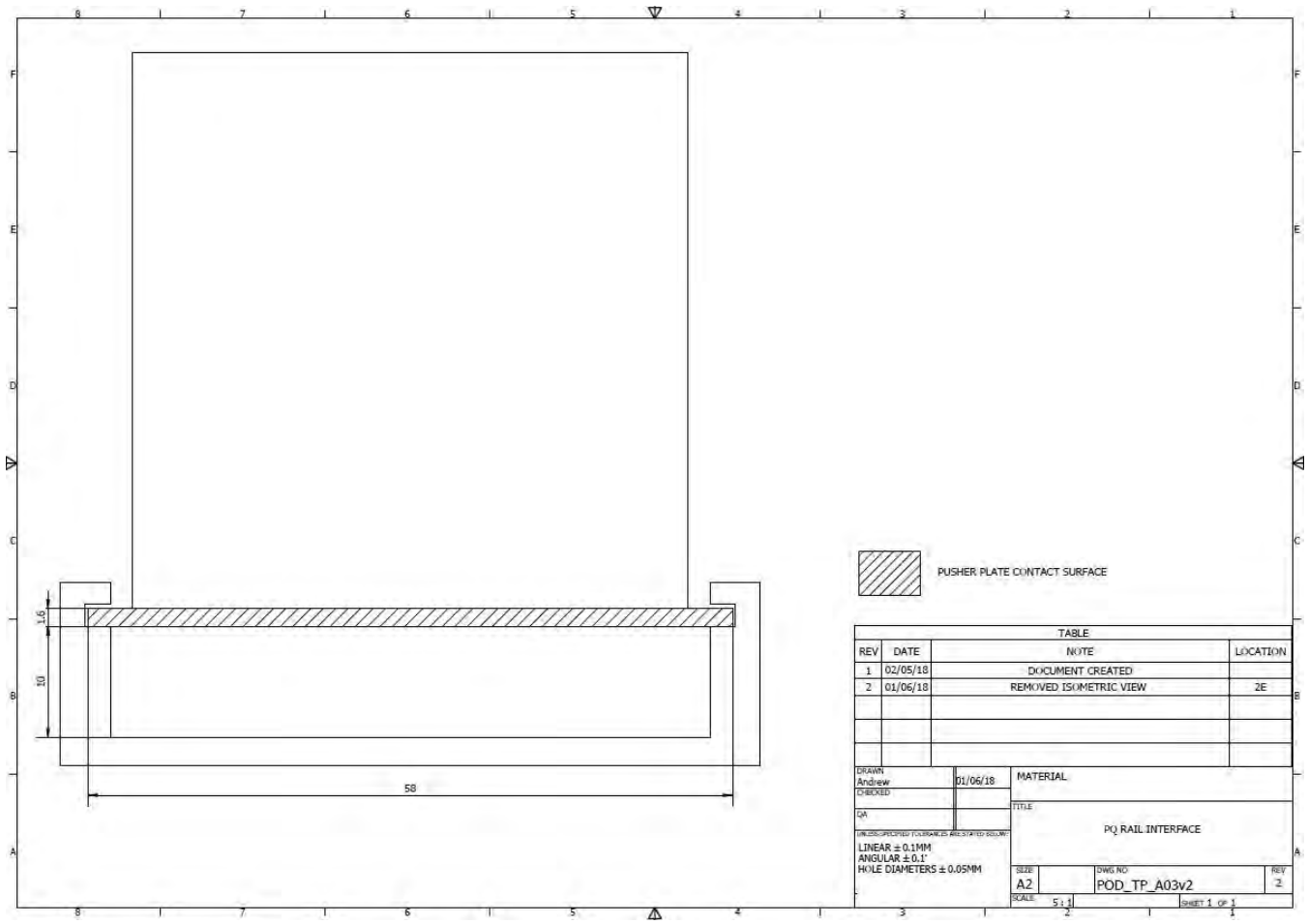

Figure 7 Contact surface (hashed area)

2.2.2 Mass

PQ-Mass-01: Each PocketQube unit (1P) shall not exceed 250 g mass.

PQ-Mass-02: Each 2P PocketQube shall not exceed 500 g mass.

PQ-Mass-03: Each 3P PocketQube shall not exceed 750 g mass.

Rationale: 1P PocketQube represents in volume one-eighth of a CubeSat. Due to the higher density of subsystems in a PocketQube, 1P shall not exceed 250 g.

PQ-Mass-04: The centre of mass of the PocketQube shall not exceed 1 cm from its geometric centre in stowed position.

Rationale: This requirement ensures the launch is safe and not jamming other payloads preventing clashes that might cause a debris.

2.2.3 Materials

PQ-Mat-01: Any structural material used for the PocketQube shall be able to withstand all required environmental tests.

PQ-Mat-02: Recommended materials for the baseplate are: FR4, Aluminium (7075,6061,6065,6082) as described in [5].

PQ-Mat-03: Potential metallic materials used for the PocketQube that are in contact with the deployer and standoffs shall be hard anodized.

Rationale: All aluminium materials specified in requirement PQ-Mat-02 that are in contact with the deployer shall be hard anodized in order to prevent cold welding.

PQ-Mat-04: For any other materials which are not specified in requirement PQ-Mat-02, the PocketQube developer shall contact the Launch Service Provider.

2.3 Electrical Requirements

To be continued in the 2nd issue. For information with respect to the electrical requirements, please contact your LSP.

2.4 Operational Requirements

To be continued in the 2nd issue. For information with respect to the operational requirements, please contact your LSP.

2.5 Testing Requirements

To be continued in the 2nd issue. For information with respect to the testing requirements, please contact your LSP.

3. Annexe 1

The PocketQube envelope waiver form

Contact _____

Contact email _____

Contact phone _____

Company/Organisation _____

PocketQube satellite _____

I acknowledge and accept that the appendages and deployable mechanisms exceed the 7 mm envelope limit which is specified in the PocketQube standard. I understand that our appendages and deployables must not exceed the 10 mm limit which is a requirement for deployers with larger envelopes.

I agree to disclose the details of the appendages and deployable mechanisms of the satellite to the launch provider in order to determine the suitability of our satellite for integrating into the <INSERT POD NAME> deployer.

Signature: _____ Date:_____/_____/_____

Print Name: _____

Refer to the figure and table below for the maximum envelope of the appendages mechanisms. If you require assistance in defining the interface between the PocketQube and the POD, contact your deployer provider.

Mechanical standard maximum envelope			Maximum envelope for larger PODs (intended for PocketQubes that require a larger envelope as per req. no PQ-Mech-08)	
Location	Max X (mm)	Max Y (mm)	Max X (mm)	Max Y (mm)
A	7	53.6	10	53.6
B	7	53.6	10	53.6
C	50	7	50	7
D	54	7	54	9

Mechanical limits:

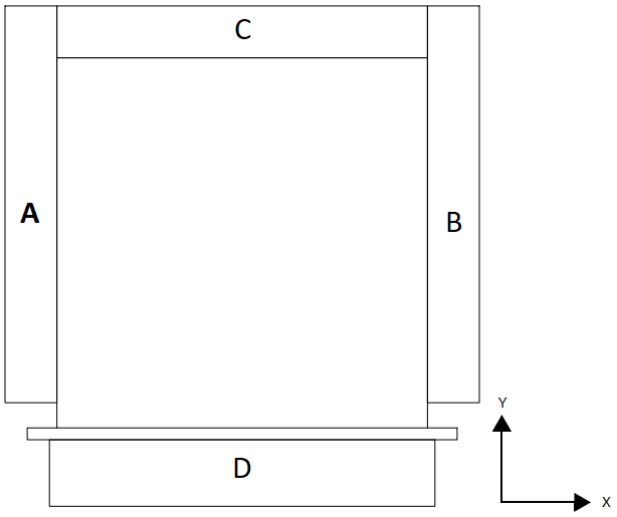

4. References

[1] “Small Launch Platforms for Microsatellites” – Cappelletti, Chantal and Battistini, Simone and Graziani, Filippo; Advances in Space Research;

[2] Cappelletti, C., 2018. Femto, pico, nano: overview of new satellite standards and applications. In: Advances in Astronautical Sciences, Proceedings of the 4th IAA Conference on University Satellite Missions and CubeSat Workshop, vol. 163, pp. 503–510;

[3] CubeSat Design Specification (CDS) revision 9, 3rd of June 2004;

[4] ECSS-Q-70-02C, 15th of November 2008 – Space Product Assurance, Thermal vacuum outgassing test for screening of space materials;

[5] ECSS-Q-ST-70-36C, 6th of March 2009 – Space Product Assurance, Material selection for controlling stress-corrosion cracking.

5. Contacts

For any additional questions with respect to the standard, please contact one of the following people:

Table 2. Contacts:

No.	Partner	Name	E-mail
1.	Alba Orbital	Andrew Dunn	andrew@pocketqubeshop.com
2.	Alba Orbital	Tom Walkinshaw	tom@pocketqubeshop.com
3.	TU Delft	Silvana Radu	s.radu@tudelft.nl
4.	TU Delft	Sevket Mehmet Uludag	m.s.uludag@tudelft.nl
5.	TU Delft	Jasper Bouwmeester	jasper.bouwmeester@tudelft.nl
6.	GAUSS Srl	Chantal Cappelletti	chantal.cappelletti@gaussteam.com
7.	GAUSS Srl	Pedro Luiz Kaled Da Cas	pedrokdc@gmail.com
8.	GAUSS Srl	Filippo Graziani	Filippo.graziani@gaussteam.com

Appendix B – Technical Drawings

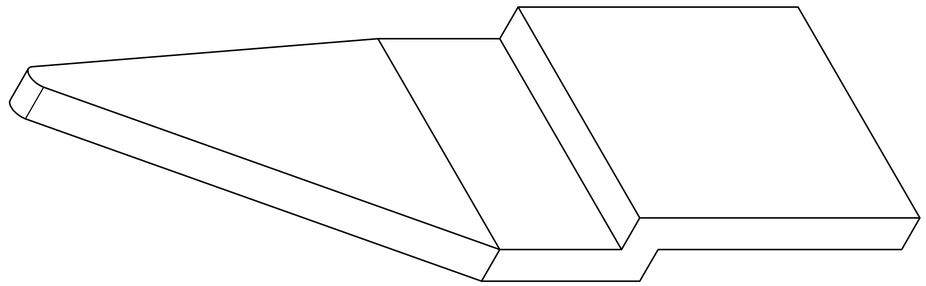

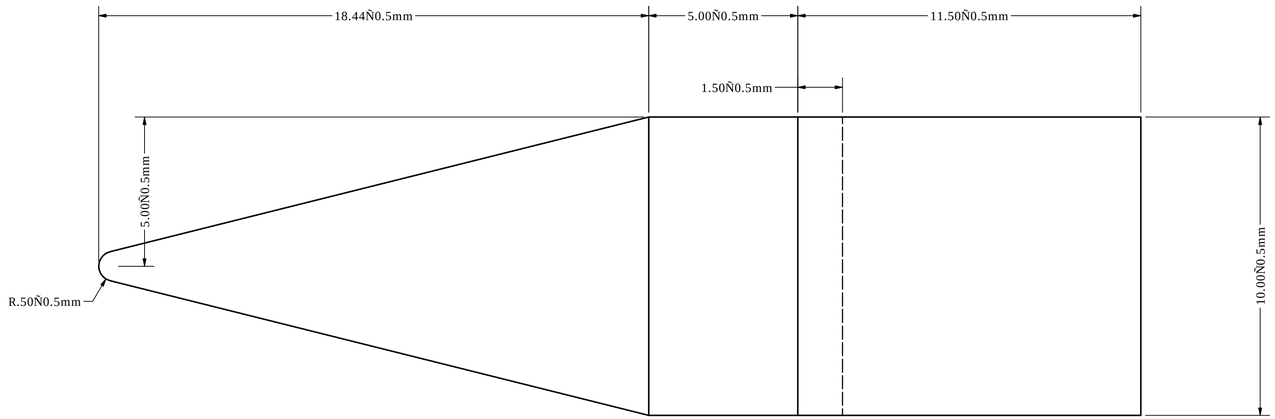

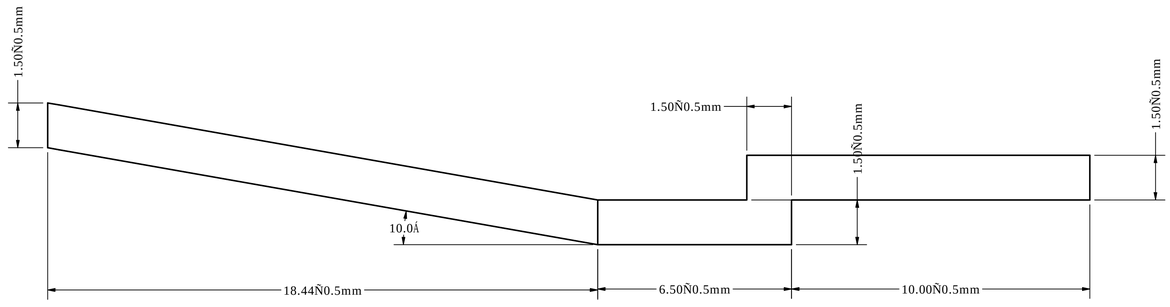

DRAWN J Bae	2021/03/01	Nelson Mandela University
CHECKED		TITLE: Micro-PPT Electrode
QA		
MFG		
APPROVED		
		SIZE D · DWG NO electrodes · REV
		SCALE 10:1 · SHEET 1 OF 1

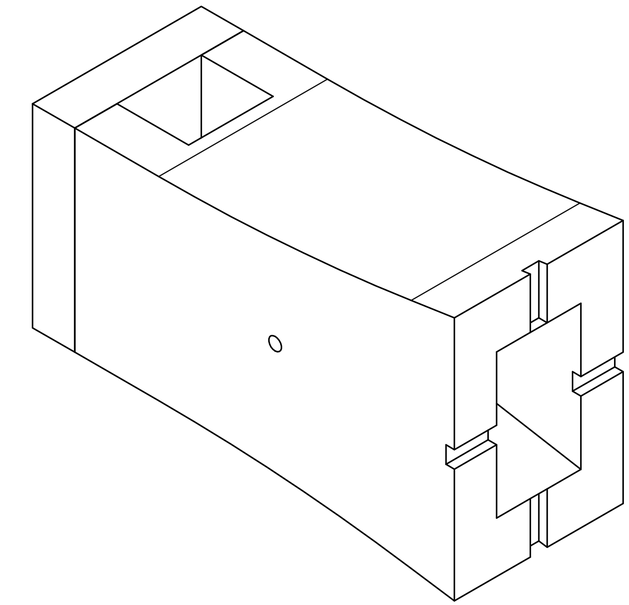

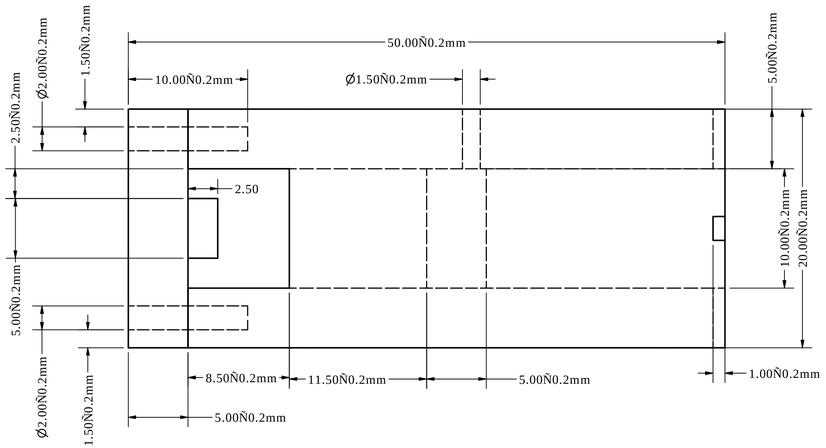

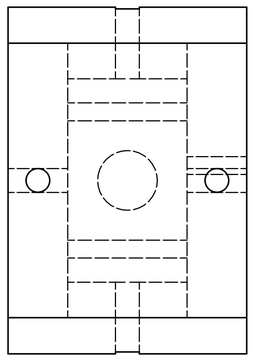

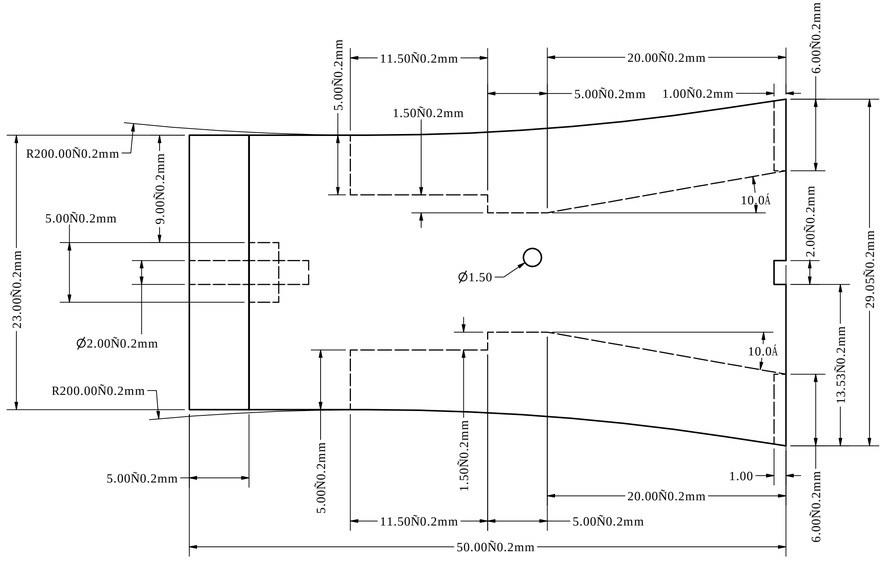

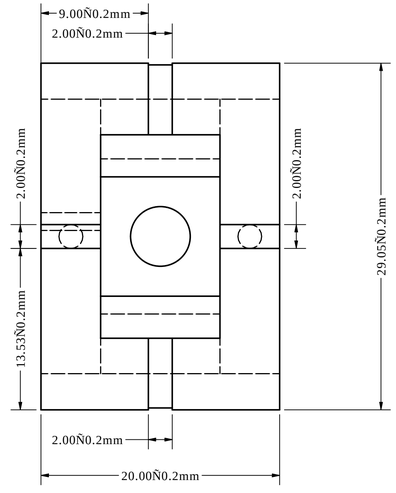

DRAWN J. Bae	2021/03/01	Nelson Mandela University
CHECKED		TITLE: PocketQube Micro-PPT
QA		
MFG		
APPROVED		SIZE: D; DWG NO: assembled housing; REV
		SCALE: 4 : 1; SHEET 1 OF 1

Appendix C – Ultem 1010 Datasheet

ULTEM 1010 Resin

ULTEM™ 1010 resin is a high-performance FDM® thermoplastic that offers excellent strength, thermal stability and the ability to withstand steam autoclaving. ULTEM 1010 resin is available in a general-purpose grade as well as a certified grade (CG) for those customers who want to take advantage of food-contact certification for special applications including food production tools and custom medical applications. ULTEM 1010 resin offers the highest heat resistance, chemical resistance and tensile strength of any FDM thermoplastic and is ideal for aerospace and automotive applications.

Mechanical Properties[1]	Test Method	Value	
		XZ Orientation	ZX Orientation
Tensile Strength, Yield (Type 1, 0.125", 0.2"/min)	ASTM D638	64 MPa (9,300 psi)	41 MPa (5,990 psi)
Tensile Strength, Ultimate (Type 1, 0.125", 0.2"/min)	ASTM D638	81 MPa (11,700 psi)	48 MPa (7,000 psi)
Tensile Modulus (Type 1, 0.125", 0.2"/min)	ASTM D638	2,770 MPa (402,000 psi)	2,200 MPa (322,000 psi)
Tensile Elongation at Break (Type 1, 0.125", 0.2"/min)	ASTM D638	3.3%	2.0%
Tensile Elongation at Yield (Type 1, 0.125", 0.2"/min)	ASTM D638	2.2%	1.5%
Flexural Strength (Method 1, 0.05"/min)	ASTM D790	144 MPa (21,000 psi)	77 MPa (11,100 psi)
Flexural Modulus (Method 1, 0.05"/min)	ASTM D790	2,820 MPa (409,000 psi)	2,230 MPa (324,000 psi)
Flexural Strain at Break (Method 1, 0.05"/min)	ASTM D790	No break	3.5%
IZOD Impact, notched (Method A, 23 °C)	ASTM D256	41 J/m (0.8 ft-lb/in)	24 J/m (0.4 ft-lb/in)
IZOD Impact, un-notched (Method A, 23 °C)	ASTM D256	326 J/m (6.1 ft-lb/in)	138 J/m (2.6 ft-lb/in)
Compressive Strength, Yield (Method 1, 0.05"/min)	ASTM D695	134 MPa (19,500 psi)	107 MPa (15,100 psi)
Compressive Strength, Ultimate (Method 1, 0.05"/min)	ASTM D695	No break	1,125 MPa (15,500 psi)
Compressive Modulus (Method 1, 0.05"/min)	ASTM D695	10,000 MPa (1,450,000 psi)	1,120 MPa (305,000 psi)

Thermal Properties[1]	Test Method	Value
Heat Deflection (HDT) @ 66 psi, 0.125"	ASTM D648	216 °C (421 °F)
Heat Deflection (HDT) @ 264 psi, 0.125"	ASTM D648	213 °C (415 °F)
Vicat Softening Temperature (Rate B/50)	ASTM D1525	214 °C (416 °F)
Glass Transition Temperature (Tg)	DSC (SSYS)	215 °C (419 °F)
Coefficient of Thermal Expansion	ASTM E831	47 µm/(m·°C) 26 uin/(in·°F)
Coefficient of Thermal Expansion (xflow)	ASTM E831	41 µm/(m·°C) 23 uin/(in·°F)

ULTEM 1010 Resin

Electrical Properties	Test Method	Value Range
Volume Resistivity	ASTM D257	1.0 x10^{14} - 8.96x10^{15} ohm-cm
Dielectric Constant	ASTM D150-98	2.67
Dissipation Factor	ASTM D150-98	.001
Dielectric Strength	ASTM D149-09, Method A	240 V/mil

Other[2]	Test Method	Value
Specific Gravity	ASTM D792	1.27
Oxygen Index	ASTM D2863	0.44
Vertical Burn	FAR 25.853 (Test a (60s), passes at)	4 seconds
OSU Total Heat Release (2 min test, . 060" thick)	FAR 25.853	35.7 kW min/m^2
Food Safety Certification[3]	NSF 51	Certified
Bio-Compatibility Certification[3]	ISO 10993	Certified

Burn Testing		
Horizontal Burn (15 sec)	14 CFR/FAR 25.853	Passed (.060" thick)
Vertical Burn (60 sec)	14 CFR/FAR 25.853	Passed (.060" thick)
Vertical Burn (12 sec)	14 CFR/FAR 25.853	Passed (.060" thick)
45° Ignition	14 CFR/FAR 25.853	Passed (.060" thick)
Heat Release	14 CFR/FAR 25.853	Passed (.060" thick)
NBS Smoke Density (flaming)	14 CFR/FAR 25.853	Passed (.060" thick)
NBS Smoke Density (non-flaming)	14 CFR/FAR 25.853	Passed (.060" thick)

ULTEM 1010 Resin

System Availability	Layer Thickness Capability	Support Structure	Available Colors
Fortus 450mc™ Stratasys F900™	0.010 inch (0.254 mm) 0.013 inch (0.333 mm) 0.020 inch (0.508 mm)[4]	Breakaway	Natural

The performance characteristics of these materials may vary according to application, operating conditions, or end use. The information presented are typical values intended for reference and comparison purposes only. They should not be used for design specifications or quality control purposes. End-use material performance can be impacted (+/-) by, but not limited to, part design, end-use conditions, test conditions, etc. Actual values will vary with build conditions. Tested parts were built on Fortus 400mc™ @ 0.010" (0.254 mm) slice. Product specifications are subject to change without notice.

The performance characteristics of these materials may vary according to application, operating conditions, or end use. Each user is responsible for determining that the Stratasys material is safe, lawful, and technically suitable for the intended application, as well as for identifying the proper disposal (or recycling) method consistent with applicable environmental laws and regulations. Stratasys makes no warranties of any kind, express or implied, including, but not limited to, the warranties of merchantability, fitness for a particular use, or warranty against patent infringement.

[1] Build orientation is on side long edge.

[2] Literature value unless otherwise noted

[3] Available for ULTEM 1010 CG (certified grade) canisters.

[4] Available on the Stratasys F900 only.

Orientation: See Stratasys Testing white paper for more detailed description of build orientations.

- XZ = X or "on edge"
- XY = Y or "flat"
- ZX = or "upright"

Stratasys Headquarters

7665 Commerce Way,
Eden Prairie, MN 55344
+1 800 801 6491 (US Toll Free)
+1 952 937-3000 (Intl)
+1 952 937-0070 (Fax)

stratasys.com
ISO 9001:2008 Certified

1 Holtzman St., Science Park,
PO Box 2496
Rehovot 76124, Israel
+972 74 745 4000
+972 74 745 5000 (Fax)

Appendix D – Arduino Code Simulation

arduino_pulser.ino

```
uint16_t dt = 1667 ;

char sdata = 0 ;

void setup() {
 Serial.begin(9600);

 pinMode(13, OUTPUT);

 pinMode(12, OUTPUT);

}

void loop() {
 digitalWrite( 12 , HIGH ) ;
 if( Serial.available() > 0 )
 {
    sdata = Serial.read() ;

    switch( sdata ){
    case 'A':
          dt = 1667 ;
          break;
    case 'B':
          dt = 1250 ;
          break;
    case 'C':
          dt = 1000 ;
          break;
    case 'D':
          dt = 833 ;
          break;
    case 'E':
          dt = 714 ;
          break;
    case 'F':
          dt = 625 ;
          break;
case 'G':
      dt = 556 ;
      break;
case 'H':
      dt = 500 ;
      break;
case 'I':
      dt = 455 ;
      break;
case 'J':
      dt = 417 ;
      break;
case 'K':
      dt = 385 ;
      break;
case 'L':
      dt = 357 ;
      break;
case 'M':
      dt = 333 ;
      break;
case 'N':
      dt = 313 ;
      break;
case 'O':
      dt = 294 ;
      break;
case 'P':
      dt = 278 ;
      break;
case 'Q':
      dt = 263 ;
      break;
case 'R':
      dt = 250 ;
      break;
case 'S':
      dt = 238 ;
      break;
case 'T':
      dt = 227 ;
```

```
        break;
    case 'U':
        dt = 217 ;
        break;
    case 'V':
        dt = 208 ;
        break;
    case 'W':
        dt = 200 ;
        break;
    case 'X':
        dt = 192 ;
        break;
    case 'Y':
        dt = 185 ;
        break;
    case 'Z':
        dt = 179 ;
        break;
    case '[':
        dt = 172 ;
        break;
    case '\\':
        dt = 167  ;
        break;
    }
  }

  digitalWrite( 13 , HIGH ) ;
  delay( dt ) ;
  digitalWrite( 13 , LOW ) ;
  delay( dt ) ;

}
```

arduino_reader.ino

```
uint8_t bank = A0, igniter = A3 ;
uint8_t mode = 5 ;
long volt = 0 ;



void set up() {
  Serial.begin(9600);
  pinMode(5, INPUT);
}

void loop() {
  if ( digitalRead(5) )
  {
    volt = analogRead( bank ) * 5 / 1023 ;
    Serial.println(volt);
    delay(1);
  }
  else
  {
    volt = analogRead( igniter ) * 5 / 1023 ;
    Serial.println(volt);
    delay(1);
  }
}
```

Appendix E – MATLAB GUI Code

GUI.m

```
function varargout = GUI(varargin)
% GUI MATLAB code for GUI.fig
%      GUI, by itself, creates a new GUI or raises the existing
%      singleton*.
%
%      H = GUI returns the handle to a new GUI or the handle to
%      the existing singleton*.
%
%      GUI('CALLBACK',hObject,eventData,handles,...) calls the local
%      function named CALLBACK in GUI.M with the given input arguments.
%
%      GUI('Property','Value',...) creates a new GUI or raises the
%      existing singleton*.  Starting from the left, property value pairs are
%      applied to the GUI before GUI_OpeningFcn gets called.  An
%      unrecognised property name or invalid value makes property application
%      stop.  All inputs are passed to GUI_OpeningFcn via varargin.
%
%      *See GUI Options on GUIDE's Tools menu.  Choose "GUI allows only one
%      instance to run (singleton)".
%
% See also: GUIDE, GUIDATA, GUIHANDLES

% Edit the above text to modify the response to help GUI

% Last Modified by GUIDE v2.5 28-Feb-2021 02:10:49

% Begin initialization code - DO NOT EDIT
gui_Singleton = 1;
gui_State = struct('gui_Name',       mfilename, ...
                   'gui_Singleton',  gui_Singleton, ...
                   'gui_OpeningFcn', @GUI_OpeningFcn, ...
                   'gui_OutputFcn',  @GUI_OutputFcn, ...
                   'gui_LayoutFcn',  [] , ...
                   'gui_Callback',   []);
if nargin && ischar(varargin{1})
    gui_State.gui_Callback = str2func(varargin{1});
end

if nargout
    [varargout{1:nargout}] = gui_mainfcn(gui_State, varargin{:});
else
    gui_mainfcn(gui_State, varargin{:});
end
% End initialisation code - DO NOT EDIT


% --- Executes just before GUI is made visible.
function GUI_OpeningFcn(hObject, eventdata, handles, varargin)
% This function has no output args, see OutputFcn.
% hObject    handle to figure
% eventdata  reserved - to be defined in a future version of MATLAB
% handles    structure with handles and user data (see GUIDATA)
% varargin   command line arguments to GUI (see VARARGIN)

% Choose default command line output for GUI
handles.output = hObject;

% Update handles structure
guidata(hObject, handles);

% UIWAIT makes GUI wait for user response (see UIRESUME)
% uiwait(handles.figure1);


% --- Outputs from this function are returned to the command line.
function varargout = GUI_OutputFcn(hObject, eventdata, handles)
% varargout  cell array for returning output args (see VARARGOUT);
% hObject    handle to figure
% eventdata  reserved - to be defined in a future version of MATLAB
% handles    structure with handles and user data (see GUIDATA)

% Get default command line output from handles structure
varargout{1} = handles.output;
```

```
% --- Executes on button press in com_open.
function com_open_Callback(hObject, eventdata,
handles)
global s
num = get( handles.com_no, 'Value' ) ;
s = serial( ['COM', num2str(num)] , 'Baudrate', 9600 )
s.BytesAvailableFcnCount = 500;
s.BytesAvailableFcnMode = 'byte' ;
s.BytesAvailableFcn = 'available' ;

fopen(s) ;
set( hObject, 'Enable' , 'off' );
set( handles.com_no, 'Enable' , 'off' );
set( handles.close_com, 'Visible' , 'on' );
set( handles.freq, 'Visible' , ' on' ) ;

% --- Executes on selection change in com_no.
function com_no_Callback(hObject, eventdata,
handles)
% hObject    handle to com_no (see GCBO)
% eventdata  reserved - to be defined in a future
version of MATLAB
% handles    structure with handles and user data
(see GUIDATA)

% Hints: contents = cellstr(get(hObject,'String'))
returns com_no contents as cell array
%        contents{get(hObject,'Value')} returns
selected item from com_no


% --- Executes during object creation, after setting all
properties.
function com_no_CreateFcn(hObject, eventdata,
handles)
% hObject    handle to com_no (see GCBO)
% eventdata  reserved - to be defined in a future
version of MATLAB
% handles    empty - handles not created until after
all CreateFcns called

% Hint: popupmenu controls usually have a white
background on Windows.
%       See ISPC and COMPUTER.
if ispc && isequal(get(hObject,'BackgroundColor'),
get(0,'defaultUicontrolBackgroundColor'))
   set(hObject,'BackgroundColor','white');
end


% --- Executes on button press in close_com.
function close_com_Callback(hObject, eventdata,
handles)
global s
fclose(s)
delete(s)
set( hObject, 'Visible' , 'off' );
set( handles.com_open, 'Enable' , 'on' );
set( handles.com_no, 'Enable' , 'on' );
set( handles.freq, 'Visible' , ' off' ) ;
set( handles.acquire, 'Visible' , ' off' );


% --- Executes on selection change in freq_val.
function freq_val_Callback(hObject, eventdata,
handles)
% hObject    handle to freq_val (see GCBO)
% eventdata  reserved - to be defined in a future
version of MATLAB
% handles    structure with handles and user data
(see GUIDATA)

% Hints: contents = cellstr(get(hObject,'String'))
returns freq_val contents as cell array
%        contents{get(hObject,'Value')} returns
selected item from freq_val


% --- Executes during object creation, after setting all
properties.
function freq_val_CreateFcn(hObject, eventdata,
handles)
% hObject    handle to freq_val (see GCBO)
% eventdata  reserved - to be defined in a future
version of MATLAB
% handles    empty - handles not created until after
all CreateFcns called

% Hint: popupmenu controls usually have a white
background on Windows.
%       See ISPC and COMPUTER.
if ispc && isequal(get(hObject,'BackgroundColor'),
get(0,'defaultUicontrolBackgroundColor'))
   set(hObject,'BackgroundColor','white');
end


% --- Executes on button press in set_frequency.
function set_frequency_Callback(hObject,
eventdata, handles)
global s
ch = [ 'ABCDEFGHIJKLMNOPQRSTUVWXYZ[\' ] ;
fr = get( handles.freq_val, 'Value' );
fprintf( s , ch(fr) )
```

```
% --- Executes when user attempts to close figure1.
function figure1_CloseRequestFcn(hObject,
eventdata, handles)
% hObject    handle to figure1 (see GCBO)
% eventdata  reserved - to be defined in a future
version of MATLAB
% handles    structure with handles and user data
(see GUIDATA)

% Hint: delete(hObject) closes the figure
delete(hObject);
delete(instrfind)


% --- Executes on button press in acquire.
function acquire_Callback(hObject, eventdata,
handles)
global s
k = get( handles.measure , 'Value' ) ;
fprintf(s, num2str(k) );
if s.BytesAvailable > 0
   data = [];
   while( s.BytesAvailable > 0 )
      data = [ data ; str2num(fscanf( s )) ] ;
   end
end
axis( handles.axes1 )
plot(data)
data


% --- Executes on selection change in measure.
function measure_Callback(hObject, eventdata,
handles)
% hObject    handle to measure (see GCBO)
% eventdata  reserved - to be defined in a future
version of MATLAB
% handles    structure with handles and user data
(see GUIDATA)

% Hints: contents = cellstr(get(hObject,'String'))
returns measure contents as cell array
%       contents{get(hObject,'Value')} returns
selected item from measure


% --- Executes during object creation, after setting all
properties.
function measure_CreateFcn(hObject, eventdata,
handles)
% hObject    handle to measure (see GCBO)
% eventdata  reserved - to be defined in a future
version of MATLAB
% handles    empty - handles not created until after
all CreateFcns called

% Hint: popupmenu controls usually have a white
background on Windows.
%       See ISPC and COMPUTER.
if ispc && isequal(get(hObject,'BackgroundColor'),
get(0,'defaultUicontrolBackgroundColor'))
   set(hObject,'BackgroundColor','white');
end


% --- Executes on selection change in popupmenu4.
function popupmenu4_Callback(hObject, eventdata,
handles)
% hObject    handle to popupmenu4 (see GCBO)
% eventdata  reserved - to be defined in a future
version of MATLAB
% handles    structure with handles and user data
(see GUIDATA)

% Hints: contents = cellstr(get(hObject,'String'))
returns popupmenu4 contents as cell array
%       contents{get(hObject,'Value')} returns
selected item from popupmenu4


% --- Executes during object creation, after setting all
properties.
function popupmenu4_CreateFcn(hObject,
eventdata, handles)
% hObject    handle to popupmenu4 (see GCBO)
% eventdata  reserved - to be defined in a future
version of MATLAB
% handles    empty - handles not created until after
all CreateFcns called

% Hint: popupmenu controls usually have a white
background on Windows.
%       See ISPC and COMPUTER.
if ispc && isequal(get(hObject,'BackgroundColor'),
get(0,'defaultUicontrolBackgroundColor'))
   set(hObject,'BackgroundColor','white');
end
```

available.m

```
function [ ] = available(hObject,eventData)
global s
data = [];
if s.BytesAvailable > 0
   while( s.BytesAvailable > 0 )
      data = [ data ; str2num(fscanf( s )) ] ;
   end
end
flushinput(s)
plot(data)
xlabel('Time (s)')
ylabel('Voltage (V)')
grid on;
grid minor;
ylim([0 6])
end
```

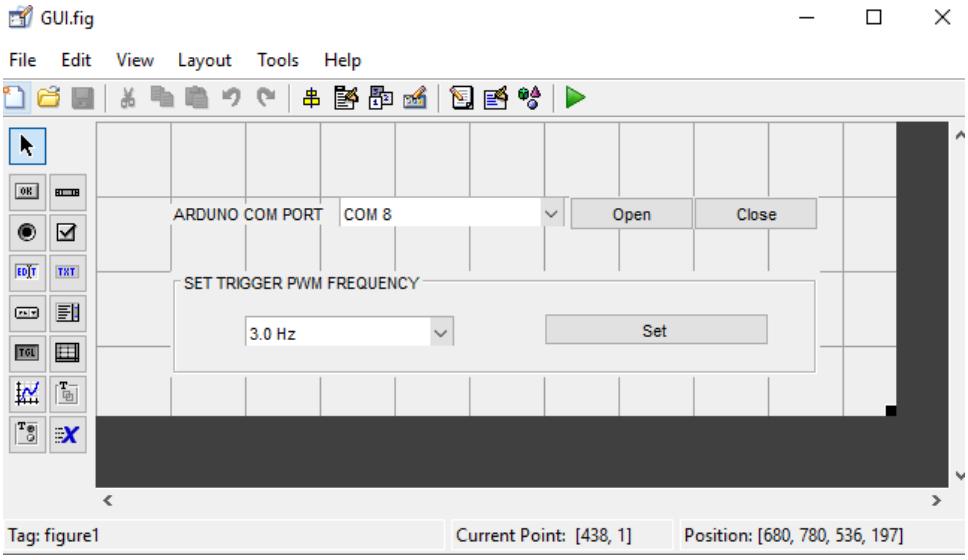

Appendix F – Electronics BoM

Supplier Part Number	Design Reference	Qty	Unit Price	Extended Price	Description	RoHS Status
296-29758-1-ND	IC1	1	R 60,59	R 60,59	IC PWR SWITCH N-CHAN 1:1 SOT23-5	ROHS3 Compliant
1470-3336-ND	HV1	1	R 2 967,89	R 2 967,89	DC DC CONVERTER -2000V 500MW	ROHS3 Compliant
1242-1169-1-ND	D1/D2	2	R 41,76	R 83,52	DIODE SCHOTTKY 1.2KV 2.5A SMB	RoHS Compliant
HVCB2512FKC10M0CT-ND	R1/R2	2	R 49,49	R 98,98	RES 10M OHM 1% 2W 2512	ROHS3 Compliant
CRHV1.00GECT-ND	R4/R6	2	R 54,46	R 108,92	RES SMD 1G OHM 1% 1W 2512	ROHS3 Compliant
RHM1180CT-ND	R5	1	R 6,13	R 6,13	RES SMD 6.8M OHM 1% 1/3W 1210	ROHS3 Compliant
RHM1065CT-ND	R7	1	R 6,13	R 6,13	RES SMD 1.5M OHM 1% 1/3W 1210	ROHS3 Compliant
RNCF1206TKY10K0CT-ND	R8/R10	2	R 29,49	R 58,98	RES 10K OHM 0.01% 1/4W 1206	ROHS3 Compliant
P4.3KCTCT-ND	R9	1	R 21,46	R 21,46	RES SMD 4.3K OHM 0.05% 1/4W 1206	ROHS3 Compliant
CRHV12.0MECT-ND	R3	1	R 53,00	R 53,00	RES SMD 12M OHM 1% 1W 2512	ROHS3 Compliant
399-13342-1-ND	C1/C2	2	R 578,31	R 1 156,62	CAP CER 0.068UF 2KV C0G/NP0 4540	ROHS3 Compliant
445-14655-1-ND	C4/C5	2	R 10,22	R 20,44	CAP CER 0.1UF 50V NP0 1206	ROHS3 Compliant
80-C4540H104KUGWCT1	C3	1	R 274,60	R 274,60	SMD/SMT 1250V .1uF 0.1	ROHS3 Compliant
1740-1095-1-ND	SCR1	1	R 12,70	R 12,70	SCR 800V 8A DPAK	RoHS Compliant
PFT-1052V	TX1	1	R 94,84	R 94,84	Trigger Coil Transformer 12KV	ROHS3 Compliant
Total				R 5 024,80		

Appendix G – Simulation Results

Input Voltage: 3V

Freq (Hz)	Pulse Time (s)	Capacitor Voltage Output (V)	Trigger Coil Voltage Output (V)
0,3	3,33	166	6640
0,4	2,50	160	6400
0,5	2,00	158	6320
0,6	1,67	154	6160
0,7	1,43	153	6120
0,8	1,25	147	5880
0,9	1,11	144	5760
1	1,00	139	5560
1,1	0,91	134	5360
1,2	0,83	127	5080
1,3	0,77	123	4920
1,4	0,71	121	4840
1,5	0,67	117	4680
1,6	0,63	113	4520
1,7	0,59	109	4360
1,8	0,56	107	4280
1,9	0,53	104	4160
2	0,50	102	4080
2,1	0,48	100	4000
2,2	0,45	97	3880
2,3	0,43	95	3800
2,4	0,42	94	3760
2,5	0,40	92	3680
2,6	0,38	90	3600
2,7	0,37	89	3560
2,8	0,36	88	3520
2,9	0,34	86	3440
3	0,33	85	3400

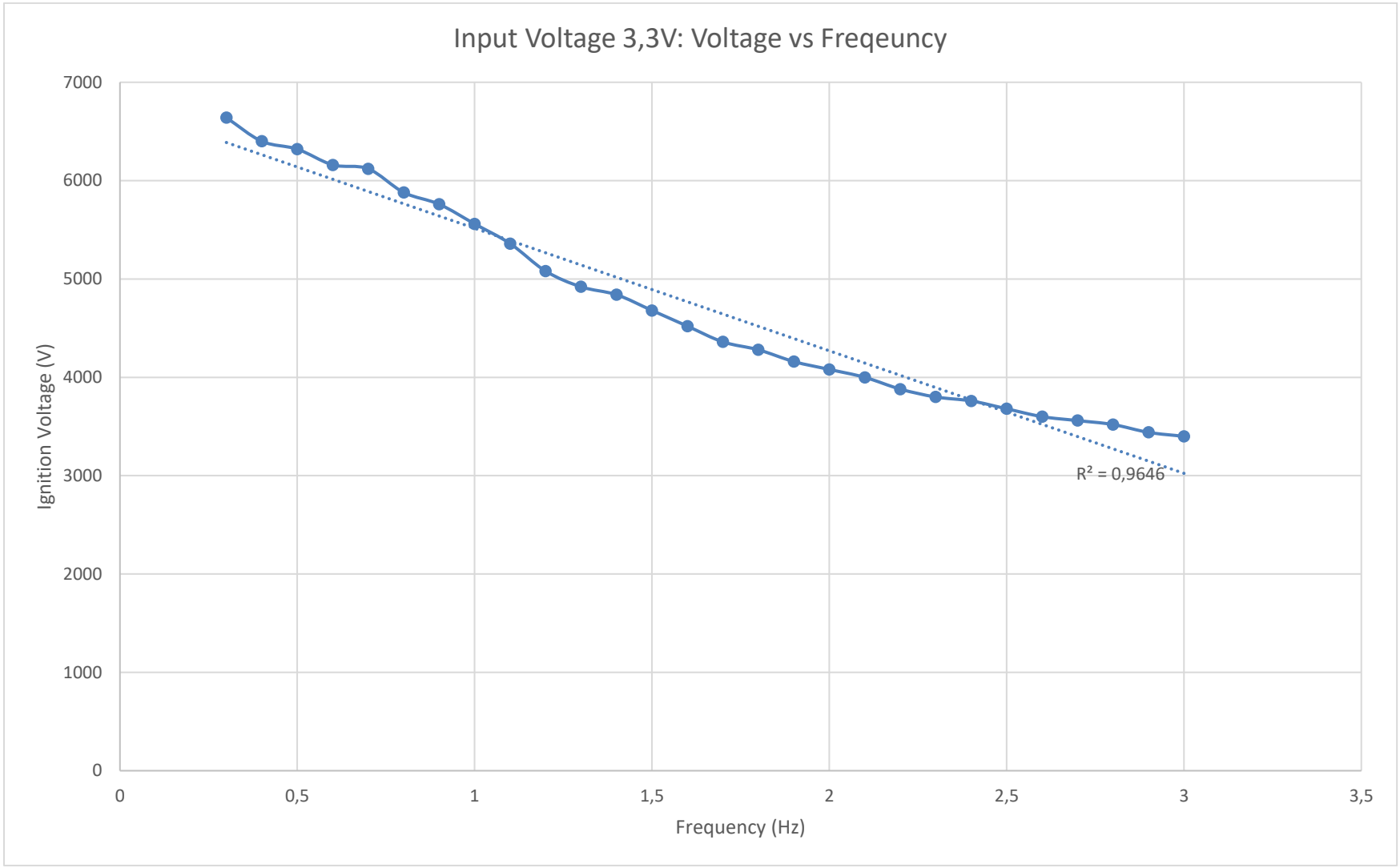
Input Voltage 3,3V: Voltage vs Freqeuncy
Ignition Voltage (V)
7000
6000
5000
4000
3000
2000
1000
0
0
0,5
1
1,5
2
2,5
3
3,5
Frequency (Hz)
R² = 0,9646

Input Voltage: 4V

Freq (Hz)	Pulse Time (s)	Capacitor Voltage Output (V)	Trigger Coil Voltage Output (V)
0,3	3,33	195	7800
0,4	2,50	190	7600
0,5	2,00	187,5	7500
0,6	1,67	185	7400
0,7	1,43	182,5	7300
0,8	1,25	177,5	7100
0,9	1,11	170	6800
1	1,00	165	6600
1,1	0,91	160	6400
1,2	0,83	155	6200
1,3	0,77	150	6000
1,4	0,71	145	5800
1,5	0,67	140	5600
1,6	0,63	135	5400
1,7	0,59	130	5200
1,8	0,56	127,5	5100
1,9	0,53	125	5000
2	0,50	123	4920
2,1	0,48	120	4800
2,2	0,45	117	4680
2,3	0,43	114	4560
2,4	0,42	113	4520
2,5	0,40	111	4440
2,6	0,38	109	4360
2,7	0,37	107	4280
2,8	0,36	106	4240
2,9	0,34	104	4160
3	0,33	103	4120

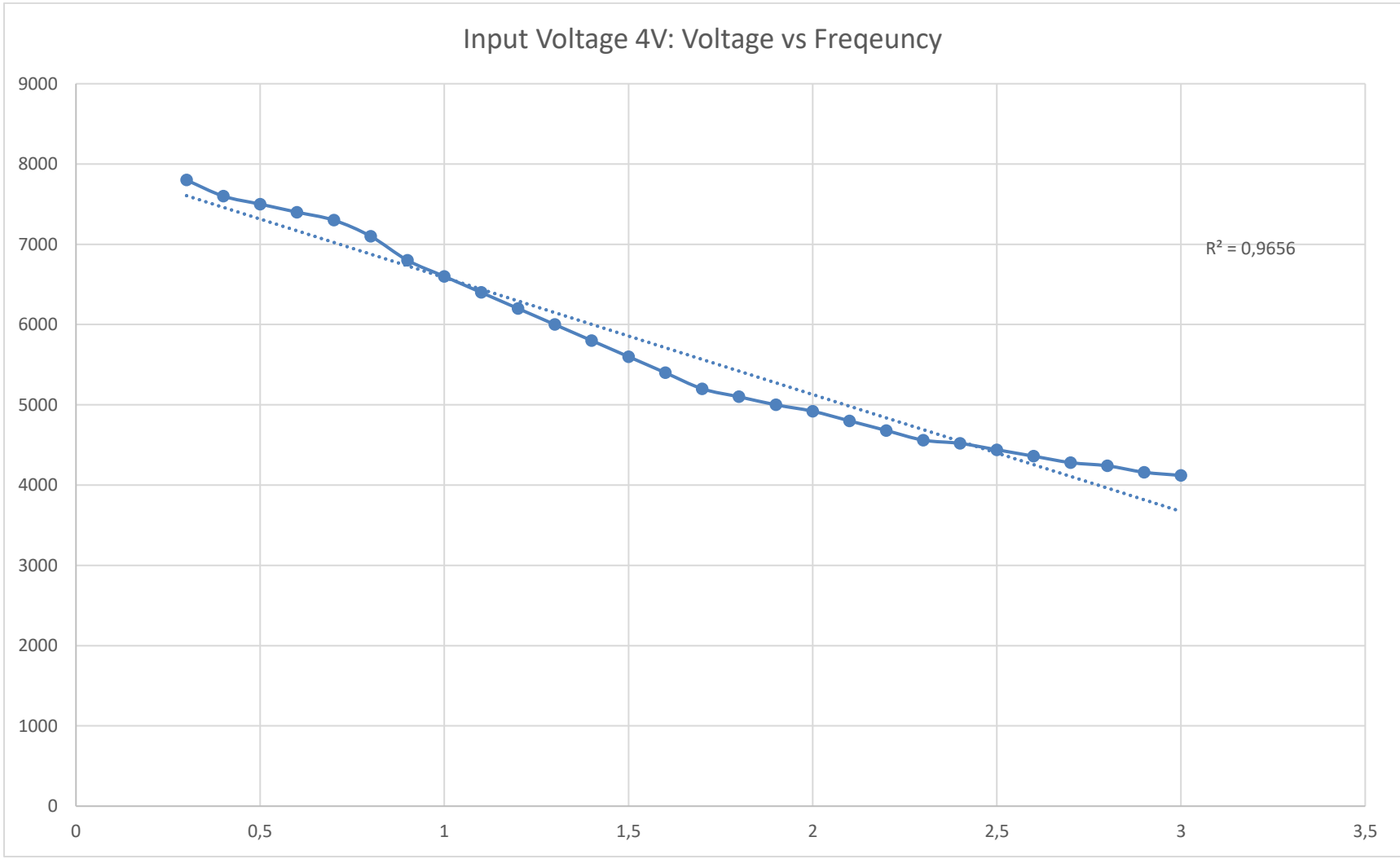
Input Voltage 4V: Voltage vs Freqeuncy
9000
8000
7000
6000
5000
4000
3000
2000
1000
0
0
0,5
1
1,5
2
2,5
3
3,5
R² = 0,9656

Input Voltage: 5V

Freq (Hz)	Pulse Time (s)	Capacitor Voltage Output (V)	Trigger Coil Voltage Output (V)
0,3	3,33	242,5	9700
0,4	2,50	235	9400
0,5	2,00	232,5	9300
0,6	1,67	225	9000
0,7	1,43	227,5	9100
0,8	1,25	217,5	8700
0,9	1,11	215	8600
1	1,00	207,5	8300
1,1	0,91	200	8000
1,2	0,83	192,5	7700
1,3	0,77	186,3	7450
1,4	0,71	180	7200
1,5	0,67	175	7000
1,6	0,63	168,8	6750
1,7	0,59	165	6600
1,8	0,56	161,3	6450
1,9	0,53	156,3	6250
2	0,50	152,5	6100
2,1	0,48	148,8	5950
2,2	0,45	146,3	5850
2,3	0,43	143,8	5750
2,4	0,42	141,3	5650
2,5	0,40	138,8	5550
2,6	0,38	136,3	5450
2,7	0,37	133,8	5350
2,8	0,36	132,5	5300
2,9	0,34	130	5200
3	0,33	128,8	5150

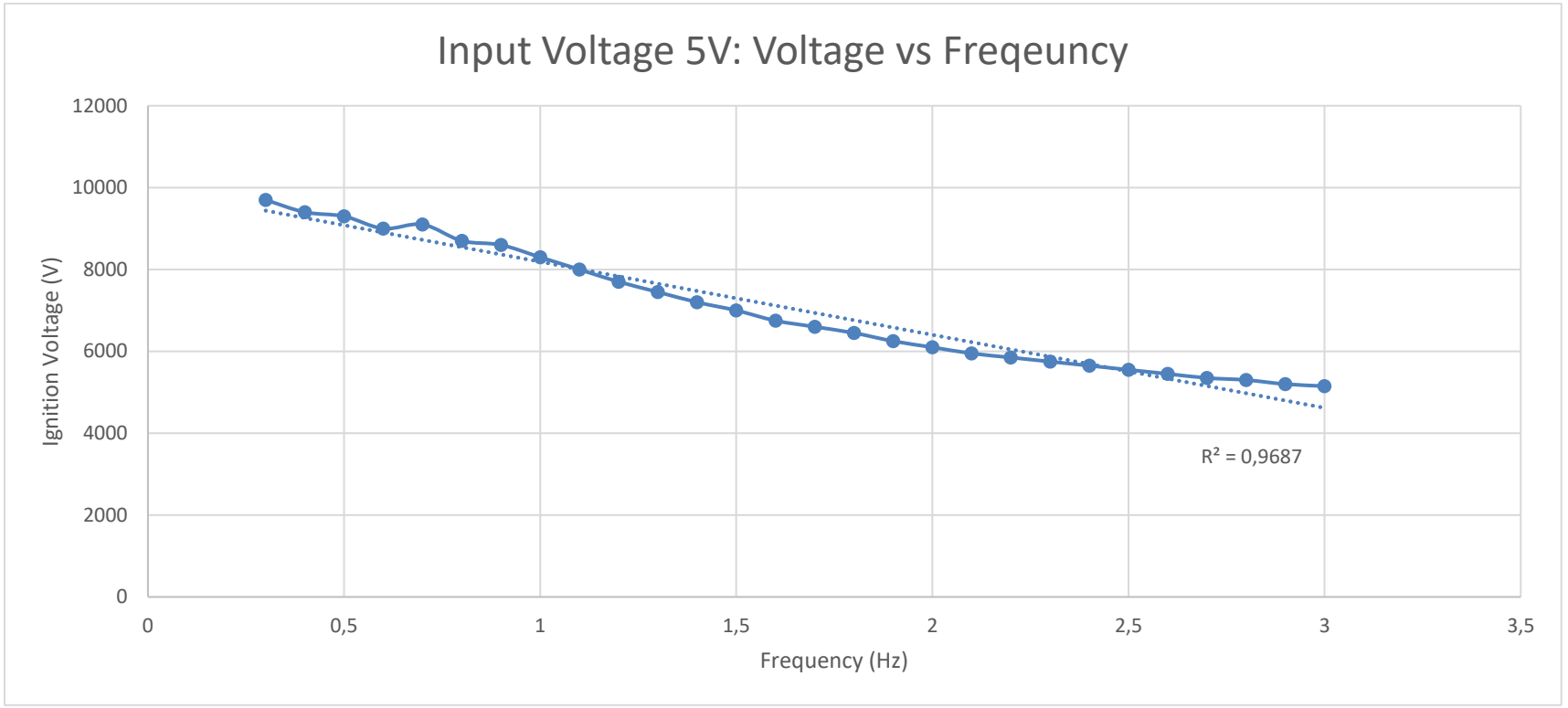
Input Voltage 5V: Voltage vs Freqeuncy
Ignition Voltage (V)
12000
10000
8000
6000
4000
2000
0
0
0,5
1
1,5
2
2,5
3
3,5
Frequency (Hz)
R² = 0,9687

Appendix H – 0.25Hz Results


1.jpg


2.jpg


3.jpg


4.jpg


5.jpg

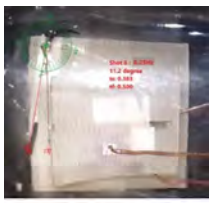
6.jpg

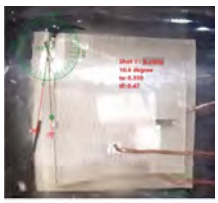
7.jpg


8.jpg


9.jpg


10.jpg

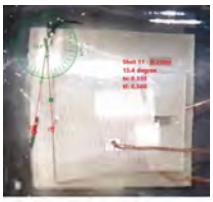
11.jpg

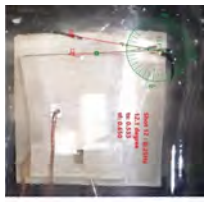
12.jpg


13.jpg


14.jpg


15.jpg


16.jpg

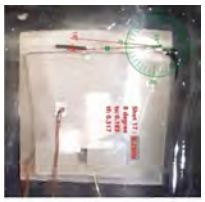
17.jpg


18.jpg


19.jpg


20.jpg


21.jpg


22.jpg


23.jpg


24.jpg


25.jpg


26.jpg


27.jpg


28.jpg


29.jpg


30.jpg


31.jpg


32.jpg


33.jpg


34.jpg


35.jpg


36.jpg


37.jpg


38.jpg


39.jpg


40.jpg


41.jpg


42.jpg


43.jpg


44.jpg

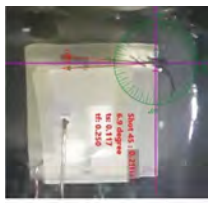
45.jpg


46.jpg


47.jpg


48.jpg


49.jpg


50.jpg


51.jpg

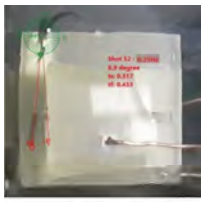
52.jpg

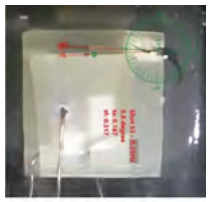
53.jpg


54.jpg


55.jpg


56.jpg

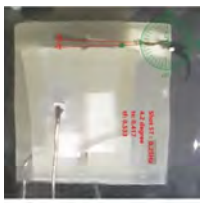
57.jpg

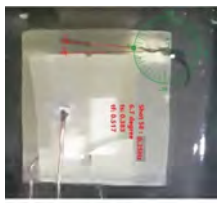
58.jpg


59.jpg


60.jpg


61.jpg


62.jpg


63.jpg


64.jpg


65.jpg


66.jpg


67.jpg


68.jpg


69.jpg


70.jpg


71.jpg


72.jpg


73.jpg


74.jpg


75.jpg

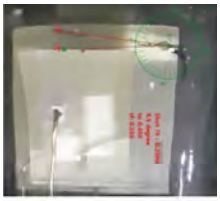
76.jpg


77.jpg


78.jpg

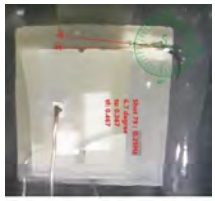
79.jpg


80.jpg


81.jpg


82.jpg


83.jpg


84.jpg

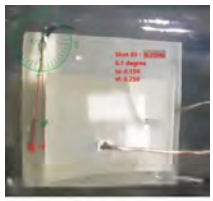
85.jpg


86.jpg


87.jpg


88.jpg


89.jpg


90.jpg


91.jpg


92.jpg


93.jpg


94.jpg


95.jpg


96.jpg


97.jpg


98.jpg


99.jpg


100.jpg


101.jpg

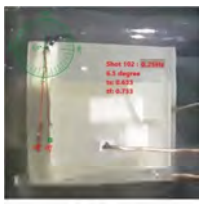
102.jpg


103.jpg


104.jpg


105.jpg

106.jpg

107.jpg

108.jpg

109.jpg

110.jpg

111.jpg

112.jpg

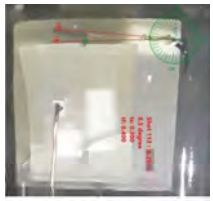

113.jpg

114.jpg

115.jpg

116.jpg

117.jpg

118.jpg

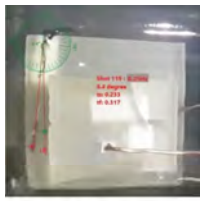

119.jpg

120.jpg

Shot #	angle (degree)	start time (s)	end time (s)	distance (m)	Ibit (µNs)	Thrust (µN)
1	9,8	0,083	0,200	0,007	1,976	0,494
2	10,0	0,367	0,517	0,007	2,018	0,504
3	8,7	0,200	0,300	0,006	1,749	0,437
4	11,1	0,500	0,600	0,008	2,247	0,562
5	14,3	0,383	0,500	0,010	2,930	0,732
6	11,2	0,383	0,500	0,008	2,268	0,567
7	10,6	0,350	0,470	0,007	2,143	0,536
8	10,8	0,383	0,500	0,008	2,185	0,546
9	11,1	0,333	0,433	0,008	2,247	0,562
10	10,3	0,517	0,633	0,007	2,080	0,520
11	13,4	0,333	0,500	0,010	2,735	0,684
12	12,1	0,533	0,650	0,009	2,458	0,615
13	8,3	0,267	0,383	0,006	1,667	0,417
14	8,9	0,167	0,300	0,006	1,791	0,448
15	9,9	0,283	0,400	0,007	1,997	0,499
16	5,5	0,167	0,300	0,004	1,099	0,275
17	8,0	0,183	0,317	0,006	1,606	0,402
18	11,6	0,183	0,283	0,008	2,352	0,588
19	10,1	0,133	0,250	0,007	2,039	0,510
20	7,5	0,150	0,333	0,005	1,504	0,376
21	11,6	0,183	0,300	0,008	2,352	0,588
22	7,0	0,200	0,300	0,005	1,402	0,351
23	5,6	0,200	0,317	0,004	1,119	0,280
24	5,2	0,200	0,383	0,004	1,038	0,260
25	7,3	0,183	0,367	0,005	1,463	0,366
26	7,4	0,017	0,217	0,005	1,484	0,371
27	6,9	0,117	0,283	0,005	1,382	0,345
28	7,3	0,117	0,300	0,005	1,463	0,366
29	6,9	0,167	0,283	0,005	1,382	0,345
30	7,1	0,083	0,233	0,005	1,423	0,356
31	7,6	0,100	0,300	0,005	1,524	0,381
32	5,4	0,200	0,350	0,004	1,079	0,270
33	6,5	0,183	0,383	0,005	1,301	0,325
34	5,6	0,133	0,283	0,004	1,119	0,280
35	7,3	0,330	0,467	0,005	1,463	0,366
36	5,6	0,150	0,350	0,004	1,119	0,280
37	6,5	0,167	0,317	0,005	1,301	0,325
38	6,7	0,150	0,300	0,005	1,341	0,335
39	6,0	0,133	0,317	0,004	1,200	0,300
40	6,3	0,067	0,250	0,004	1,260	0,315
41	6,1	0,083	0,233	0,004	1,220	0,305
42	5,6	0,067	0,233	0,004	1,119	0,280
43	6,4	0,233	0,433	0,004	1,281	0,320
44	7,6	0,400	0,500	0,005	1,524	0,381
45	6,9	0,117	0,250	0,005	1,382	0,345
46	7,8	0,283	0,367	0,005	1,565	0,391

47	8,5	0,333	0,467	0,006	1,708	0,427
48	8,0	0,330	0,467	0,006	1,606	0,402
49	9,4	0,300	0,433	0,007	1,894	0,473
50	8,9	0,350	0,467	0,006	1,791	0,448
51	7,2	0,433	0,533	0,005	1,443	0,361
52	8,9	0,317	0,433	0,006	1,791	0,448
53	5,8	0,167	0,317	0,004	1,159	0,290
54	7,1	0,360	0,467	0,005	1,423	0,356
55	7,7	0,417	0,533	0,005	1,545	0,386
56	7,5	0,417	0,567	0,005	1,504	0,376
57	4,2	0,417	0,533	0,003	0,838	0,209
58	6,7	0,383	0,517	0,005	1,341	0,335
59	10,1	0,200	0,317	0,007	2,039	0,510
60	4,8	0,417	0,517	0,003	0,958	0,240
61	7,7	0,417	0,517	0,005	1,545	0,386
62	7,5	0,250	0,367	0,005	1,504	0,376
63	9,3	0,367	0,467	0,007	1,873	0,468
64	7,2	0,350	0,467	0,005	1,443	0,361
65	8,9	0,433	0,533	0,006	1,791	0,448
66	6,6	0,567	0,667	0,005	1,321	0,330
67	6,9	0,450	0,567	0,005	1,382	0,345
68	6,8	0,417	0,500	0,005	1,362	0,340
69	8,4	0,417	0,517	0,006	1,688	0,422
70	6,7	0,367	0,467	0,005	1,341	0,335
71	6,5	0,400	0,500	0,005	1,301	0,325
72	7,1	0,433	0,533	0,005	1,423	0,356
73	7,0	0,617	0,717	0,005	1,402	0,351
74	6,9	0,400	0,500	0,005	1,382	0,345
75	7,4	0,450	0,550	0,005	1,484	0,371
76	9,5	0,450	0,550	0,007	1,914	0,479
77	8,0	0,633	0,733	0,006	1,606	0,402
78	6,6	0,300	0,400	0,005	1,321	0,330
79	6,7	0,367	0,467	0,005	1,341	0,335
80	5,7	0,350	0,450	0,004	1,139	0,285
81	7,0	0,483	0,567	0,005	1,402	0,351
82	6,1	0,500	0,600	0,004	1,220	0,305
83	6,5	0,500	0,617	0,005	1,301	0,325
84	6,1	0,667	0,767	0,004	1,220	0,305
85	6,1	0,150	0,250	0,004	1,220	0,305
86	6,6	0,383	0,483	0,005	1,321	0,330
87	7,1	0,367	0,467	0,005	1,423	0,356
88	7,6	0,533	0,650	0,005	1,524	0,381
89	6,0	0,300	0,450	0,004	1,200	0,300
90	6,8	0,517	0,600	0,005	1,362	0,340
91	8,0	0,350	0,450	0,006	1,606	0,402
92	6,3	0,383	0,483	0,004	1,260	0,315
93	6,5	0,483	0,600	0,005	1,301	0,325

94	8,6	0,483	0,567	0,006	1,729	0,432
95	8,6	0,417	0,517	0,006	1,729	0,432
96	10,6	0,367	0,467	0,007	2,143	0,536
97	8,6	0,533	0,650	0,006	1,729	0,432
98	5,0	0,500	0,583	0,003	0,998	0,250
99	9,9	0,600	0,717	0,007	1,997	0,499
100	4,9	0,367	0,500	0,003	0,978	0,245
101	7,5	0,433	0,533	0,005	1,504	0,376
102	6,5	0,633	0,733	0,005	1,301	0,325
103	9,1	0,367	0,450	0,006	1,832	0,458
104	7,7	0,367	0,450	0,005	1,545	0,386
105	7,5	0,383	0,483	0,005	1,504	0,376
106	7,3	0,317	0,417	0,005	1,463	0,366
107	7,7	0,300	0,400	0,005	1,545	0,386
108	8,4	0,367	0,467	0,006	1,688	0,422
109	8,5	0,200	0,317	0,006	1,708	0,427
110	8,7	0,283	0,367	0,006	1,749	0,437
111	6,8	0,367	0,450	0,005	1,362	0,340
112	5,6	0,617	0,700	0,004	1,119	0,280
113	8,5	0,300	0,400	0,006	1,708	0,427
114	7,7	0,283	0,367	0,005	1,545	0,386
115	7,5	0,350	0,450	0,005	1,504	0,376
116	7,4	0,517	0,617	0,005	1,484	0,371
117	8,6	0,467	0,567	0,006	1,729	0,432
118	5,2	0,450	0,550	0,004	1,038	0,260
119	6,4	0,233	0,317	0,004	1,281	0,320
120	6,8	0,267	0,350	0,005	1,362	0,340

Appendix I – 0.5Hz Results

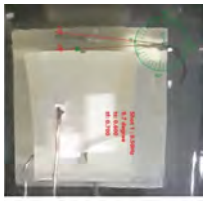
1.png


2.png

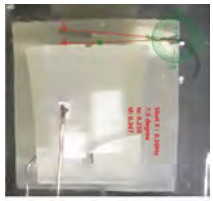
3.png

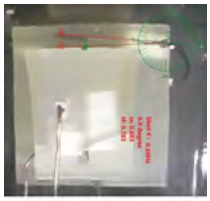
4.png

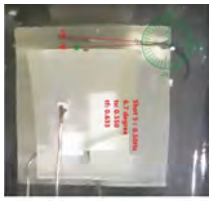
5.png


6.png


7.png


8.png

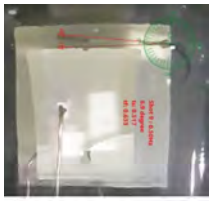
9.png

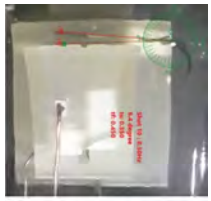
10.png

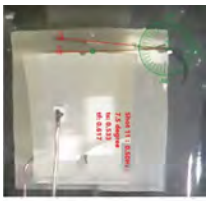
11.png


12.png

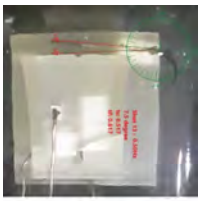
13.png

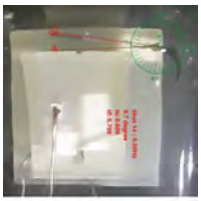
14.png

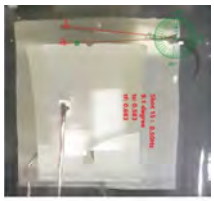
15.png

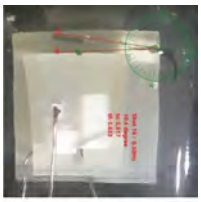
16.png


17.png

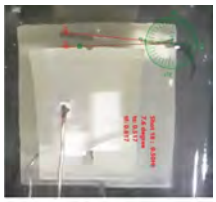
18.png


19.png

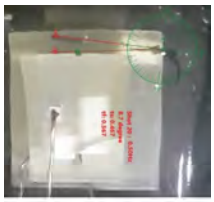
20.png

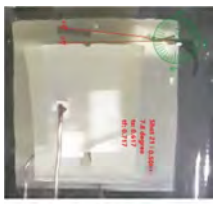
21.png

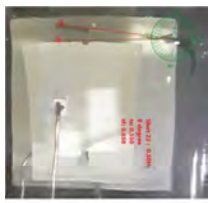
22.png


23.png

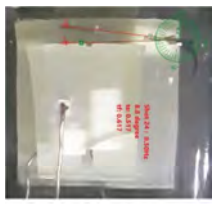
24.png

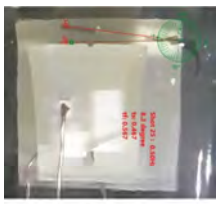
25.png

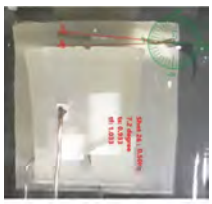
26.png

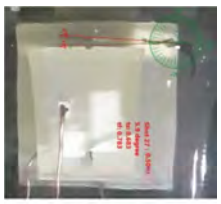
27.png

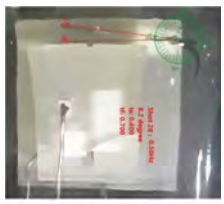
28.png

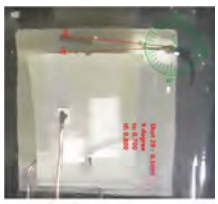
29.png


30.png

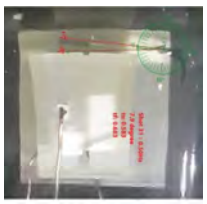
31.png

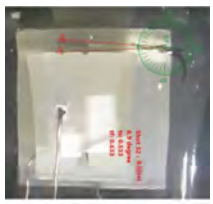
32.png


33.png

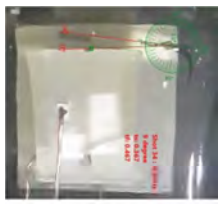
34.png

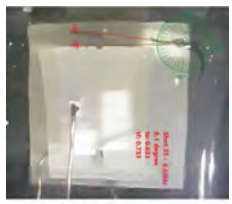
35.png

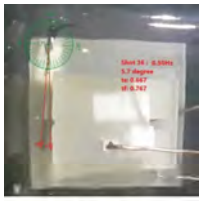
36.png


37.png


38.png

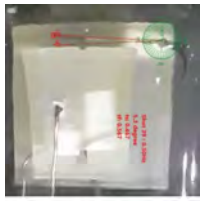
39.png


40.png

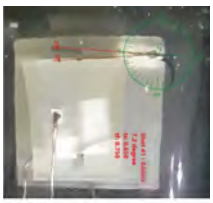
41.png

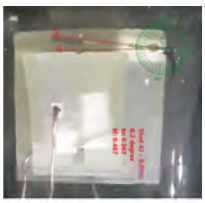
42.png


43.png

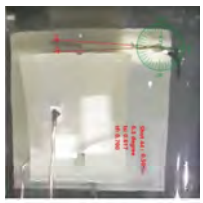
44.png


45.png

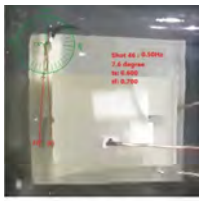
46.png


47.png

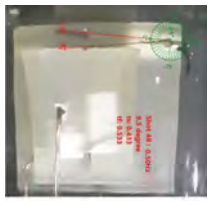
48.png

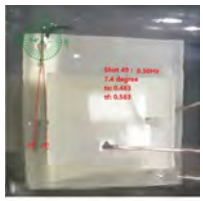
49.png

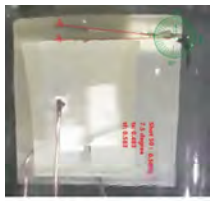
50.png

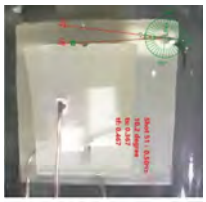
51.png

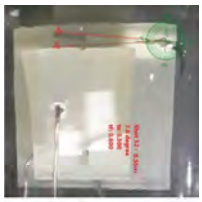
52.png

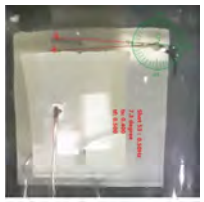
53.png


54.png


55.png

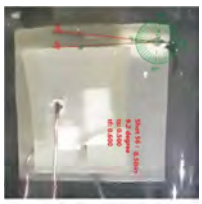
56.png

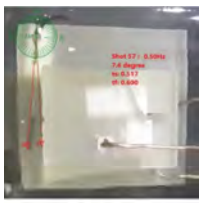
57.png

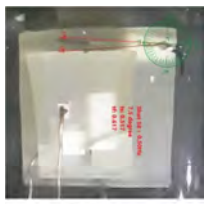
58.png


59.png

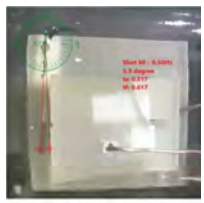
60.png


61.png

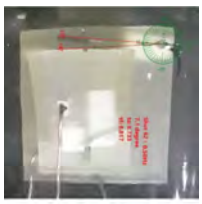
62.png

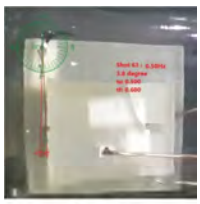
63.png

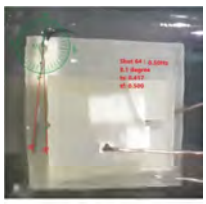
64.png


65.png

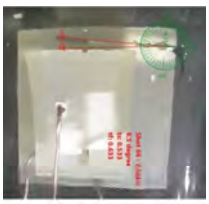
66.png


67.png

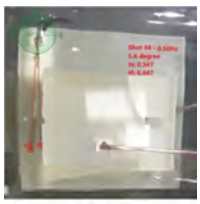
68.png

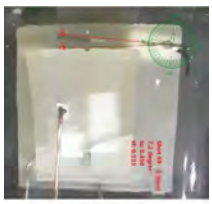
69.png


70.png

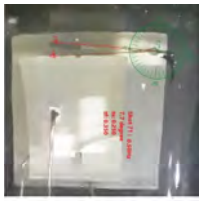
71.png

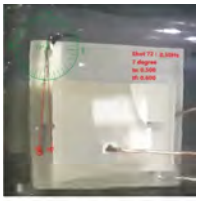
72.png


73.png


74.png

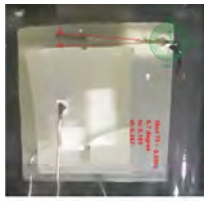
75.png


76.png

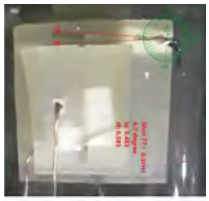
77.png

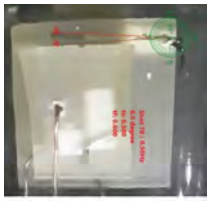
78.png


79.png

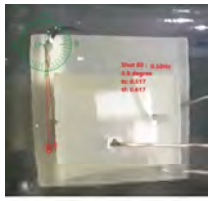
80.png


81.png


82.png

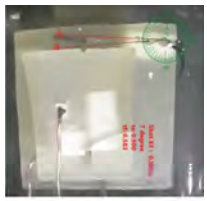
83.png


84.png


85.png

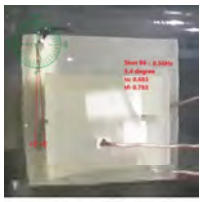
86.png

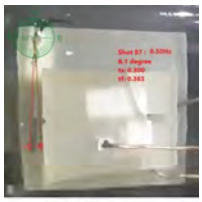
87.png

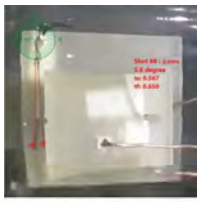
88.png

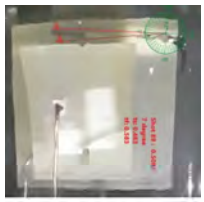
89.png

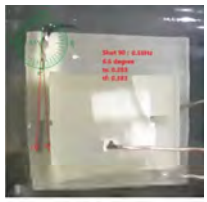
90.png


91.png

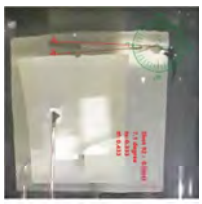
92.png

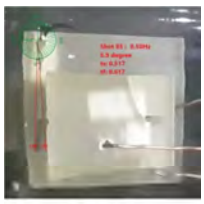
93.png


94.png

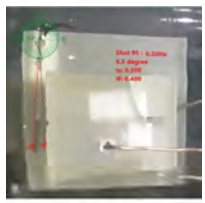
95.png

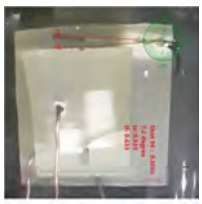
96.png


97.png


98.png


99.png


100.png


101.png

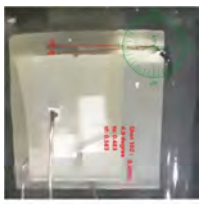
102.png

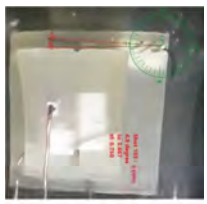
103.png


104.png

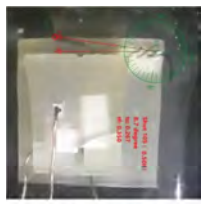
105.png

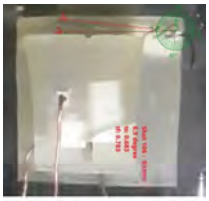

106.png

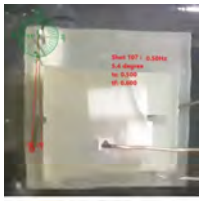

107.png

108.png

109.png

110.png

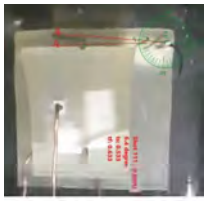

111.png

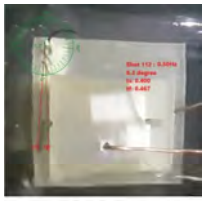

112.png

113.png

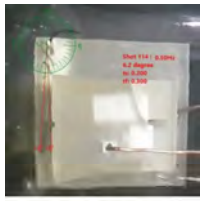

114.png

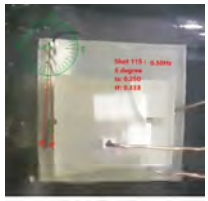

115.png

116.png

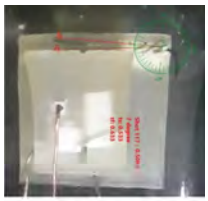

117.png

118.png

119.png

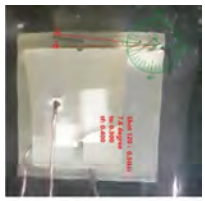

120.png

Shot #	angle (degree)	start time (s)	end time (s)	distance (m)	Ibit (μNs)	Thrust (μN)
1	9,7	0,600	0,700	0,007	1,956	0,978
2	6,5	0,450	0,550	0,005	1,301	0,650
3	7,5	0,250	0,367	0,005	1,504	0,752
4	6,9	0,683	0,783	0,005	1,382	0,691
5	6,7	0,550	0,633	0,005	1,341	0,671
6	7,8	0,600	0,700	0,005	1,565	0,783
7	6,8	0,583	0,683	0,005	1,362	0,681
8	6,1	0,567	0,667	0,004	1,220	0,610
9	6,9	0,517	0,633	0,005	1,382	0,691
10	6,4	0,350	0,450	0,004	1,281	0,640
11	7,5	0,533	0,617	0,005	1,504	0,752
12	7,2	0,450	0,533	0,005	1,443	0,721
13	7,5	0,517	0,617	0,005	1,504	0,752
14	9,7	0,600	0,700	0,007	1,956	0,978
15	9,1	0,583	0,683	0,006	1,832	0,916
16	10,6	0,517	0,633	0,007	2,143	1,071
17	6,6	0,450	0,550	0,005	1,321	0,661
18	7,6	0,517	0,617	0,005	1,524	0,762
19	9,5	0,617	0,717	0,007	1,914	0,957
20	8,7	0,467	0,567	0,006	1,749	0,875
21	7,8	0,617	0,717	0,005	1,565	0,783
22	8,0	0,550	0,650	0,006	1,606	0,803
23	8,9	0,450	0,550	0,006	1,791	0,895
24	8,8	0,517	0,617	0,006	1,770	0,885
25	8,2	0,467	0,567	0,006	1,647	0,823
26	7,2	0,933	1,033	0,005	1,443	0,721
27	5,9	0,683	0,783	0,004	1,180	0,590
28	8,2	0,600	0,700	0,006	1,647	0,823
29	9,0	0,700	0,800	0,006	1,811	0,906
30	7,6	0,650	0,750	0,005	1,524	0,762
31	7,9	0,583	0,683	0,006	1,586	0,793
32	6,9	0,533	0,633	0,005	1,382	0,691
33	7,5	0,700	0,800	0,005	1,504	0,752
34	9,0	0,367	0,467	0,006	1,811	0,906
35	8,1	0,633	0,733	0,006	1,626	0,813
36	5,7	0,667	0,767	0,004	1,139	0,570
37	8,4	0,500	0,600	0,006	1,688	0,844
38	9,8	0,317	0,417	0,007	1,976	0,988
39	5,3	0,467	0,567	0,004	1,059	0,529
40	7,5	0,467	0,567	0,005	1,504	0,752
41	7,2	0,650	0,750	0,005	1,443	0,721
42	8,2	0,367	0,467	0,006	1,647	0,823
43	8,2	0,667	0,750	0,006	1,647	0,823
44	6,3	0,617	0,700	0,004	1,260	0,630
45	7,7	0,650	0,733	0,005	1,545	0,772
46	7,6	0,600	0,700	0,005	1,524	0,762

47	7,6	0,550	0,650	0,005	1,524	0,762
48	9,5	0,433	0,533	0,007	1,914	0,957
49	7,4	0,483	0,583	0,005	1,484	0,742
50	7,5	0,483	0,583	0,005	1,504	0,752
51	10,2	0,367	0,467	0,007	2,059	1,030
52	7,8	0,500	0,600	0,005	1,565	0,783
53	7,3	0,400	0,500	0,005	1,463	0,732
54	7,2	0,567	0,667	0,005	1,443	0,721
55	4,4	0,517	0,617	0,003	0,878	0,439
56	9,2	0,500	0,600	0,006	1,852	0,926
57	7,6	0,517	0,600	0,005	1,524	0,762
58	7,5	0,517	0,617	0,005	1,504	0,752
59	6,5	0,333	0,417	0,005	1,301	0,650
60	5,3	0,517	0,617	0,004	1,059	0,529
61	6,9	0,550	0,633	0,005	1,382	0,691
62	7,1	0,733	0,817	0,005	1,423	0,711
63	3,8	0,500	0,600	0,003	0,758	0,379
64	8,1	0,417	0,500	0,006	1,626	0,813
65	3,5	0,533	0,633	0,002	0,698	0,349
66	6,5	0,533	0,633	0,005	1,301	0,650
67	6,8	0,450	0,533	0,005	1,362	0,681
68	5,6	0,567	0,667	0,004	1,119	0,560
69	7,2	0,450	0,533	0,005	1,443	0,721
70	7,9	0,417	0,517	0,006	1,586	0,793
71	7,7	0,250	0,350	0,005	1,545	0,772
72	7,0	0,500	0,600	0,005	1,402	0,701
73	6,6	0,267	0,367	0,005	1,321	0,661
74	6,6	0,350	0,433	0,005	1,321	0,661
75	6,7	0,183	0,267	0,005	1,341	0,671
76	6,2	0,283	0,383	0,004	1,240	0,620
77	6,7	0,483	0,583	0,005	1,341	0,671
78	6,5	0,500	0,600	0,005	1,301	0,650
79	6,6	0,483	0,583	0,005	1,321	0,661
80	3,9	0,517	0,617	0,003	0,778	0,389
81	6,9	0,533	0,633	0,005	1,382	0,691
82	7,3	0,450	0,533	0,005	1,463	0,732
83	7,0	0,500	0,583	0,005	1,402	0,701
84	7,2	0,317	0,400	0,005	1,443	0,721
85	6,9	0,600	0,683	0,005	1,382	0,691
86	5,4	0,683	0,783	0,004	1,079	0,539
87	6,1	0,300	0,383	0,004	1,220	0,610
88	5,6	0,567	0,650	0,004	1,119	0,560
89	7,0	0,483	0,583	0,005	1,402	0,701
90	6,6	0,283	0,383	0,005	1,321	0,661
91	7,4	0,000	0,083	0,005	1,484	0,742
92	7,1	0,333	0,433	0,005	1,423	0,711
93	5,9	0,517	0,617	0,004	1,180	0,590

94	7,6	0,117	0,217	0,005	1,524	0,762
95	6,5	0,300	0,400	0,005	1,301	0,650
96	7,2	0,533	0,633	0,005	1,443	0,721
97	7,7	0,550	0,650	0,005	1,545	0,772
98	8,1	0,217	0,317	0,006	1,626	0,813
99	6,5	0,533	0,633	0,005	1,301	0,650
100	6,6	0,583	0,667	0,005	1,321	0,661
101	6,5	0,000	0,083	0,005	1,301	0,650
102	4,9	0,483	0,583	0,003	0,978	0,489
103	4,9	0,667	0,750	0,003	0,978	0,489
104	6,9	0,367	0,467	0,005	1,382	0,691
105	8,7	0,267	0,350	0,006	1,749	0,875
106	6,9	0,683	0,783	0,005	1,382	0,691
107	5,4	0,500	0,600	0,004	1,079	0,539
108	5,3	0,483	0,550	0,004	1,059	0,529
109	5,8	0,550	0,650	0,004	1,159	0,580
110	5,8	0,533	0,617	0,004	1,159	0,580
111	6,4	0,533	0,633	0,004	1,281	0,640
112	6,3	0,400	0,467	0,004	1,260	0,630
113	7,2	0,333	0,433	0,005	1,443	0,721
114	6,2	0,200	0,300	0,004	1,240	0,620
115	6,0	0,250	0,333	0,004	1,200	0,600
116	6,6	0,583	0,667	0,005	1,321	0,661
117	7,0	0,533	0,633	0,005	1,402	0,701
118	7,0	0,650	0,733	0,005	1,402	0,701
119	6,4	0,267	0,367	0,004	1,281	0,640
120	7,6	0,300	0,400	0,005	1,524	0,762

Appendix J – Total BoM

This total BoM estimates the cost for the manufacturing of one micro-PPT and micro-pendulum used in the experiment. This does not reflect the true total cost of the dissertation. All customs and shipping were excluded from the costs.

Date	Company	Amount	Material
2021/04/06	Big Ideas 3D Printing	R 2 173,60	ULTEM 1010 3D Printing
2021/05/06	Metals Centre CC	R 46,00	Copper Sheet
2020/12/15	Digikey	R 5 024,80	Electric Components
2020/12/15	Mouser (USD)	R 2 035,84	Electric Components
2020/12/15	Xenon Flash	R 918,92	Electric Component
2021/09/30	RS Components	R 630,49	Electric Components
Total		R 10 829,65	

Appendix K – KiCAD Circuit Schematic and PCB Layout

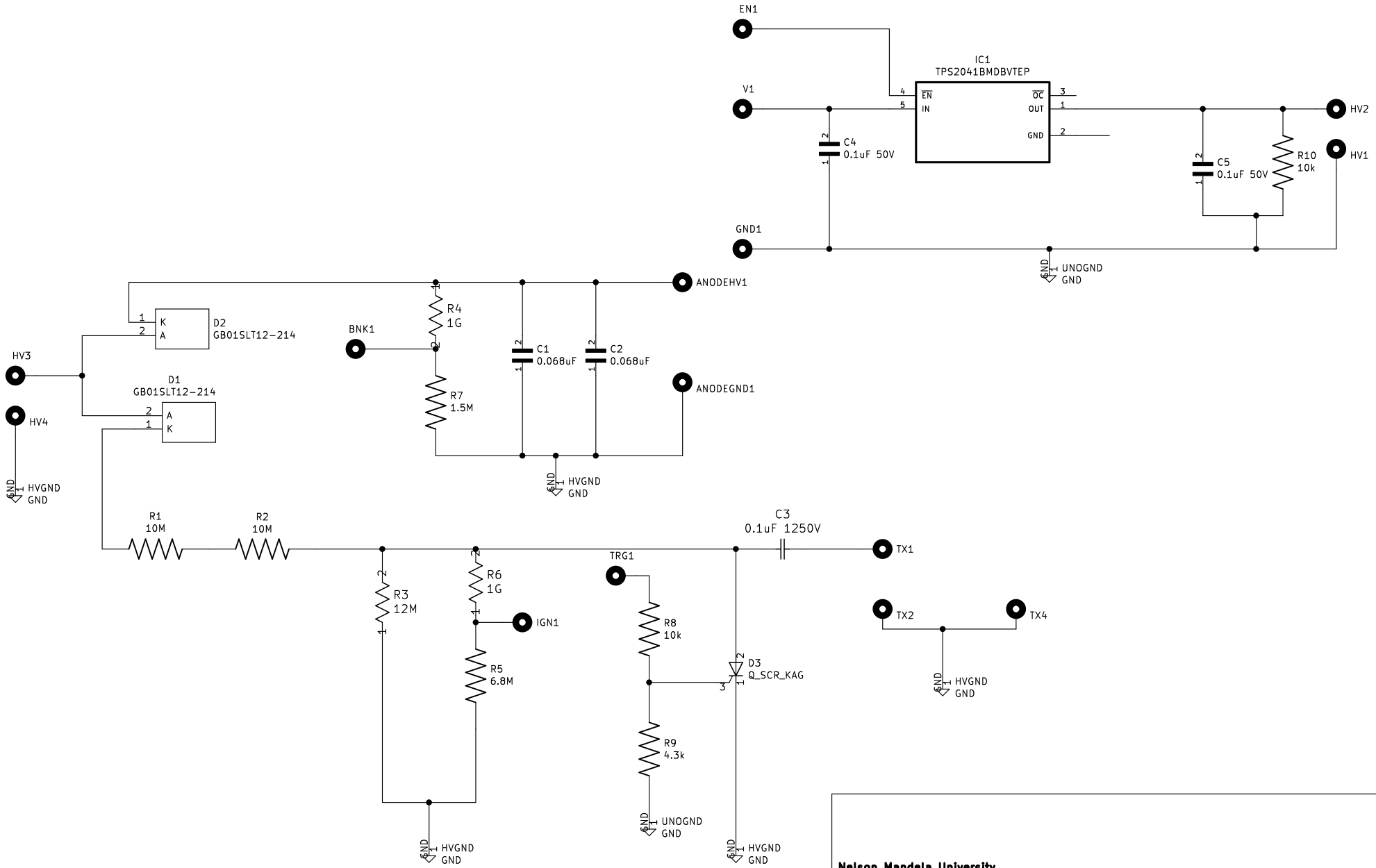

Nelson Mandela University

Sheet: /
File: Circuit V2.sch

Title: Micro-PPT control circuit

Size: A4	Date: 2021-03-19	**Rev:**
KiCad E.D.A. kicad (5.1.6)-1		Id: 1/1

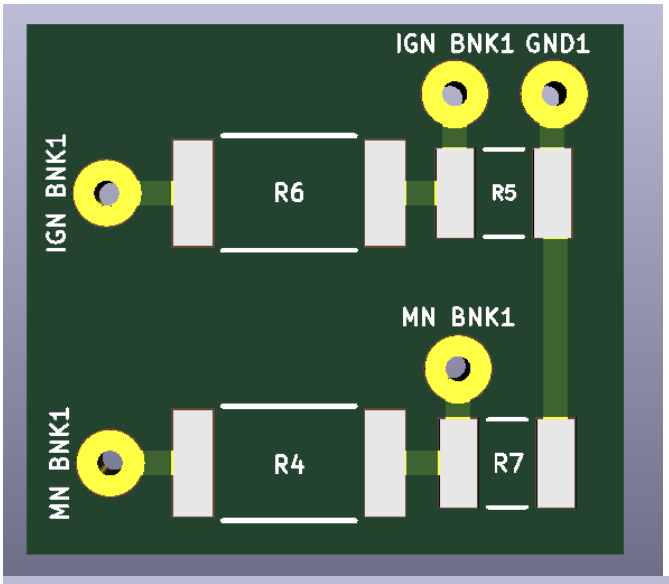
IGN BNK1 GND1
IGN BNK1
R6
R5
MN BNK1
MN BNK1
R4
R7

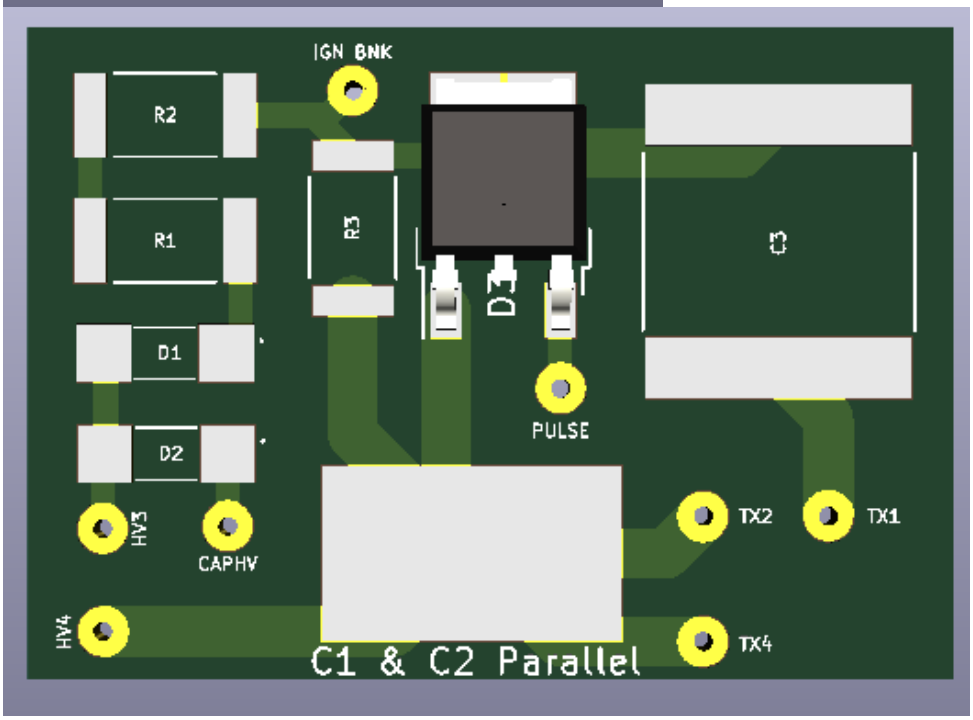
IGN BNK
R2
R1
R3
D3
D1
D2
PULSE
HV3
CAPHV
TX2
TX1
HV4
TX4
C1 & C2 Parallel

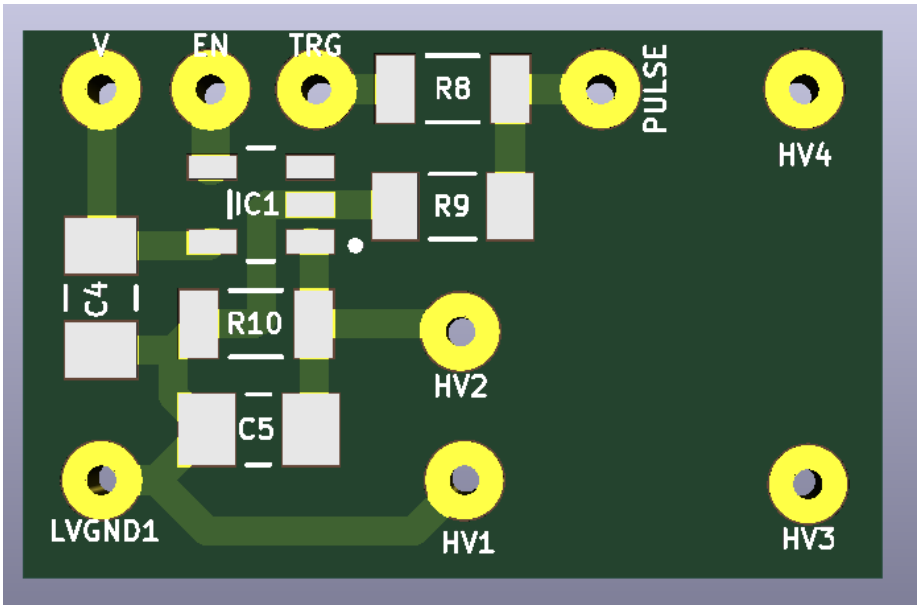
V
EN
TRG
R8
PULSE
HV4
IC1
R9
C4
R10
HV2
C5
LVGND1
HV1
HV3

Appendix L –Micro-pendulum Test Stand

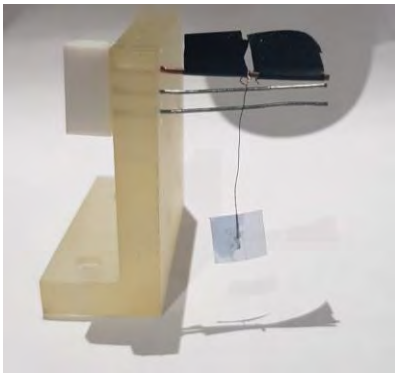
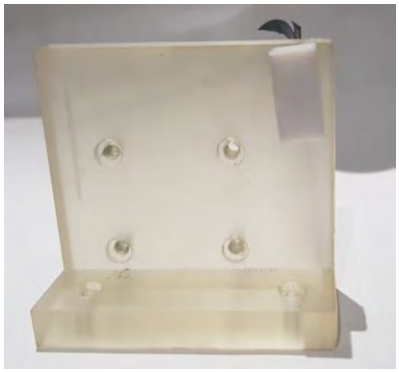
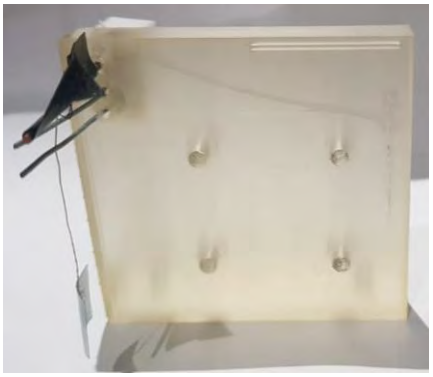

The micro-pendulum test stand used in the experiment was 3D printed with Formlabs High Temp V2 liquid using SLA 3D technology. The special pendulum target mass was made from an SCS 1000 flapper attached to a thin copper wire. Assuming the thin wire's weight was negligible and had a density of 0.001408g/mm^3, the calculated pendulum target mass came to an estimated weight of 0.0182g. A guiding bar was on the micro-pendulum was to ensure that the flapper fell to the right position after each pulse. *Table 15* shows a summary of the pendulum properties used in the calculation of the thrust produced in the experiments.

Table 15: Summary of the micro-pendulum properties

Property	Value
Length (mm)	40mm
Mass (g)	0,0182g
g (m/s^2)	9.807